



**NAVAL
POSTGRADUATE
SCHOOL**

MONTEREY, CALIFORNIA

THESIS

**IMPROVEMENT OF THE PERFORMANCE OF A TURBO-
RAMJET ENGINE FOR UAV AND MISSILE
APPLICATIONS**

by

Dimitrios Krikellas

December 2003

Thesis Advisor:
Second Reader:

Garth V. Hobson
Kai E. Woehler

Approved for public release; distribution is unlimited.

THIS PAGE INTENTIONALLY LEFT BLANK

REPORT DOCUMENTATION PAGE

Form Approved OMB No. 0704-0188

Public reporting burden for this collection of information is estimated to average 1 hour per response, including the time for reviewing instruction, searching existing data sources, gathering and maintaining the data needed, and completing and reviewing the collection of information. Send comments regarding this burden estimate or any other aspect of this collection of information, including suggestions for reducing this burden, to Washington headquarters Services, Directorate for Information Operations and Reports, 1215 Jefferson Davis Highway, Suite 1204, Arlington, VA 22202-4302, and to the Office of Management and Budget, Paperwork Reduction Project (0704-0188) Washington DC 20503.

1. AGENCY USE ONLY (Leave blank)		2. REPORT DATE December 2003	3. REPORT TYPE AND DATES COVERED Master's Thesis
4. TITLE AND SUBTITLE Improvement of the Performance of a Turbo-Ramjet Engine for UAV and Missile Applications		5. FUNDING NUMBERS	
6. AUTHOR (S) Dimitrios Krikellas		8. PERFORMING ORGANIZATION REPORT NUMBER	
7. PERFORMING ORGANIZATION NAME(S) AND ADDRESS(ES) Naval Postgraduate School Monterey, CA 93943-5000		10. SPONSORING/MONITORING AGENCY REPORT NUMBER	
9. SPONSORING / MONITORING AGENCY NAME(S) AND ADDRESS(ES) N/A		11. SUPPLEMENTARY NOTES The views expressed in this thesis are those of the author and do not reflect the official policy or position of the U.S. Department of Defense or the U.S. Government.	
12a. DISTRIBUTION / AVAILABILITY STATEMENT Approved for public release; distribution is unlimited		12b. DISTRIBUTION CODE	
13. ABSTRACT (maximum 200 words) An existing turbo-ramjet engine was modified in order to increase the produced thrust and sustain combustion at increased freejet Mach numbers. The engine's afterburner fuel system was redesigned to improve the vaporization and atomization of the fuel. The engine performed satisfactorily at speeds up to Mach 0.3, producing 100% more thrust over the baseline turbojet. The data acquisition system of the turbo-ramjet engine's performance measurement in a freejet facility was also updated. Various Computational Fluid Dynamics models of the flow through the turbo-ramjet engine were developed to visualize the flow and to predict the engine performance at different Mach numbers.			
14. SUBJECT TERMS : turbo-ramjet, afterburner, UAV propulsion, missile propulsion, Computational Fluid Dynamics, OVERFLOW, freejet, small-scale engines			15. NUMBER OF PAGES 157
16. PRICE CODE			
17. SECURITY CLASSIFICATION OF REPORT Unclassified	18. SECURITY CLASSIFICATION OF THIS PAGE Unclassified	19. SECURITY CLASSIFICATION OF ABSTRACT Unclassified	20. LIMITATION OF ABSTRACT UL

NSN 7540-01-280-5500

Standard Form 298 (Rev. 2-89)
Prescribed by ANSI Std. Z39-18

THIS PAGE INTENTIONALLY LEFT BLANK

Approved for public release; distribution is unlimited.

**IMPROVEMENT OF THE PERFORMANCE OF A TURBO-RAMJET ENGINE
FOR UAV AND MISSILE APPLICATIONS**

Dimitrios Krikellas

Captain, Hellenic Air Force

B.S., Hellenic Air Force Academy, 1993

B.S., National Technical University of Athens, 1999

Submitted in partial fulfillment of the
requirements for the degree of

**MASTER OF SCIENCE IN APPLIED PHYSICS
MASTER OF SCIENCE IN AERONAUTICAL ENGINEERING**

from the

**NAVAL POSTGRADUATE SCHOOL
December 2003**

Author: Dimitrios Krikellas

Approved by: Garth V. Hobson
Thesis Advisor

Kai E. Woehler
Co-Advisor

James Luscombe
Chairman, Department of Physics

Anthony J. Healey
Chairman, Department of Mechanical and Astronautical
Engineering

THIS PAGE INTENTIONALLY LEFT BLANK

ABSTRACT

An existing turbo-ramjet engine was modified in order to increase the produced thrust and sustain combustion at increased freejet Mach numbers. The engine's afterburner fuel system was redesigned to improve the vaporization and atomization of the fuel. The engine performed satisfactorily at speeds up to Mach 0.3, producing 100% more thrust over the baseline turbojet. The data acquisition system of the turbo-ramjet engine's performance measurement in a freejet facility was also updated. Various Computational Fluid Dynamics models of the flow through the turbo-ramjet engine were developed to visualize the flow and to predict the engine performance at different Mach numbers.

THIS PAGE INTENTIONALLY LEFT BLANK

*ΣΤΟΥΣ ΓΟΝΕΙΣ ΜΟΥ ΧΡΩΣΤΑΩ ΤΟ ΖΕΙΝ,
ΣΤΟΥΣ ΔΙΔΑΣΚΑΛΟΥΣ ΜΟΥ ΤΟ ΕΥ ΖΕΙΝ*

ΜΕΓΑΣ ΑΛΕΞΑΝΔΡΟΣ

*TO MY PARENTS I OWE MY EXISTENCE,
TO MY TEACHERS MY PROSPERITY*

ALEXANDER THE GREAT

THIS PAGE INTENTIONALLY LEFT BLANK

TABLE OF CONTENTS

I.	INTRODUCTION	1
II.	ENGINE DEVELOPMENT PROGRAM	5
A.	EXPERIMENTAL SETUP.....	5
1.	Engine Test Facility	5
2.	Turbo-ramjet Engine	6
a.	Sofia J450 Engine	7
b.	Ramjet Engine.....	7
(1)	Intake.....	7
(2)	Afterburner Duct.....	8
(3)	Flame Holders.....	8
3.	Air Supply System	9
4.	Thrust Stand.....	10
B.	DATA ACQUISITION SYSTEM.....	11
1.	Overview.....	11
2.	Sensors.....	12
3.	Program Analysis.....	13
4.	Program Operation.....	13
C.	AFTERBURNER FUEL SYSTEM DEVELOPMENT	15
1.	Overview.....	15
2.	Fuel Pump.....	15
3.	Afterburner Fuel Tank	16
4.	Fuel Lines.....	17
5.	Fuel Manifolds	18
a.	Propane Manifold.....	18
b.	Liquid Fuel Spray Rings	18
6.	Fuel Preheating	19
7.	Fuel Injectors..	20
D.	ENGINE PERFORMANCE	22

1.	Overview.....	22
2.	Spray Ring Configurations with Fuel Preheating	22
3.	Fuel Injector Configurations	26
a.	Six-Injector Configurations	26
b.	Twelve-Injector Configuration	29
D.	RESULTS	32
1.	Spray Ring Configuration with Fuel Preheating.....	32
2.	Fuel Injector Configurations	33
III.	TURBOJET ENGINE PERFORMANCE PREDICTION	35
A.	INTRODUCTION	35
B.	RESULTS	35
IV.	COMPUTATIONAL FLUID DYNAMICS (CFD) ANALYSIS.....	37
A.	INTRODUCTION	37
B.	SOFTWARE	38
1.	GRIDGEN.....	38
2.	GRIDDED.....	38
3.	OVERFLOW.....	38
4.	FAST.....	38
C.	GRID GENERATION	39
D.	TURBULENCE MODELS.....	40
1.	Introduction.....	40
2.	$k - \omega$ Turbulence Model.....	41
3.	Baldwin-Barth Turbulence Model.....	41
4.	Spalart-Allmaras Turbulence Model.....	42
E.	RESULTS	43
1.	Overview.....	43
2.	Ramjet Shroud with Nose Cone and Engine (Small Grid)	43
3.	Ramjet Shroud with Shock Cone and Engine (large grid).....	46
4.	Ramjet Shroud with Shock Cone, Engine and Flameholder.....	49
5.	Investigation of Various Turbulence Models	54

a. k- ω Turbulence Model	54
b. Baldwin-Barth Turbulence Model	54
c. Spalart-Allmaras Turbulence Model.....	55
6. Simulations Using the Engine Model	56
a. Creation of the Solution Files (Q files).....	56
b. Results.....	58
7. Limiting Factors of the Models.....	61
V. CONCLUSIONS AND RECOMMENDATIONS	63
APPENDIX A. SOPHIA J450 ENGINE AND FUEL PUMP	
SPECIFICATIONS	65
APPENDIX B. INSTRUMENTATION CALIBRATION RESULTS AND	
THRUST MEASUREMENTS	67
APPENDIX C. RESULTS AND INPUT FILES TO OVERFLOW.....	79
APPENDIX D. FORTRAN PROGRAMS AND INPUT FILES.....	123
APPENDIX E. DATA ACQUISITION PROGRAM ANALYSIS	125
1. Block Diagram of the Program Operation	125
2. Main Page Analysis	126
3. “Channel” Function Analysis	128
4. “Fuel_Flow” Function Analysis	129
5. “Thrust1” Function Analysis	130
6. “Static_Pres” and “Stagn_Pres” Functions Analysis.....	131
LIST OF REFERENCES	133
INITIAL DISTRIBUTION LIST.....	135

THIS PAGE INTENTIONALLY LEFT BLANK

LIST OF FIGURES

Figure 1. SFC vs Mach Number for Airbreathing Engines (Ref 1).....	2
Figure 2. Schematic of Engine Test Facility (Ref 1.)	5
Figure 3. Engine Test Rig and Controls.....	6
Figure 4. Turbo-ramjet Engine Configuration (Ref. 1).....	6
Figure 5 Typical Flame Holder (Ref. 8)	8
Figure 6. Flame Holder Configuration with Propane Manifold (Ref 1)	9
Figure 7. Engine Test Rig	10
Figure 8. Data Acquisition System	11
Figure 9. Data Control and Storage System.....	12
Figure 10. Control Panels	14
Figure 11. Afterburner Fuel System Schematic (Ref. 1)	15
Figure 12. New Fuel Pump and Suction Line.....	16
Figure 13. Fuel Tank and Feeding Line.....	17
Figure 14. Afterburner Rigid Lines (Back View).....	18
Figure 15. Coleman/Kerosene Fuel Manifold	19
Figure 16. Afterburner Rigid Lines and Fuel Preheat Setup (Side View)	20
Figure 17. Fuel Spray from M1 Injectors at 20 psi.....	21
Figure 18. Fuel Spray from M1 Injectors at 20 psi (detail)	21
Figure 19. Manifold for the Fuel Injector Configuration.....	22
Figure 20. Additional Afterburner Duct with Spiral.....	24
Figure 21. Additional Afterburner Duct with Insulation around the Spiral.....	24
Figure 22. Evidence of High Temperature in Preheating Spiral.....	25
Figure 23. Final Configuration with Fuel Reheating	26
Figure 24. Configuration with six 90° elbow fittings	27
Figure 25. Configuration with six 45° elbow fittings	28
Figure 26. Position of the Injectors Relative to the Turbojet Exhaust Cone (45° Elbow Fittings).....	29
Figure 27. Final Configuration with 12 Injectors	30
Figure 28. Manifold for the Final Configuration	31
Figure 29. Position of Injectors Inside the Turboramjet Engine.....	31
Figure 30. Thrust Measurements (Analytically).....	32
Figure 31. Thrust Measurements (Summary)	33
Figure 32. Thrust Measurements for Turbojet Engine operating at 60%	34
Figure 33. Grid Boundaries.....	40
Figure 34. Mach Number Distribution at $M_{\infty}=0.6$	44
Figure 35. Mach Number Distribution for $M_{\infty}=1.5$	45
Figure 36. Mach Number Distribution for $M_{\infty}=1.5$ (New Boundary Condition).....	46
Figure 37. Mach Number Distribution for $M_{\infty}=0.6$ (Large Grid)	47
Figure 38. Mach Number Distribution for $M_{\infty}=1.5$ (Boundary Condition # 32)	48
Figure 39. Mach Number Distribution for $M_{\infty}=1.5$ (Boundary Condition # 31)	49

Figure 40. Mach Number Distribution for $M_{\infty} = 0.6$ (with Flameholder).....	50
Figure 41. Mach Number Distribution for $M_{\infty} = 1.5$ (with Flameholder, BC #32)	50
Figure 42. Mach Number Distribution for $M_{\infty} = 1.5$ (with Flameholder, BC #31)	51
Figure 43. Pressure Distribution for the Turbo-Ramjet Engine at $M_{\infty} = 0.6$ (with Flameholder).....	52
Figure 44. Velocity vectors aft from flameholder for $M_{\infty} = 0.6$	53
Figure 45. Velocity vectors aft from flameholder for $M_{\infty} = 1.5$	53
Figure 46. Mach distribution for $M_{\infty} = 0.6$ with Baldwin-Barth Model	54
Figure 47. Mach distribution for $M_{\infty} = 0.6$ with Spalart-Allmaras Model.....	55
Figure 48. Velocity vectors aft from flameholder for $M_{\infty} = 0.6$	56
Figure 49. Detail of first grid without any grid points inside the turbojet engine	58
Figure 50. Detail of the second grid with grid points inside the turbojet engine.....	59
Figure 51. Mach distribution for $M_{\infty} = 0.6$ with Spalart-Allmaras Model and Engine Modeling with Q-files.....	60
Figure 52. Mach distribution for $M_{\infty} = 0.6$ with Spalart-Allmaras Model and Long Afterburner Duct.....	61
Figure A1. Fuel Pump Characteristics	65
Figure B1. Thrust Beam Calibration.....	68
Figure C1. Temperature Distribution for the Turbo-Ramjet Engine at $M_{\infty} = 0.6$ (Inflow/Outflow BC)	79
Figure C2. Pressure Distribution for the Turbo-Ramjet Engine at $M_{\infty} = 0.6$ (Inflow/Outflow B.C.)	79
Figure C3. Convergence History for Turbo-Ramjet Engine at $M_{\infty} = 0.6$ (Small Grid - Inflow/Outflow B.C.).....	80
Figure C4. Temperature Distribution for the Turbo-Ramjet Engine at $M_{\infty} = 1.5$ (Small Grid - Inflow/Outflow B.C.)	83
Figure C5. Pressure Distribution for the Turbo-Ramjet Engine at $M_{\infty} = 1.5$ (Small Grid - Inflow/Outflow B.C.).....	83
Figure C6. Convergence History for Turbo-Ramjet Engine at $M_{\infty} = 1.5$ (Small Grid - Inflow/Outflow B.C.).....	84
Figure C7. Temperature Distribution for the Turbo-Ramjet Engine at $M_{\infty} = 1.5$ (Riemann Invariants B.C.)	87
Figure C8. Pressure Distribution for the Turbo-Ramjet Engine at $M_{\infty} = 1.5$ (Riemann Invariants B.C.)	87
Figure C9. Convergence History for Turbo-Ramjet Engine at $M_{\infty} = 1.5$ (Small Grid - Riemann Invariants B.C.)	88
Figure C10. Temperature Distribution for the Turbo-Ramjet Engine at $M_{\infty} = 0.6$ (Large Grid – Inflow/Outflow B.C.)	91
Figure C11. Pressure Distribution for the Turbo-Ramjet Engine at $M_{\infty} = 0.6$ (Large Grid - Inflow/Outflow B.C)	91

Figure C12. Convergence History for Turbo-Ramjet Engine at $M_{\infty} = 0.6$ (Large Grid - Inflow/Outflow B.C.).....	92
Figure C13. Temperature Distribution for the Turbo-Ramjet Engine at $M_{\infty} = 1.5$ (Large Grid - Inflow/Outflow B.C.).....	95
Figure C14. Pressure Distribution for the Turbo-Ramjet Engine at $M_{\infty} = 1.5$ (Large Grid - Inflow/Outflow B.C.)	95
Figure C15. Convergence History for Turbo-Ramjet Engine at $M_{\infty} = 1.5$ (Large Grid - Inflow/Outflow B.C).....	96
Figure C16. Temperature Distribution for the Turbo-Ramjet Engine at $M_{\infty} = 1.5$ (Large Grid – Riemann Invariants B.C.)	99
Figure C17. Pressure Distribution for the Turbo-Ramjet Engine at $M_{\infty} = 1.5$ (Large Grid - Riemann Invariants B.C.)	99
Figure C18. Convergence History for Turbo-Ramjet Engine at $M_{\infty} = 1.5$ (Large Grid - Riemann Invariants B.C.)	100
Figure C19. Temperature Distribution for the Turbo-Ramjet Engine at $M_{\infty} = 0.6$ (with Flameholder – Inflow/Outflow B.C.).....	103
Figure C20. Pressure Distribution for the Turbo-Ramjet Engine at $M_{\infty} = 0.6$ (with Flameholder – Inflow/Outflow B.C.).....	103
Figure C21. Convergence History for Turbo-Ramjet Engine at $M_{\infty} = 0.6$ (Flameholder – Inflow/Outflow B.C.).....	104
Figure C22. Temperature Distribution for the Turbo-Ramjet Engine at $M_{\infty} = 1.5$ (with Flameholder – Inflow/Outflow B.C.).....	107
Figure C23. Pressure Distribution for the Turbo-Ramjet Engine at $M_{\infty} = 1.5$ (with Flameholder – Inflow/Outflow B.C.).....	107
Figure C24. Convergence History for Turbo-Ramjet Engine at $M_{\infty} = 1.5$ (with Flameholder – Inflow/Outflow B.C.).....	108
Figure C25. Pressure Distribution for the Turbo-Ramjet Engine at $M_{\infty} = 1.5$ (with Flameholder – Riemann Invariants B.C.)	111
Figure C26. Temperature Distribution for the Turbo-Ramjet Engine at $M_{\infty} = 1.5$ (with Flameholder – Riemann Invariants B.C.)	111
Figure C27. Convergence History for Turbo-Ramjet Engine at $M_{\infty} = 1.5$ (with Flameholder – Riemann Invariants B.C.)	112
Figure C28. Pressure Distribution for the Turbo-Ramjet Engine at $M_{\infty} = 0.6$ (Engine Modeling with Q-files –Short Afterburner Duct).....	115
Figure C29. Temperature Distribution for the Turbo-Ramjet Engine at $M_{\infty} = 1.5$ (Engine Modeling with Q-files – Short Afterburner Duct).....	115
Figure C30. Convergence History for Turbo-Ramjet Engine at $M_{\infty} = 0.6$ with Engine Modeling with Q-files (Short Afterburner Duct).....	116
Figure C31. Pressure Distribution for the Turbo-Ramjet Engine at $M_{\infty} = 0.6$ (Long Afterburner Duct).....	119

Figure C32. Temperature Distribution for the Turbo-Ramjet Engine at $M_{\infty} = 0.6$ (Long Afterburner Duct).....	119
Figure C33. Convergence History for Turbo-Ramjet Engine at $M_{\infty} = 0.6$ with Engine Modeling with Q-files (Long Afterburner Duct).....	120
Figure E1. Control Panels	125
Figure E2. Main Page Block Diagram.....	128
Figure E3. “Channel” Function Diagram.....	129
Figure E4. “Fuel_Flow” Function Diagram.....	130
Figure E5. “Thrust1” Function Diagram	131
Figure E6. “Static_Pres” Function Diagram.....	132
Figure E7. “Stagn_Pres” Function Diagram.....	132

LIST OF TABLES

Table A1. Sophia J450 Engine Specifications	65
Table B1. Plume's Static Differential Pressure and Corresponding Mach Numbers	67
Table B2. Thrust Beam Calibration Values	68
Table B3. Run 2, 20 Oct. 2003	69
Table B4. Run 4, 22 Oct. 2003	70
Table B5. Run 5, 22 Oct. 2003	71
Table B6. Run 6, 22 Oct. 2003	72
Table B7. Thrust Measurements for Configuration with Six M1 Injectors Spraying Axially.....	73
Table B8. Thrust Measurements for Configuration with Six M2 Injectors Spraying at 45° Relative to the Flow.....	74
Table B9. Thrust Measurements for Configuration with Twelve M2 Injectors	75
Table B10. Measurements with AB ON (Ref. 1).....	76
Table B11. Measurements with AB OFF (Ref. 6).....	77

THIS PAGE INTENTIONALLY LEFT BLANK

ACKNOWLEDGMENT

I would like to express my deep appreciation to all those who helped me in different ways in the completion of this demanding research.

Thanks to Dr. Anthony Gannon, Mr. Rick Still and Mr. John Gibson for their continuous help and advice in materializing my thoughts.

Most of all I would like to thank my thesis advisor Prof. Garth V. Hobson of the Department of Mechanical and Astronautical Engineering for his tireless support, guidance and advice, which enabled the successful conclusion of this project.

THIS PAGE INTENTIONALLY LEFT BLANK

I. INTRODUCTION

There is an increasing interest worldwide in the long-range tactical missiles as well as high performance Unmanned Aerial Vehicles (UAVs) or Unmanned Combat Aerial Vehicles (UCAVs). They can be launched from remote positions outside the enemy's defenses, can operate efficiently under dangerous conditions (bad weather, air defense), are very difficult to detect and thus to intercept. The biggest advantage is their ability to carry out a variety of missions autonomously thus avoiding the loss of valuable pilots, especially in the early days of potential conflicts.

Some of the main performance requirements of these vehicles are high flight speed, long range and long endurance. Thus being able to reach their target or area of operation in minimum time or remain airborne as long as possible. To achieve this, a powerplant able to operate efficiently in a wide range of altitudes and flight speeds is required.

A measure of the efficiency of modern engines is, among others, the Specific Fuel Consumption (SFC), which is defined as the fuel mass flow rate divided by the thrust

$$\text{produced, } SFC = \frac{\dot{m}_{fuel}}{T}.$$

Different types of engines operate efficiently over a relatively narrow Mach number range as discussed by Piper (Ref 1). This behavior is shown in Figure 1. It can be seen that the *SFC* of a high bypass turbofan engine is a minimum at subsonic speeds, a low bypass turbofan engine is optimized in the supersonic range below Mach 2 and a turbojet engine operates most efficiently between Mach 3 and 4. For flight speeds higher than Mach 4 and up to Mach 6, the ramjet is most suitable and for hypersonic speeds (greater than Mach 7) the Supersonic Combustion Ramjet (SCRAMJET) seems has been predicted to be the most efficient.

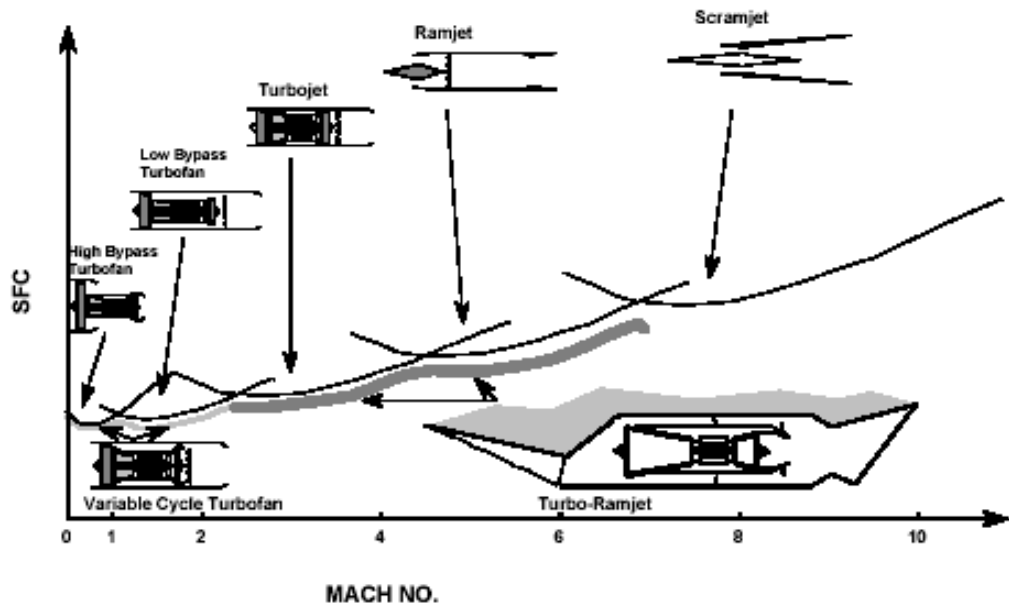


Figure 1. SFC vs Mach Number for Airbreathing Engines (Ref 1)

The main powerplants installed in UAVs, UCAVs and long-range tactical missiles are the internal-combustion propeller-driven or turbofan engines. The latter are similar in design and operation to the jet engines used to power modern fighter or commercial planes but in a smaller scale.

From the preceding it is clear that today's engines limit the flight speeds to high subsonic and low supersonic. In order to achieve efficient operation in higher Mach numbers and most importantly in a wide range of flight speeds, the use of Combined Cycle Engines (CCE) is of great interest.

The CCEs consists of a combination of engines (usually turbofans, turbojets and ramjet engines), which can operate simultaneously or separately to accelerate and sustain high flight speeds. They combine the advantages of both types of engines; for example, the turbofan/turbojet engine can be used to accelerate the UAV up to Mach 2 and then the ramjet can be turned on for acceleration to and cruise at Mach 4. If the vehicle is required to fly at low speeds, the ramjet can be turned off and the turbofan/turbojet can be used again.

The Nord Aviation Griffon II aircraft (1953) was the first to use a CCE. It was powered by a ramjet wrapped around a SNECMA Atar 101 E3 turbojet engine, and flew at Mach 2.1 at 18,600 m (61,000 ft) of altitude. Also, the SR-71 Blackbird (1960) had

two Pratt & Whitney J58 turbo-ramjet engines, each producing 32,500 lbs of thrust. It was capable of flying at Mach 3.0 at an altitude of 24,400 m (Ref.1).

A lot of work has been done since June 1998 at the Naval Postgraduate School's Gas Dynamics Laboratory (GDL) in order to design, develop and test a small turbo-ramjet engine capable of flying at high speeds.

Initially, Rivera (Ref 2) tested the performance of the Sophia J450 engine, a commercially available small turbojet engine for model aircraft. In March 1999, Hackaday (Ref. 3) performed a study of the static performance of the J450 with a constant area ejector. In September 1999, Andreou (Ref. 4) tested the J450 in a shrouded duct of varying lengths with an elliptical intake.

In June 2000, al-Namani (Ref. 5) continued the testing of the J450 in a shrouded duct of varying lengths. He measured the engine shaft rotational speed and exhaust gas temperature on a remotely controlled and instrumented engine. Finally, he designed the current supersonic intake for a flight Mach number of 2.0.

In December 2000, Garcia (Ref. 6) tested the ducted engine in a newly designed and constructed freejet facility. Tests of the engine running with elliptical and supersonic intakes were completed. He also tested the shrouded engine in the freejet facility at speeds less than Mach 0.5 and at different engine spool speeds. He also used Computational Fluid Dynamics (CFD) to analyze the Mach number and pressure distributions of the shrouded engine intake at Mach 2. Finally, Garcia completed preliminary design and testing of the fuel injection system (spray bars) for a possible afterburner/turbo-ramjet configuration.

In March 2003, Piper (Ref. 1) designed, developed and tested a combustor or afterburner for the turbo-ramjet engine. Experimental and computational tools were developed for the study of the engine, which was also analyzed with currently available performance prediction software for conventional engines (GASTURB 9.0 for WINDOWS).

The objective of this thesis was the improvement of the design and testing of an existing turbo-ramjet engine in order to operate with increasing forward speed. Variou

s computational models were also developed to further analyze the engine using the computational fluid dynamics code OVERFLOW coupled with the thermodynamics model GASTURB.

II. ENGINE DEVELOPMENT PROGRAM

A. EXPERIMENTAL SETUP

1. Engine Test Facility

The test facility used during this thesis project is presented in Figures 2 and 3.

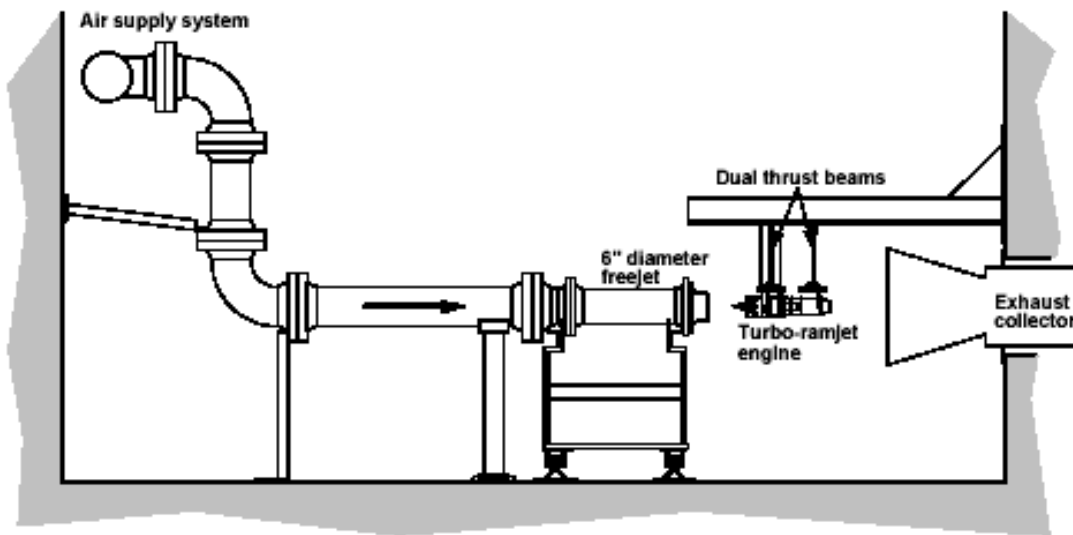


Figure 2. Schematic of Engine Test Facility (Ref 1.)

It consists of the following:

- Turbo-ramjet engine
- Air supply system
- Thrust beams
- Data acquisition system (not shown in Figure 2).
- Engine - afterburner fuel and lubricating systems.

All of the above will be described briefly in the following paragraphs.



Figure 3. Engine Test Rig and Controls

2. Turbo-ramjet Engine

The turbo-ramjet engine consisted of a SOFIA J450 Turbojet engine and the ramjet inlet ducting, combustor and exhaust nozzle as shown in Figure 4.

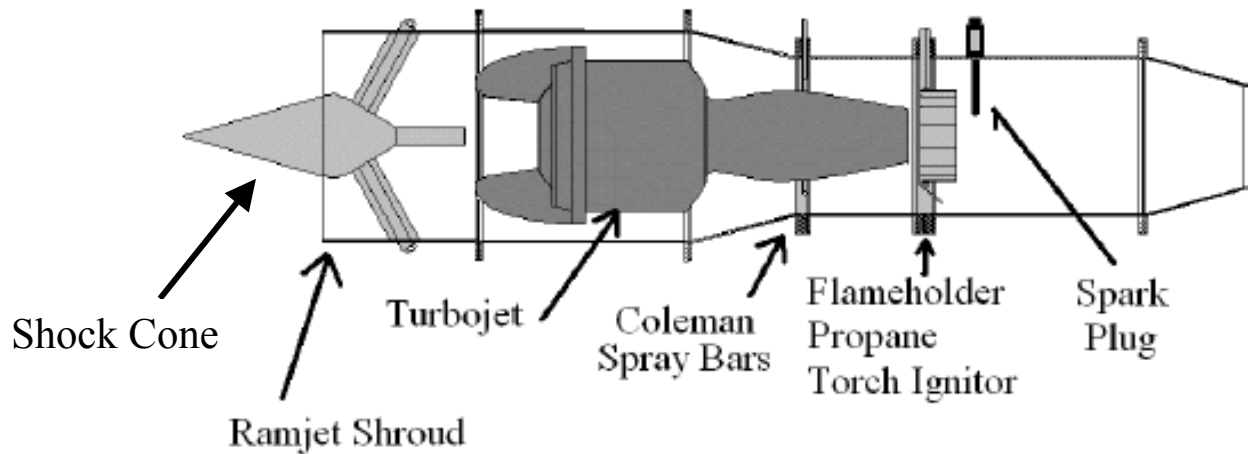


Figure 4. Turbo-ramjet Engine Configuration (Ref. 1)

a. Sofia J450 Engine

The Sofia J450 jet engine is a small commercially available turbojet engine, the performance characteristics of which are presented in Appendix A as Table A1. It has the standard configuration of a turbojet engine, that is :

- intake,
- centrifugal compressor,
- radial turbine,
- annular combustion chamber and
- nozzle.

This engine is used to power small model airplanes and hence was suitable for the gas generator of a small turbo-ramjet.

b. Ramjet Engine

The main parts of the ramjet engine are :

- the intake,
- the afterburner duct,
- the flame holders and
- the fuel manifolds,

Details of each will be presented in the following paragraphs.

(1) Intake

The supersonic portion of the intake consisted of a solid cone, which was designed to decelerate the incoming flow from supersonic to subsonic inside the engine. The principal of operation was the creation of an oblique shock, which decelerated the flow from high to low supersonic speeds, so that it could be further decelerated to subsonic through a normal shock formed at the minimum area location. The flow was to be decelerated inside the inlet due to subsonic diffusion.

The importance of this device was that both the turbojet engine and the ramjet combustor had to operate at subsonic conditions. The first one in order to avoid the creation of shocks in the blades and the second in order to sustain combustion.

The supersonic intake was designed by al-Namani (Ref. 5) using conic shock tables at a design Mach number of 2.0.

(2) Afterburner Duct

The afterburner duct was designed by Piper (Ref. 1) and had a diameter of 4.5 inches and a length of 6 inches, which was selected for maximum thrust by the J450 turbojet engine without afterburner, as discussed by al-Namani, (Ref. 5). No study was undertaken regarding the length required for flame stabilization and effective combustion.

(3) Flame Holders

The flame holders were used in order to stabilize the flame in the afterburner. The wake of the flame holders was divided in two regions: a recirculation and a mixing zone, as shown in Figure 5 (Ref 8). The recirculation zone is characterized by a strongly recirculating flow, very low reaction rates and a temperature that is nearly equal to the adiabatic flame temperature corresponding to the fuel-air mixture ratio in the approaching system. The mixing zones are characterized as turbulent regions of very strong shear, steep temperature gradients and vigorous chemical reaction.

A stable flame is established in the mixing zones by a balance of the continuing entrainment of cool unburned gas and the heat and species transfer from the hot burned gases.

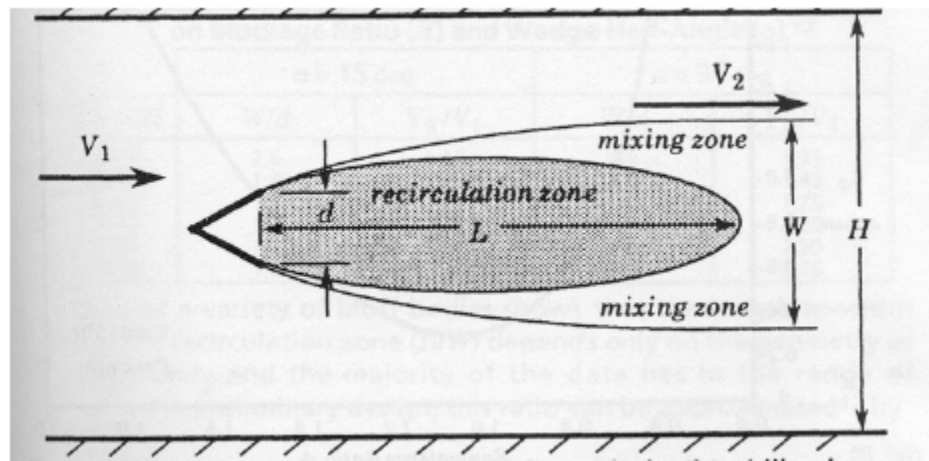


Figure 5 Typical Flame Holder (Ref. 8)

In the turbo-ramjet engine the flame holders were of the modified vee-gutter geometry, as shown in Figure 6 and had a blockage ratio of 0.3. The inner ring of the flameholder was continuous and was orientated axially (Figure 4), whereas the outer ring was discontinuous but was angled radially at about 60 degrees. Since the flow exiting the nozzle of the turbojet had significant swirl, the freestream flow onto the flameholders was not purely axial, thus the inclination of the vee-gutters was deemed acceptable.

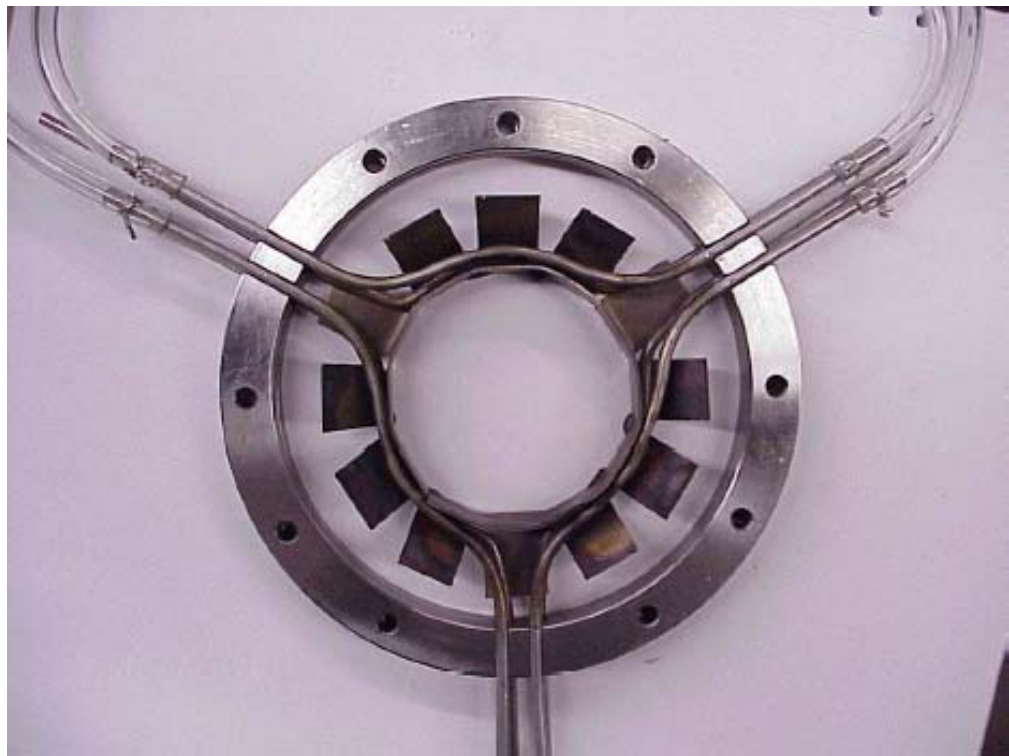


Figure 6. Flame Holder Configuration with Propane Manifold (Ref 1)

3. Air Supply System

The freejet facility used the compressed air supply system of the Gas Dynamics Laboratory (GDL). The amount of compressed air released could be varied in order to adjust the freejet Mach number. A pitot tube was installed upstream of the freejet nozzle to monitor the plenum chamber stagnation pressure. The differential pressure (plenum static-to-ambient pressure) and the corresponding Mach numbers are presented in Appendix B as Table B1.

4. Thrust Stand

The thrust stand was used to mount the turbo-ramjet as well as carry the various tubing, gauges and sensors, Figure 7.

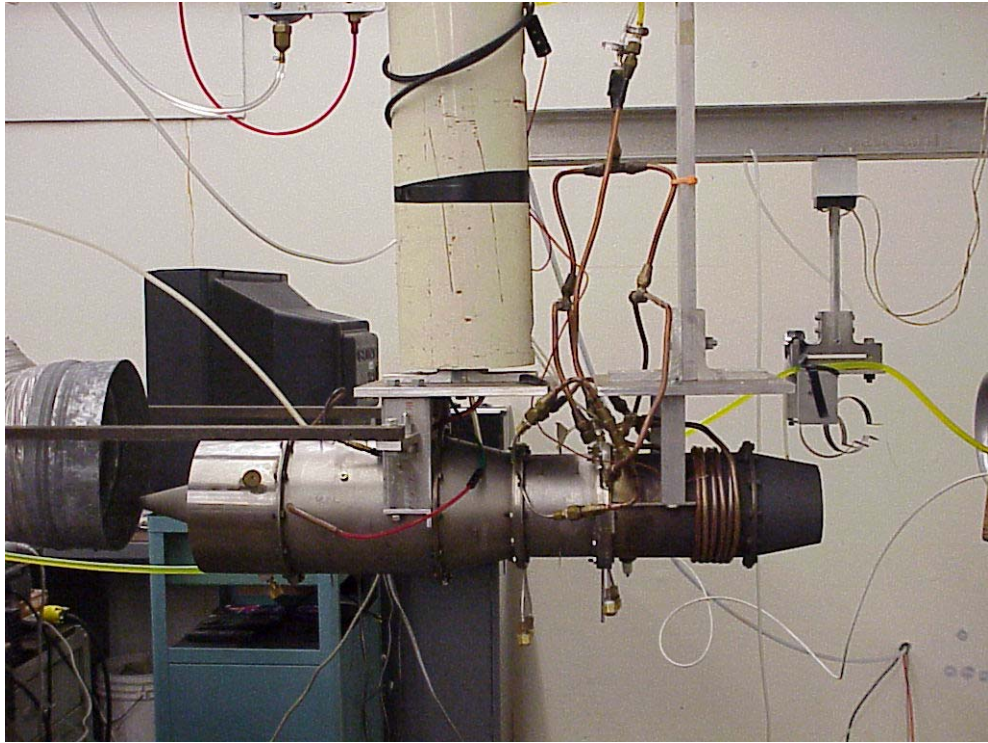


Figure 7. Engine Test Rig

It consisted of a horizontal I-beam section mounted to the wall of the GDL and two vertical beams, which held the engine horizontal and prevented it from pitching at high Mach numbers, as discussed by Piper (Ref. 1). Two strain gage Wheatstone bridges were installed on each beam in order to measure their deflection and consequently the forces produced on the engine.

Two additional horizontal beams were mounted from the nozzle of the freejet, which touched the sides of the forward thrust beam with roller bearings. These were installed in order to minimize the lateral vibrations of the engine.

B. DATA ACQUISITION SYSTEM

1. Overview

The data acquisition system consisted of a HP 6944A DACU in conjunction with a HP digital voltmeter (DVM), which received the signals from the various sensors through a signal conditioner (Figure 8). The signals were sent to a workstation via an IEEE-488 interface bus.

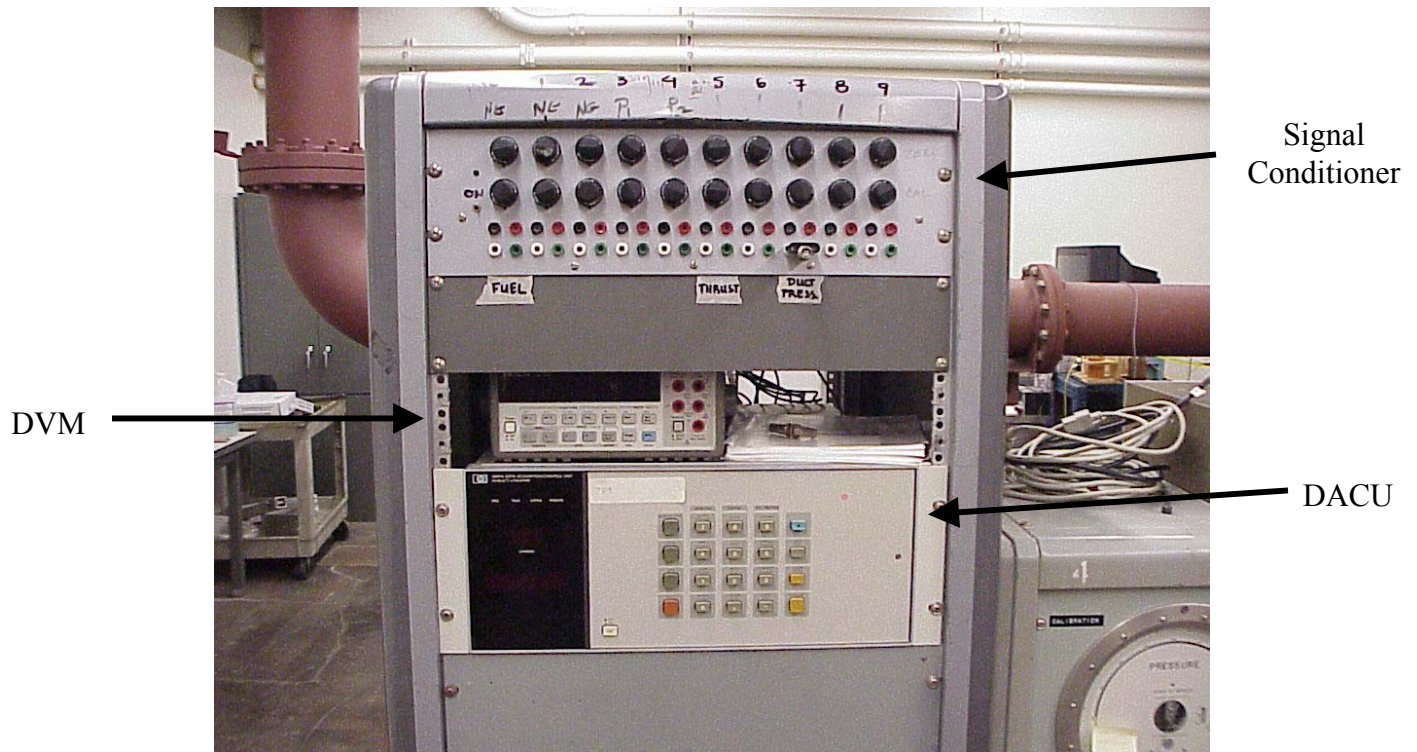


Figure 8. Data Acquisition System

The system was upgraded by replacing the old HP9000 Series 300 workstation by a Pentium 233MHz PC using the HP VEE 4.0 program development application (Figure 9). This application enabled the creation of programs in block diagram form, instead of lines of code and had extensive libraries of functions and subroutines for most programming tasks.

The '*Engine_Test2*' program was created for data acquisition and control, using the above application. The program recorded the data measured by the various sensors of

the system, calculated many performance parameters and saved them in a text file for further processing.



Figure 9. Data Control and Storage System

2. Sensors

The system used a number of sensors to measure the net engine thrust, engine fuel flow rate, freejet plenum static and total pressure as well as the afterburner duct temperature.

The thrust, fuel flow rate and pressure measurements are described by Piper (Ref. 1).

A total pressure pitot tube was installed in addition to the existing static one in order to calculate more accurately the freejet Mach number. The resulted total pressure value was very close to the measured static pressure, which corresponded in a negligible difference in Mach number.

A iron-constantine (J-type) thermocouple with a digital readout was installed to measure the afterburner duct's outer temperature as will be discussed later.

Finally, a video camera was used to record the behavior of the engine during all the test runs. It was most useful in monitoring the flame position during the acceleration of the freejet, in order to coordinate the increase of Mach number to the increase of fuel flow inside the afterburner in real time.

3. Program Analysis

The program '*Engine_Test2*' consisted of the Main page and five user-defined subroutines (*Channel*, *Fuel_Flow*, *Stag_Pres*, *Static_Pres* and *Thrust1*). The modular design of the program simplified its appearance, made it easy for the user to make modifications and/or expand for the acquisition of additional data.

The data were saved in files, which could be easily read by Microsoft Excel and MATLAB programs.

Each subroutine is analyzed in Appendix E.

4. Program Operation

The program could be controlled and run by the Main page front panel shown in Figure 10.

The user input the path in which the output file would be saved, the date and the run number as well as the calibration constants for the fuel flow and the thrust.

The program started by pressing the “Run” button. The number of iterations and the measured values of fuel flow rate, thrust, static and stagnation pressure during each iteration were presented in the corresponding windows. The program would keep running until the “Stop” button was pressed.

The program was also used to calibrate the thrust and fuel flow measurements, by selecting the individual functions (*Thrust1* and *Fuel_Flow*, respectively) and pressing the ‘START’ icon. This would run those functions only and not the rest of the application.

It was important to reset the DVM after each calibration; otherwise it would not respond to other commands.

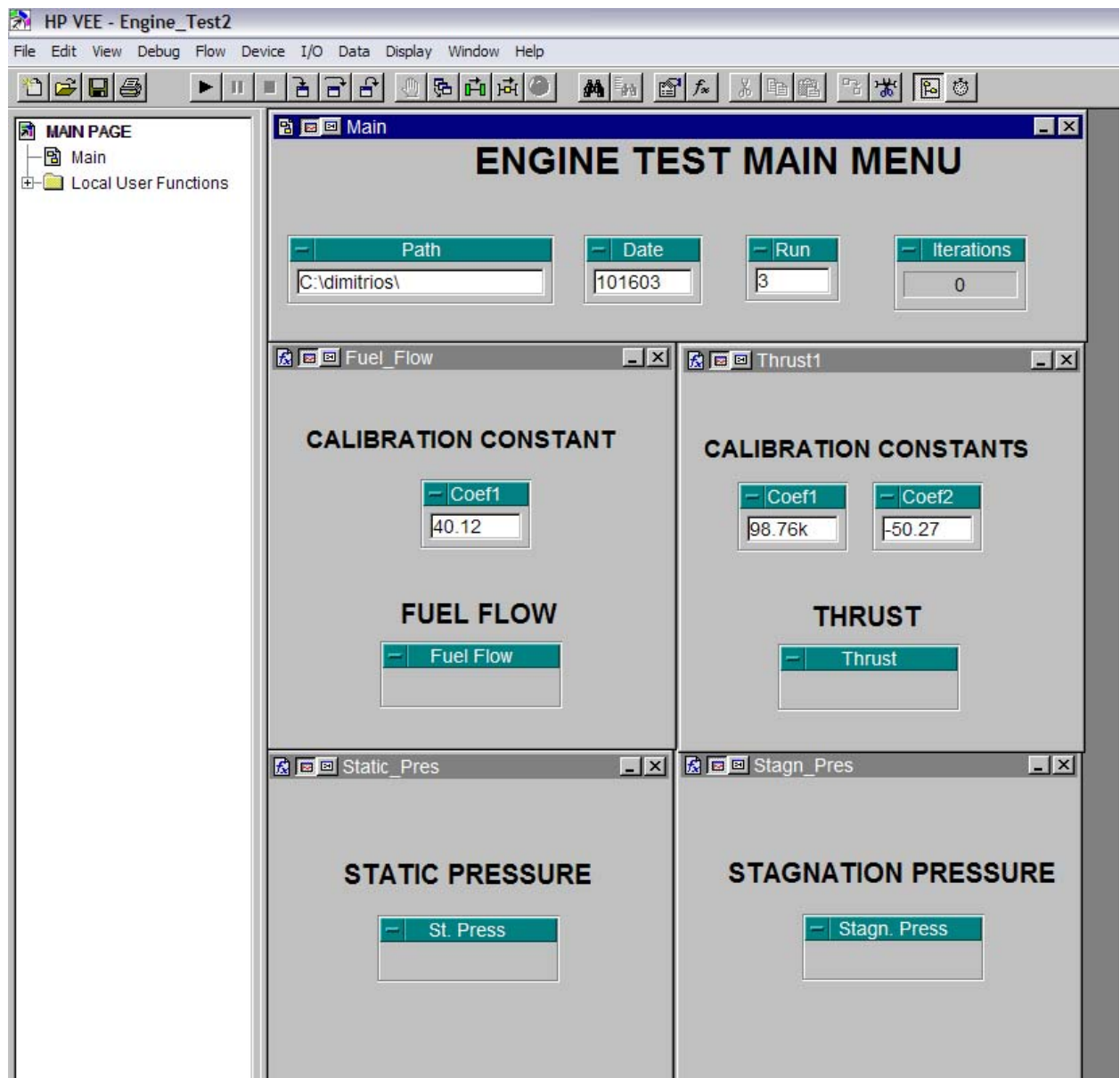


Figure 10. Control Panels

C. AFTERBURNER FUEL SYSTEM DEVELOPMENT

1. Overview

The existing afterburner fuel system was modified in order to enable the operation of the turbo-ramjet engine at increased Mach numbers. This modification included a new fuel pump, new suction line, new fuel tank and the replacement of the flexible fuel lines by rigid ones. The redesign of the spray rings, the preheating of the fuel and the use of fuel injectors were also considered during the course of the project.

The afterburner used both liquid fuel (Coleman fuel or Kerosene) and propane and its fuel system is shown in Figure 11. It consisted of the fuel tanks (propane and Coleman fuel), the electric fuel pump for the liquid fuel and two solenoid-controlled valves, which controlled the delivery of the propane to the afterburner.

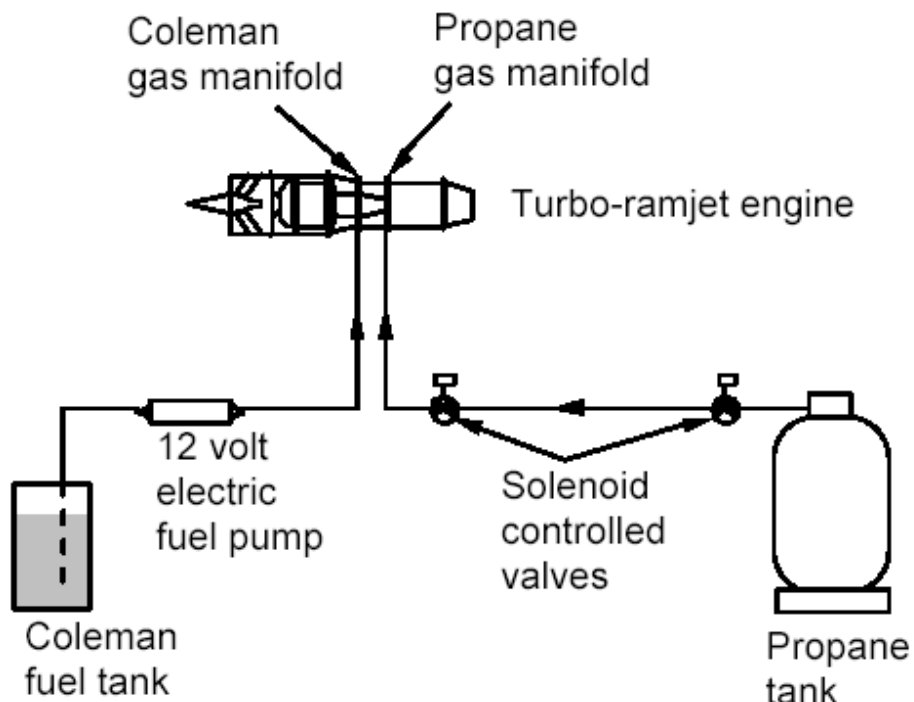


Figure 11. Afterburner Fuel System Schematic (Ref. 1)

2. Fuel Pump

Early in the tests it was revealed that the existing 12 Volt electric fuel pump was not able to provide the fuel flow rate required to sustain combustion at increased freejet Mach numbers. It was remarkable that as the Mach number increased, the air flow

through the afterburner sucked all the fuel from the lines, thus causing the pump to cavitate and not allowing the control of the fuel flow rate.

A Holley Inline Fuel Pump capable of injecting 52 GPH of fuel at 15 psi or 45 GPH at 40 psi replaced the fuel pump. A power supply was used to control the pump's flow rate. The performance characteristics of this pump, as given by the manufacturer, are shown in Appendix A as Figure A1.

Initially, a 1/8 inch suction line was used to feed the fuel pump but it proved to restrict its performance, not allowing it to provide the fuel flow rate required for the stabilization of the flame at high freejet Mach numbers. Hence, it was replaced by one with a 3/8 inch diameter (Figure 12).

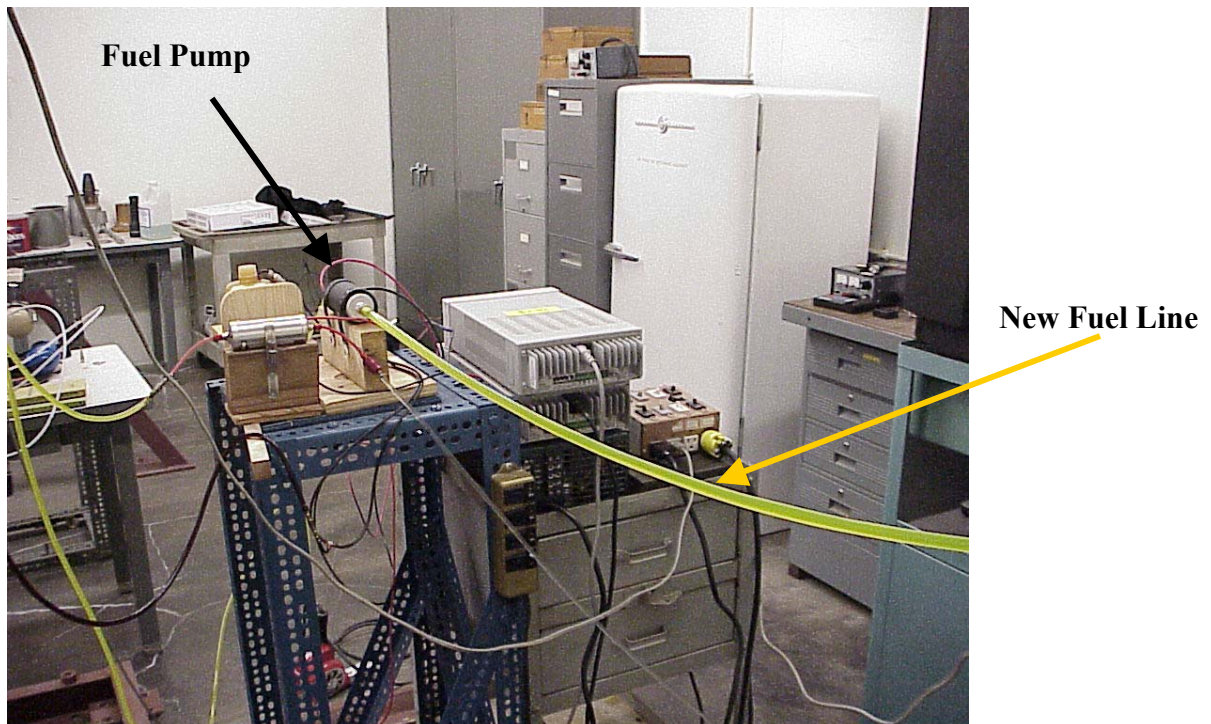


Figure 12. New Fuel Pump and Suction Line

3. Afterburner Fuel Tank

In order to operate in high Mach numbers, the required amount of fuel increased and a new 5-gallon fuel tank replaced the existing 1-gallon tank.

The fuel feed line was installed on the bottom of the tank and the whole assembly was put on an elevated position with respect to the fuel pump, in order to reduce any pressure losses and facilitate the fuel flow (Figure 13).



Figure 13. Fuel Tank and Feeding Line

4. Fuel Lines

The plastic Tygon^R tubing lines, used by Piper (Ref. 1), were replaced with brass tubing, in order to:

- reduce the danger of external fire in case of hot-gas leak from the afterburner, and
- provide a more rigid and permanent construction, as shown in Figure 14.

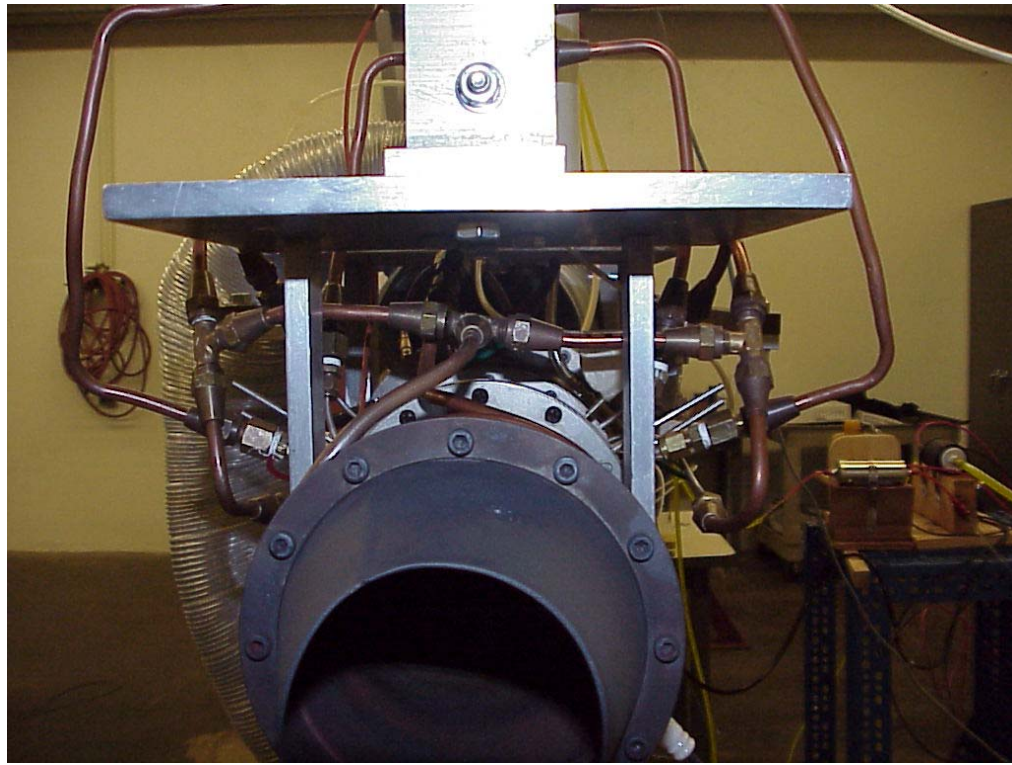


Figure 14. Afterburner Rigid Lines (Back View)

Finally, all the remaining flexible plastic lines were replaced by fuel resistant Tygon tubing, as they had become brittle from their exposure to fuel and weather conditions.

5. Fuel Manifolds

a. *Propane Manifold*

The fuel manifold that Piper (Ref.1) designed and tested did not atomized the fuel enough to ignite with a spark plug. Hence, propane was used to create a pilot flame, which ensured the ignition of the liquid fuel. The propane manifold, Figure 6, was designed by Piper (Ref. 1) and had 24 holes with a diameter of 0.050 inches, spraying inwards and outwards within the flame holder.

b. *Liquid Fuel Spray Rings*

Two configurations for the liquid fuel spray rings (Figure 15) were used:

- The first one had nine injection ports with a diameter of 0.050 inches each, spraying axially downstream. This configuration created a jet of fuel instead of a well atomized spray, resulting in limited ignition of the injected fuel, a significant amount of which drained out of the engine. Hence, the thrust generation was poor and the afterburner could not sustain combustion at high Mach numbers.
- The second one had fifteen injection ports with a diameter of 0.020 inch each, spraying radially inwards onto the hot turbojet nozzle and each hole had a small metal ring inserted over the port. This concept was originally designed and tested by Garcia (Ref 6) and facilitated the vaporization of the fuel. This configuration in conjunction with the preheating of the fuel and the improvement of the fuel delivery system, as will be discussed later, provided more efficient combustion and enabled the operation of the turbo-ramjet at higher Mach numbers.

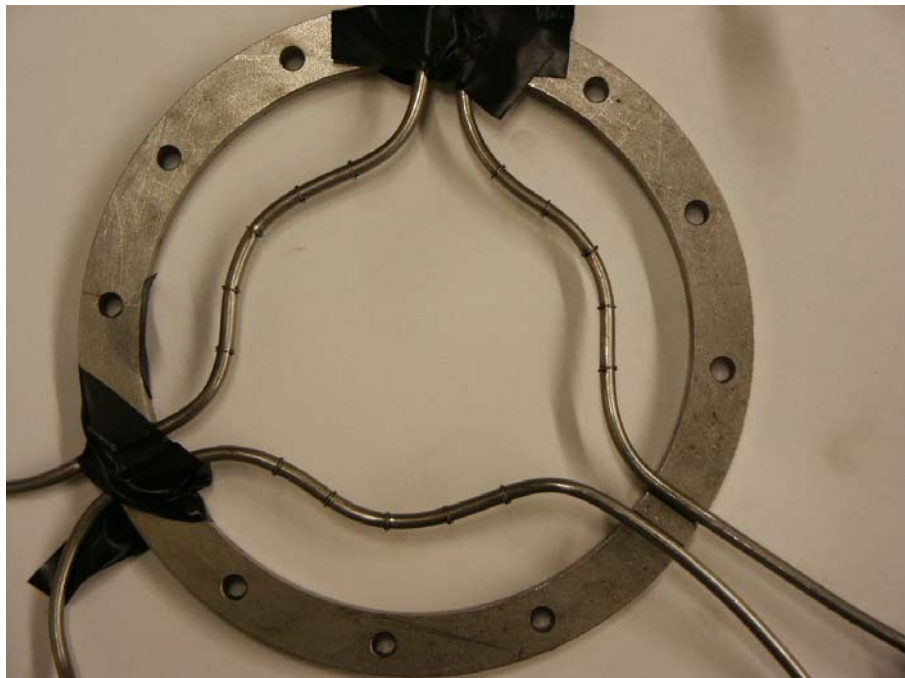


Figure 15. Coleman/Kerosene Fuel Manifold

6. Fuel Preheating

During the tests it was noticed that a large amount of fuel was draining outside the afterburner duct, thus revealing that some amount of the fuel was liquefied and hence it

could not be burned. This also restricted the freejet Mach number at which the afterburner could operate.

Hence, a fuel preheating setup was designed, consisting of spiral copper tubing around the afterburner duct (Figure 16).

This construction utilized the heat released by the afterburner in order to preheat the liquid fuel before injecting it in the engine. The spiral was positioned near the nozzle of the turbo-ramjet, where the temperature was higher.

As the spiral was made of copper having a low melting point, the temperature of the afterburner's shell was monitored using a digital thermometer.



Figure 16. Afterburner Rigid Lines and Fuel Preheat Setup (Side View)

7. Fuel Injectors

Fuel injectors were used in place of the liquid fuel manifolds in order to produce a fine spray of fuel and a more uniform air-fuel mixture inside the afterburner. Two types of injectors were used, each one designated as:

- M1, which had a maximum flow rate of 1 gal/h and

- M2, which had a maximum flow rate of 2 gal/h.

The M1s created the finest spray and increased the pressure inside the fuel line, the maximum value of which reached 90 psi. The same value for the M2s was 50 psi.

Figures 17 and 18 show the mist produced by 3 M1 injectors at fuel pressure of 20 psi.

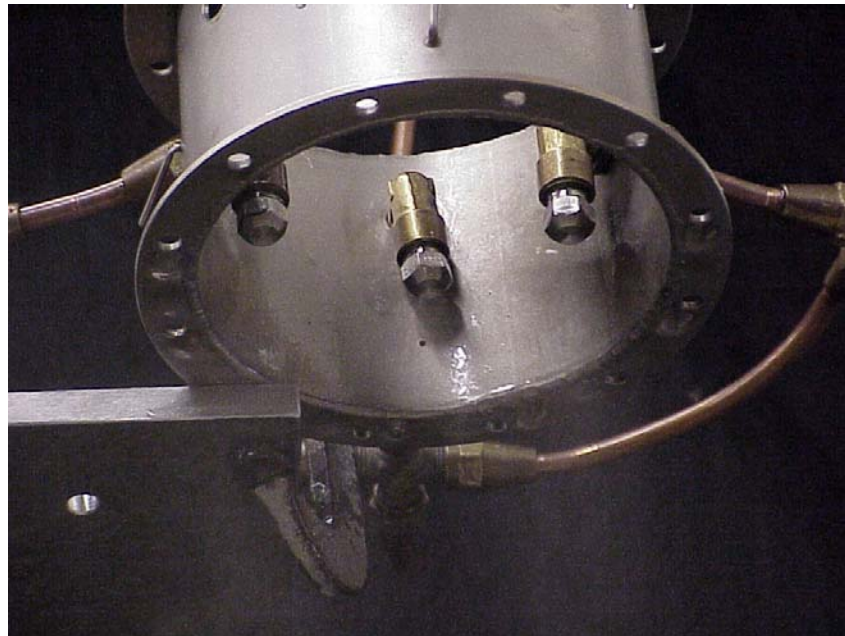


Figure 17. Fuel Spray from M1 Injectors at 20 psi



Figure 18. Fuel Spray from M1 Injectors at 20 psi (detail)

New manifolds were also constructed to provide the required fuel to the injectors, Figure 19.

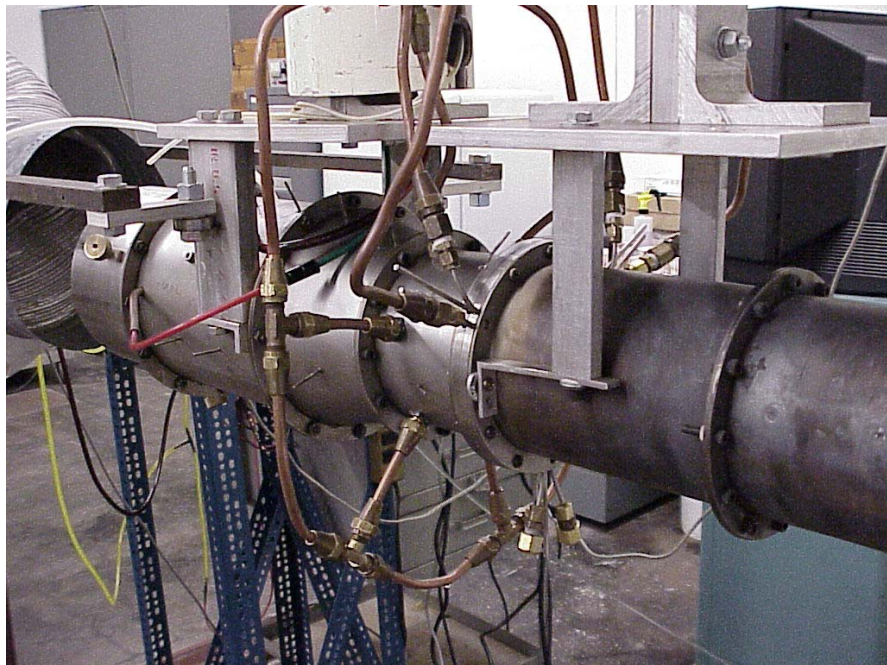


Figure 19. Manifold for the Fuel Injector Configuration

D. ENGINE PERFORMANCE

1. Overview

Two major configurations for the afterburner were used. The first one combined the use of fuel spray rings with a short and a long duct, as well as fuel preheating. The second one incorporated the use of fuel injectors in the long duct, without preheating.

2. Spray Ring Configurations with Fuel Preheating

As was stated previously, the most successful spray ring configuration was the one with the 0.0020 inches' diameter ports. This configuration created a well-atomized spray, which enabled the operation of the engine up to freestream Mach number of 0.2.

Furthermore, the use of the preheating set up was intended to help the fuel vaporization thus reducing the amount of fuel draining out of the engine and creating a rich, uniform fuel-air mixture.

The efficiency of the preheating system reduced as the freejet Mach number increased. At high Mach numbers, the heat transfer between the duct and the surrounding air increased, thus lowering its temperature. Temperatures from 600 to 1000 °F were easily achieved for speeds up to Mach 0.2, but at greater speeds, the temperature reduced to around 300 °F. This phenomenon affected the heating of the fuel and consequently its degree of vaporization, resulting in the reduction of thrust with increasing Mach number and the extinguishing of the flame at Mach 0.3 and higher.

Two solutions to this problem were considered:

- The cover of the aft section of the afterburner duct and the spiral by an insulating sheet, so as to reduce the heat losses.
- The use of kerosene, which released more heat than the Coleman fuel.

Both these options were applied, but although the duct's outside temperature was increased and under specific conditions exceeded 1400 °F, the stability of the flame didn't improve and the combustion could not be sustained.

As a next step, it was considered that the length of the afterburner duct wasn't enough to allow the stabilization of the flame and the ignition of all the fuel injected. Thus, a 6 inches duct was added and a new bigger spiral was made so as to increase the combustion area and the preheating/vaporization of the fuel (Figure 20).

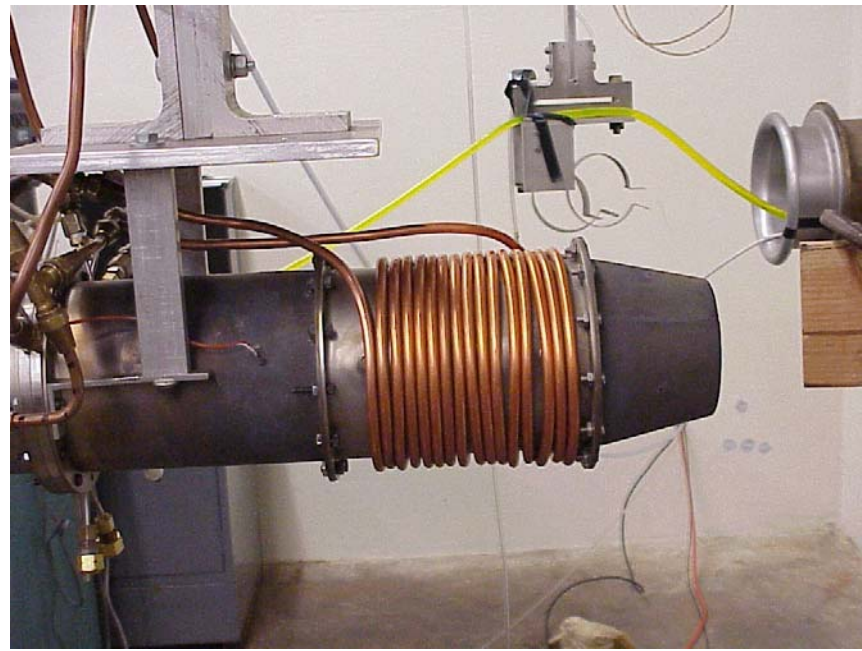


Figure 20. Additional Afterburner Duct with Spiral

The spiral was also surrounded by insulation, to reduce the heat losses (Figure 21).

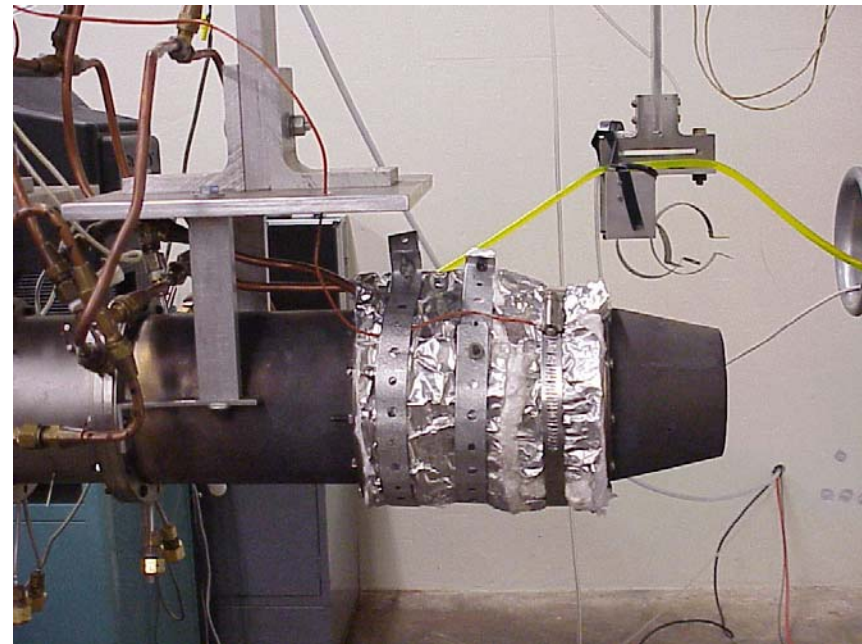


Figure 21. Additional Afterburner Duct with Insulation around the Spiral

This new design increased the vaporization of the fuel, thus giving the capability to relight the kerosene in ‘flight’ conditions once it was extinguished. On the other hand, the vast preheating of the fuel created a high fuel backpressure, which reached 60 psi, that didn’t allow the sufficient control of the fuel flow and induced instability to the fuel flow and the flame.

The cause of this problem was thought to be:

- the high temperature of the fuel, which caused it to vaporize partially or completely inside the spiral. The created gas or bubbles expanded and increased the backpressure in the fuel lines.
- the small diameter of the injector ports, which did not allow the proper flow of the fuel, thus again increasing the back pressure.

Evidence of the high temperature of the fuel lines is presented in Figure 22, where the tubing shows variable coloring.

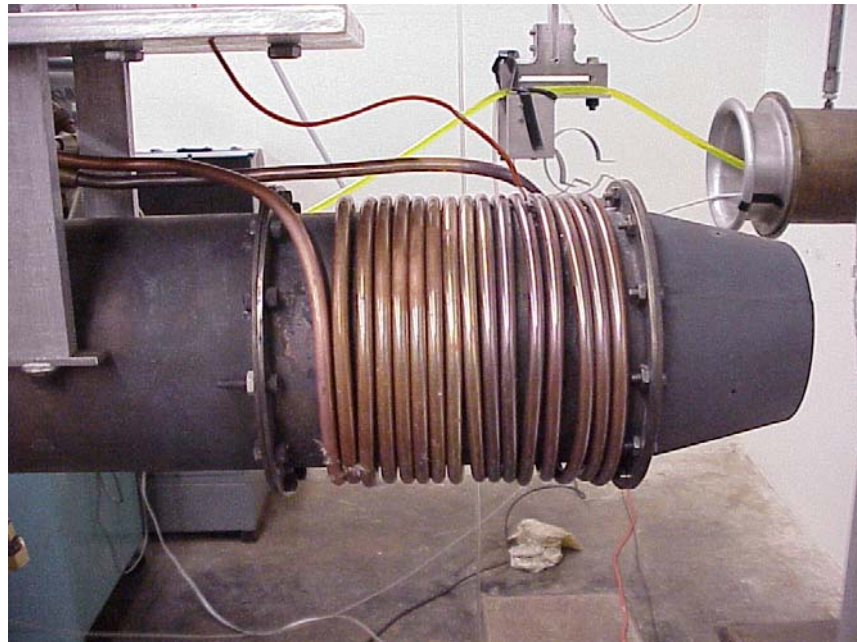


Figure 22. Evidence of High Temperature in Preheating Spiral

For the above reasons, the injectors’ diameter was increased to 0.040 inch and the insulation was removed, but again the flame was very unstable and extinguished at small Mach number.

The next step was to use a smaller preheating spiral, Figure 23, in an effort to reduce the vaporization of the fuel. This preheating configuration was expected to create a stable flame while the longer duct would contain the flame inside the engine and would increase the efficiency of the combustion. Unfortunately, the instability of the flame was maintained although the engine was more controllable and again the flame extinguished at small Mach numbers.

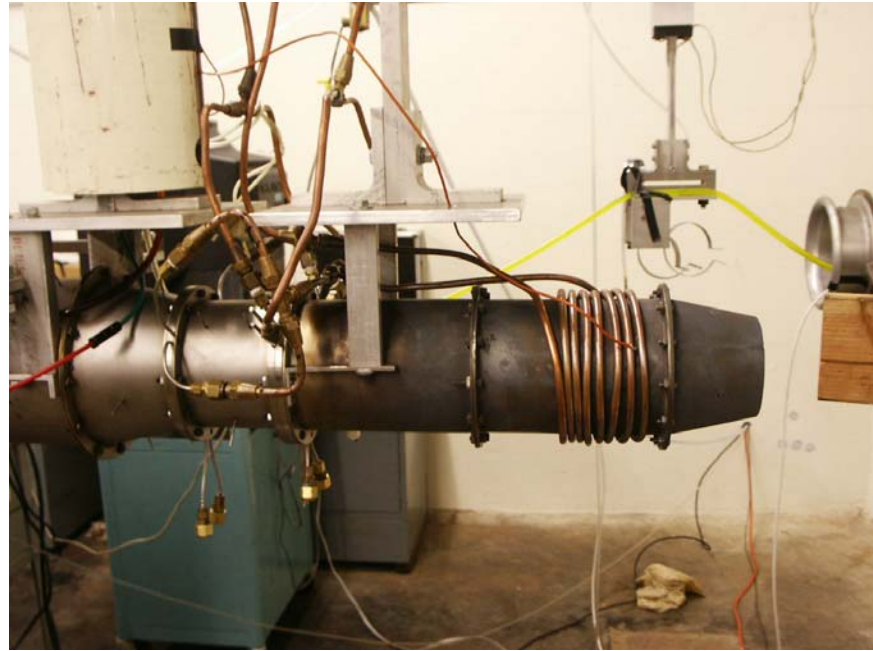


Figure 23. Final Configuration with Fuel Reheating

At this point, the existing engine's configuration development (with the spray rings and/or the preheating setup) was considered to be terminated as it could not make the engine operate at Mach numbers higher than 0.3 and produce positive thrust, the main reason being the inability to provide the proper atomized/vaporized fuel flow rate in order to sustain combustion with increasing Mach number.

3. Fuel Injector Configurations

a. *Six-Injector Configurations*

Six injectors were initially used to create the fuel spray inside the afterburner. These were placed circumferentially inside the duct, 3 inches upstream the previous position of the spray rings.

Two choices were available for the installation of the injectors. The first one used a 90° elbow fitting for each injector, Figure 24, while the second one used a 45° one, Figure 31.

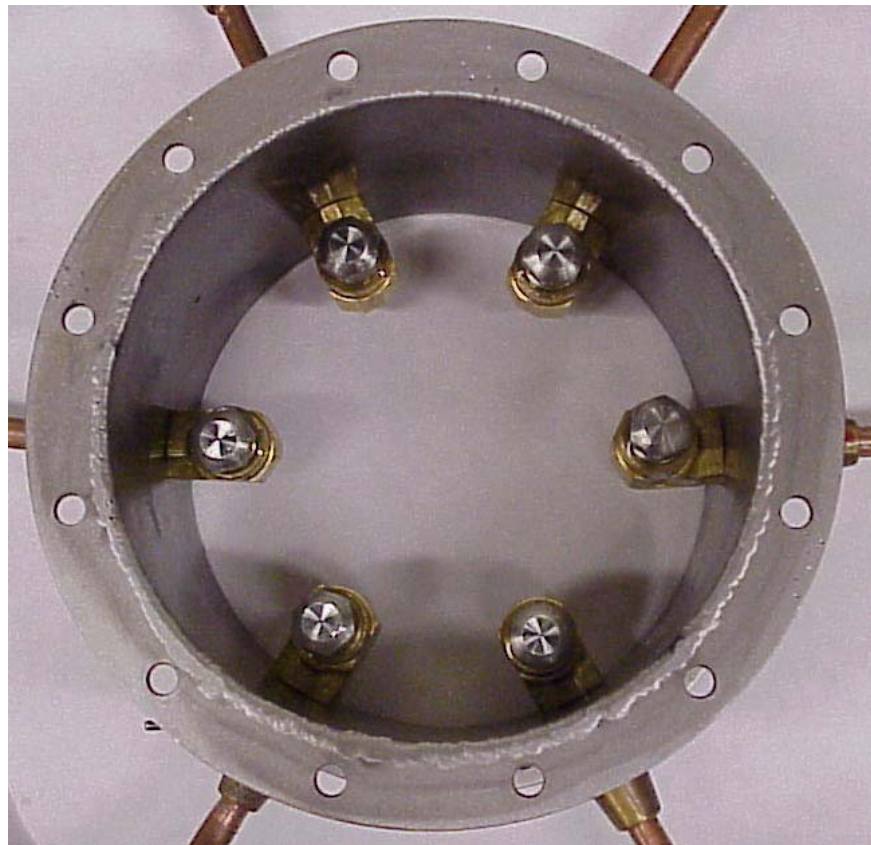


Figure 24. Configuration with six 90° elbow fittings

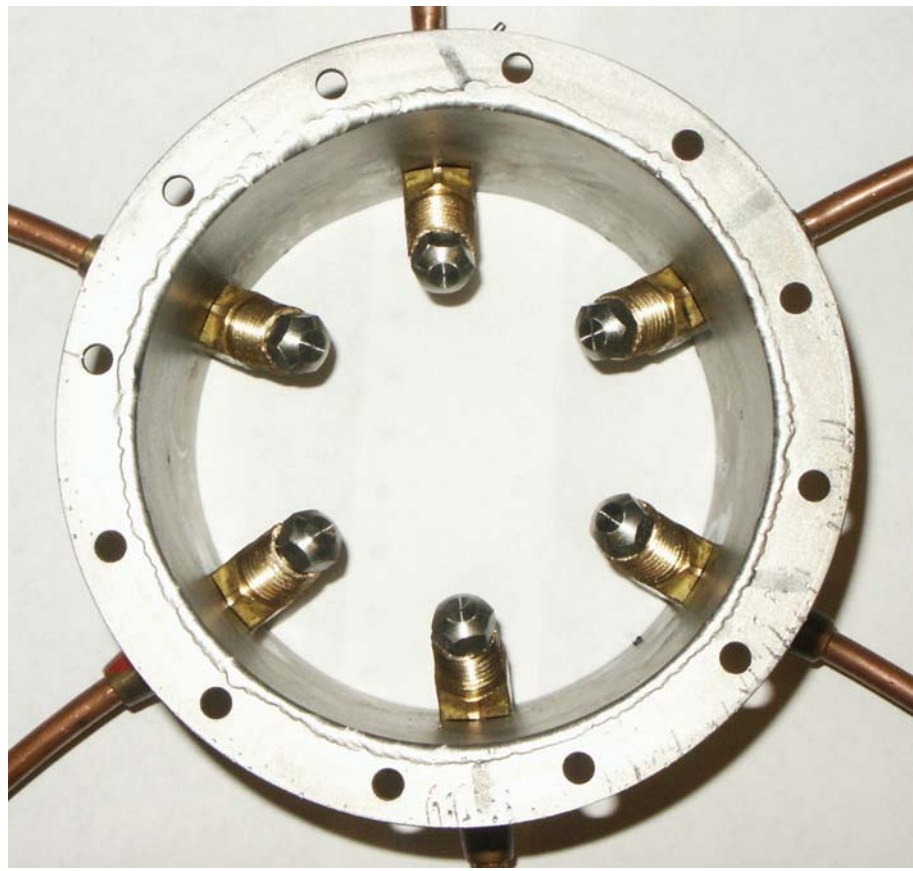


Figure 25. Configuration with six 45° elbow fittings

The difference between the two choices was that the first one placed the injector very close to the cold outer afterburner duct and sprayed axially, thus causing a great amount of fuel to be liquefied and drain outside the engine as it hit the cold outer skin of the engine. The second configuration, with the 45 ° elbows, positioned the injectors very close to the hot exhaust nozzle of the turbojet engine (Figure 26), thus improving the vaporization and the combustion of the fuel inside the afterburner. This resulted in more uniform combustion. The latter was revealed by the fact that in the first configuration the flame was annular close to the engine wall, while in the second one it covered the whole inner area of the engine.

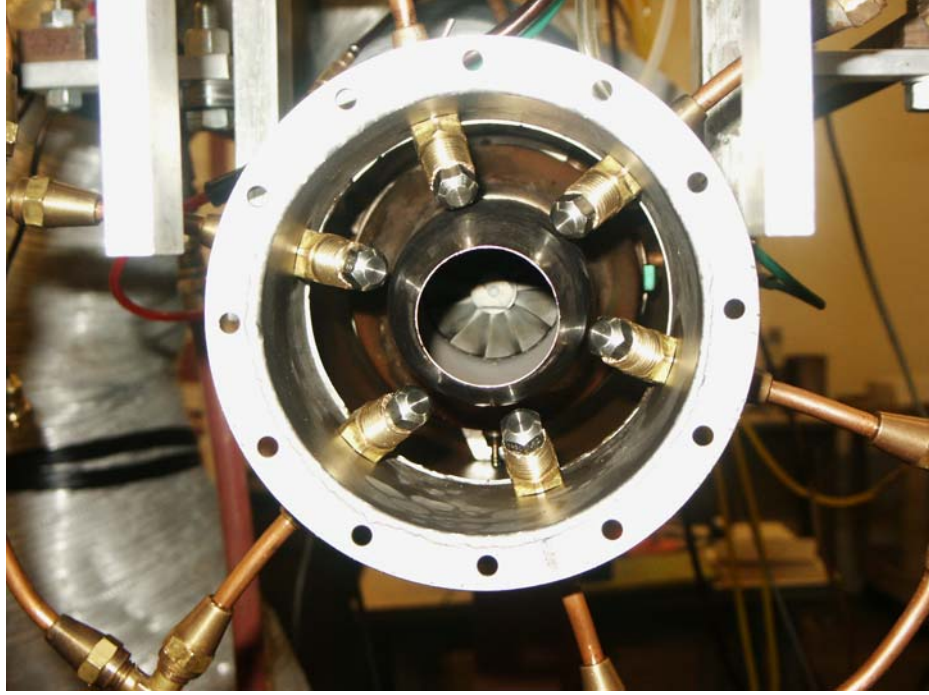


Figure 26. Position of the Injectors Relative to the Turbojet Exhaust Cone (45° Elbow Fittings)

The addition of the long afterburner duct and the 45° elbow fittings for the injectors were beneficial to the operation of the turbo-ramjet engine. The combustion was improved as was indicated by the small flame coming out of the nozzle, proving that most of the fuel was burned inside the afterburner duct. Secondly, the flame was very stable and controllable and little amount of fuel was draining outside the engine.

The turbo-ramjet engine operated up to $M_{\infty} = 0.24$ with the M1s and up to $M_{\infty} = 0.30$ with the M2s. This difference resulted from the higher fuel flow rate provided by the M2 injectors. It has to be noted that in one run with the M2s the afterburner operated up to $M_{\infty} = 0.40$ but this condition was not repeatable.

b. Twelve-Injector Configuration

The final configuration consisted of twelve injectors, half of which sprayed radially and half at 45° with respect to the air flow (Figure 27).

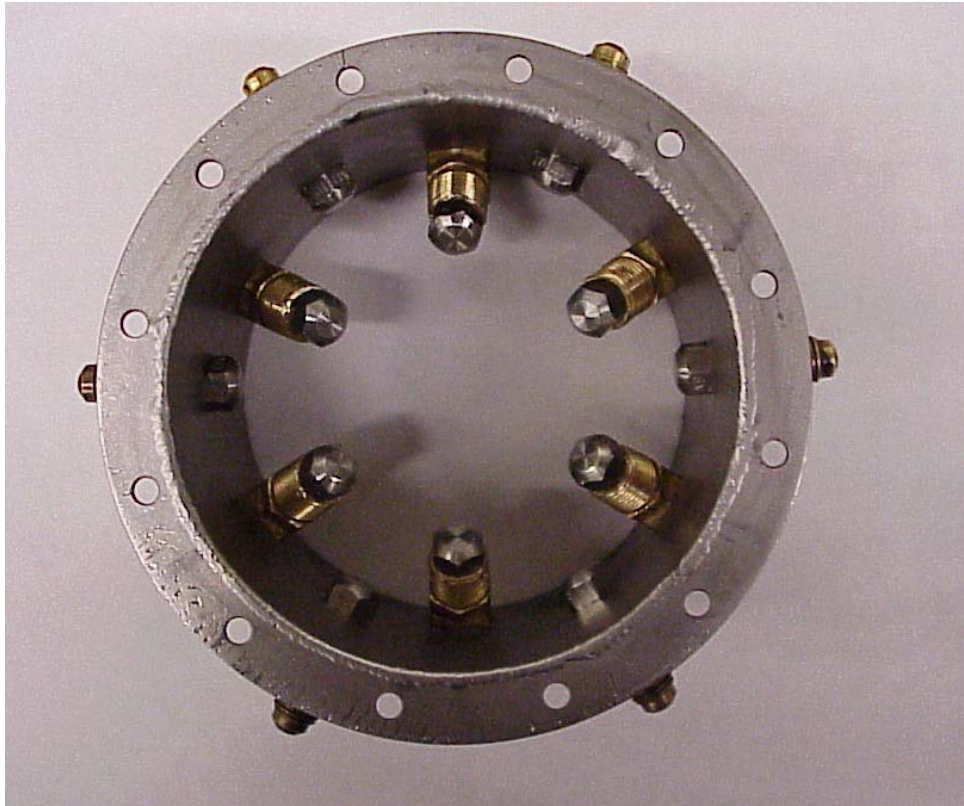


Figure 27. Final Configuration with 12 Injectors

The purpose of this configuration was to increase the fuel flow rate inside the afterburner and to produce a much more uniform air – fuel mixture by adding fuel both to the hot air flow close to the turbojet exhaust and the cold air flow near the skin of the turbo-ramjet engine. Additionally, the fuel sprayed close to turbojet exhaust would be better vaporized and it could perform like a pilot flame, which could facilitate the combustion of the whole mixture. Both M1 and M2 injectors were used.

The manifold for this configuration is shown in Figure 27 and the position of the injectors inside the engine is presented in Figure 29.

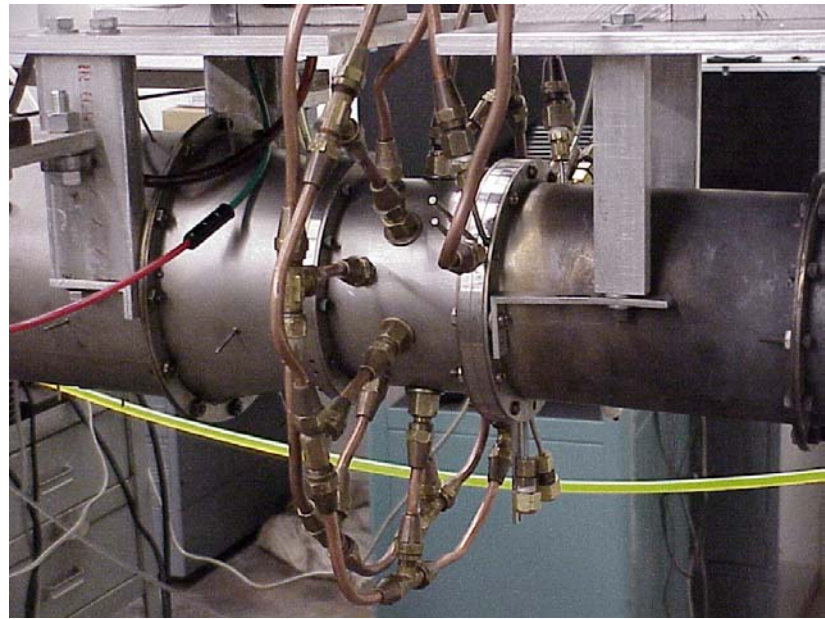


Figure 28. Manifold for the Final Configuration

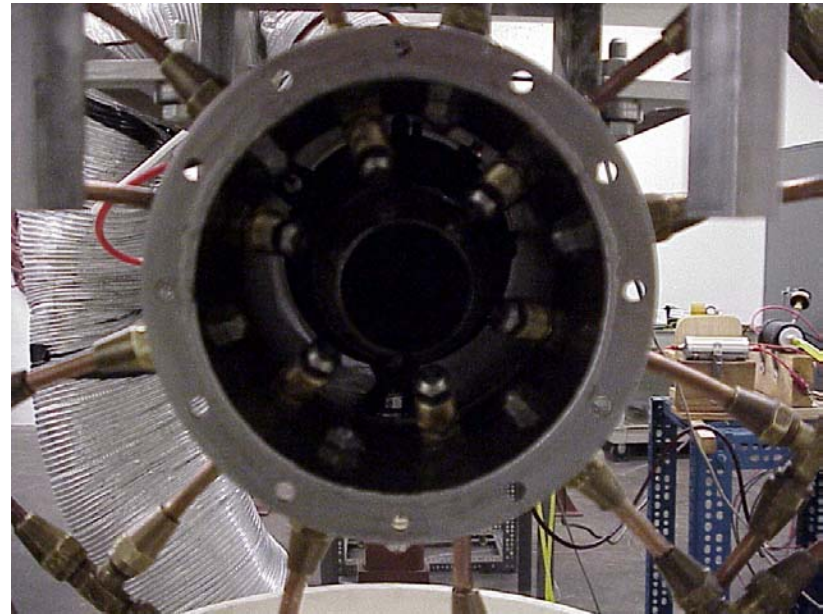


Figure 29. Position of Injectors Inside the Turbo-ramjet Engine

The engine operation for the configuration with the 12 M1 injectors was similar to the one with the 6 M2 injectors (at 45° angle), regarding the produced thrust and the maximum operating Mach number. On the other hand, the stability of the flame was better for the M1 nozzles, due to their finer spray.

The configuration with the M2 injectors produced an unstable flame, which did not permit the engine operation for freestream Mach numbers greater than $M_{\infty} = 0.30$, although the fuel flow rate was doubled.

D. RESULTS

1. Spray Ring Configuration with Fuel Preheating

Figure 30 depicts the measured net thrust versus freestream Mach number for the afterburner configuration consisting of the spray rings with the small duct and fuel preheating. These results are compared to the ones measured by Piper (Ref. 1) (initial configuration with running afterburner) and Garcia (Ref. 6) (shrouded engine without running the afterburner). The values of the measurements are presented in Appendix B.

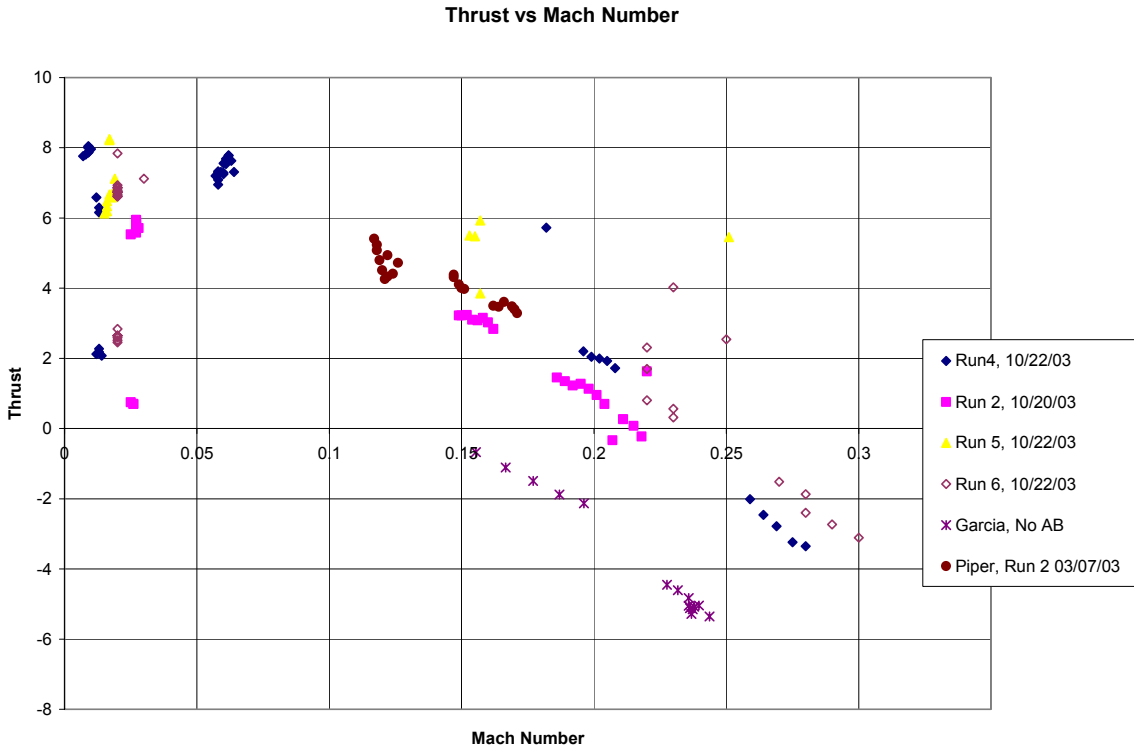


Figure 30. Thrust Measurements (Analytically)

Figure 31 shows a summary of the results. The graph is separated in bins of $M_{\infty} = 0.05$. The blue line gives the mean values and the error bars the standard deviation of the measurements in each bin.

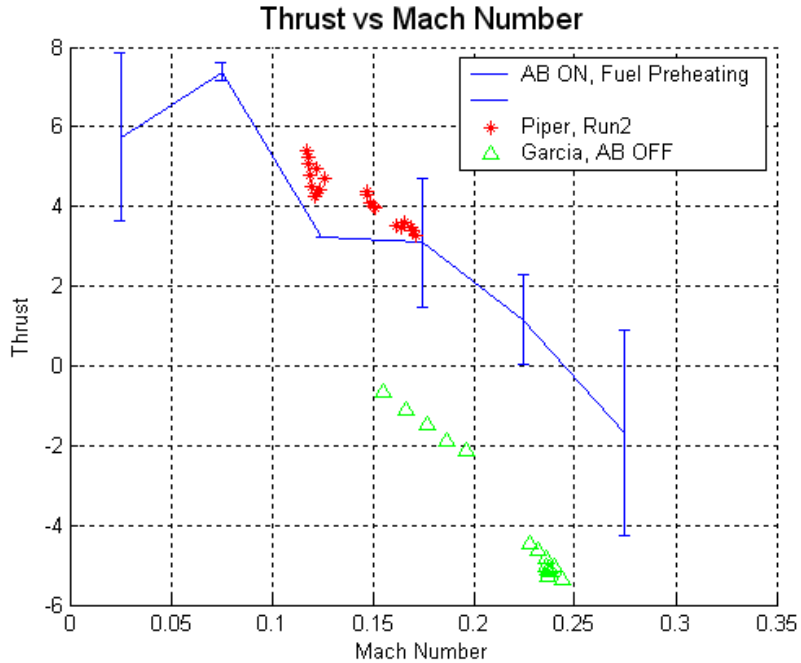


Figure 31. Thrust Measurements (Summary)

The negative values of thrust indicate that the drag produced by the turbo-ramjet engine and the surrounding structure and fuel lines was greater than the net thrust produced by the engine.

An increase of thrust of 4 to 5 lbf on average for Mach numbers greater than 0.15, due to the afterburner is clear, and was mainly due to the more efficient fuel spray inside the afterburner compared to the previous setups.

The measurements obtained for the larger fuel preheating line and the longer afterburner duct were worst than the ones shown in the previous graphs and they are not presented.

2. Fuel Injector Configurations

The thrust versus Mach number for three engine's configurations with the fuel spray nozzles are presented in Figure 32. These configurations are :

- 6 M1 injectors, spraying axially
- 6 M2 injectors, spraying at 45° with respect to the air flow
- 12 M1 injectors (6 radial and 6 at 45°)

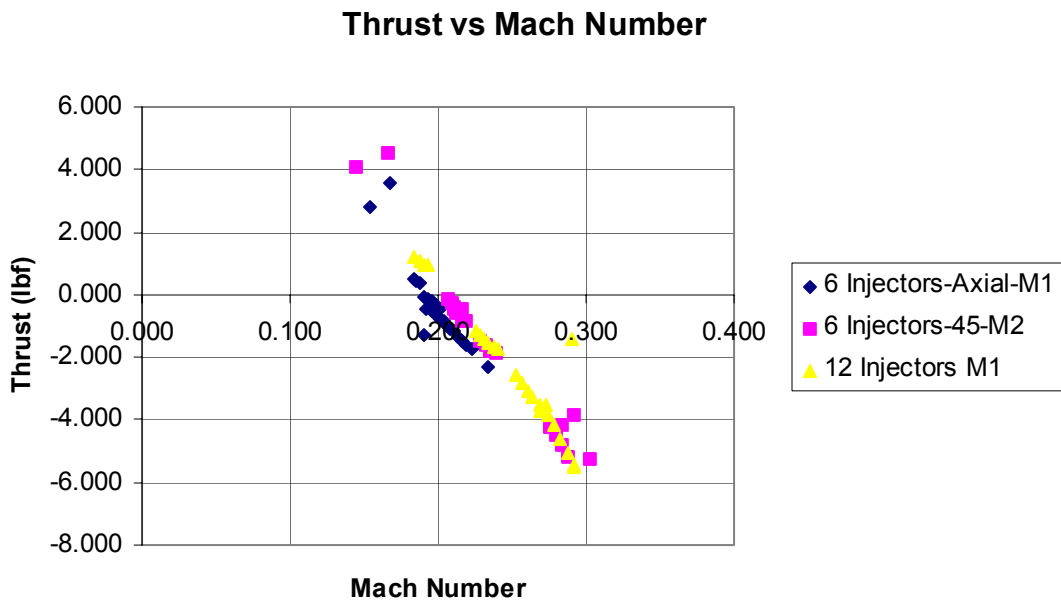


Figure 32. Thrust Measurements for Turbojet Engine operating at 60%

Figure 36 shows that the thrust produced by the 6 M2 and the 12 M1 injectors was slightly increased compared to that of the 6 M1 injectors. The maximum freestream Mach number at which the turbo-ramjet engine operated is also higher. These facts were due to the increased fuel flow rate (2 gals/h compared to 1 gal/h) but mainly to the more uniform air-flow mixture achieved in the first case.

It's also clear that the thrust measurements of the 6 M2 and 12 M1 injector configurations coincide, which was expected, as the fuel flow rate was the same.

The thrust measurements were lower than the ones recorded for the spray ring configuration. The reason for this behavior was that the turbojet engine was operated at 60% in the first case and at 80% in the second.

III. TURBOJET ENGINE PERFORMANCE PREDICTION

A. INTRODUCTION

The performance prediction code GASTURB 9.0 for WINDOWS was used to compute the performance of the turbojet engine at different free stream Mach numbers and air mass flow rates.

The code used the performance characteristics of J450 engine, the GARETT compressor map and the RADTUR turbine map, which gave reasonable results as computed by Garcia (Ref 1).

B. RESULTS

The predicted results of GASTURB 9.0 are presented in Table 1., in the form of the following parameters:

- M_2 : Mach number at the compressor's entrance
- T_2, T_{t2} : Static and stagnation temperature at the compressor's entrance
- P_2, P_{t2} : Static and stagnation pressure at the compressor's entrance
- M_8 : Mach number at the nozzle's exit
- T_{t8} : Stagnation temperature at the nozzle's exit
- P_{t8} : Stagnation pressure at the nozzle's exit
- $Thrust$: Engine's net thrust
- \dot{m}_{air} : Air mass flow rate

M_2	T_2	T_{t2}	P_2	P_{t2}	T_{t8}	P_{t8}	M_8	$Thrust$	\dot{m}_{air}
0.2	522	526.17	15.11	15.54	1802.44	25.70	0.65	8.49	0.27
0.3	528	537.50	15.64	16.65	1763.00	26.54	0.67	8.04	0.28
0.4	535.3	552.42	16.41	18.32	1709.58	27.88	0.7	7.67	0.30
0.5	544.62	571.85	17.43	20.67	1644.61	29.30	0.725	7.38	0.32
0.6	556	596.03	18.74	23.90	1587.05	31.57	0.765	7.19	0.35
0.7	569.42	625.22	20.38	28.27	1537.52	34.70	0.813	7.11	0.38
0.8	584.92	659.79	22.40	34.14	1504.85	39.08	0.87	7.16	0.42
0.9	602.5	700.10	24.85	42.03	1496.30	45.34	0.938	7.43	0.47

Table 1. Predicted Off-Design Values for J450 Turbojet Engine

These results were slightly different from the ones computed by Piper (Ref. 1), who used a previous version of the same code (GASTURB 7.0).

The values of $T_2, P_2, M_2, P_{t8}, T_{t8}, M_8$ were used as inputs in the OVERFLOW code in order to simulate the turbojet engine's operation at various flight conditions, and compute the bypass ratio of the turbo-ramjet engine.

IV. COMPUTATIONAL FLUID DYNAMICS (CFD) ANALYSIS

A. INTRODUCTION

There are basically three approaches or methods, which can be used to solve a problem in fluid mechanics: the experimental, theoretical and numerical (CFD) one.

The experimental approach has the capability of producing the most realistic answers for many flow problems; however the costs are becoming greater every day.

The big advantage of the theoretical approach is that general information can be obtained in many cases from a simple formula. This approach is quite useful in preliminary design work since reasonable answers can be obtained in a minimum amount of time.

In the numerical approach a limited number of assumptions are made and a high-speed digital computer is used to solve the resulting governing fluid dynamic equations.

Comparing the methods, it has to be noted that a computer simulation is free of some of the constraints imposed on the experimental method for obtaining information upon which to base a design. For example, it is very difficult to simulate the large Reynolds numbers of aircraft in flight, atmospheric re-entry conditions or the severe operating conditions of some turbomachines in existing test facilities. On the other hand, computational methods have the limitations of computer storage and speed as well as our inability to understand and mathematically model certain complex phenomena, such as turbulence and combustion.

The Naval Postgraduate School (NPS) currently has a number of numerical applications for solving problems of fluid mechanics. One of them is the NASA supported CFD code OVERFLOW 1.8w, which has been used extensively to model the Space Shuttle aerodynamics.

The code was used to create a model of the engine which would be used to analyze the flow inside and outside the turbo-ramjet engine in an effort to estimate the by-pass ratio, that is the ratio of the air mass flow through the turbojet engine to the total one through the whole turbo-ramjet. This value is needed in order to predict the performance characteristics of the turbo-ramjet using the GASTURB code.

B. SOFTWARE

1. GRIDGEN

GRIDGEN is a software package for the generation of 3D, multiple block, and structured grids. The code may also be used to generate single block structured grids, single surface structured grids, and overset structured grids. The Version 9 of the software system was used during the current research. The code can be used to convert a 3D domain into blocks, distribute grid points on curves, initialize and refine grid points on surfaces, and initialize volume grid points. The code was written using the Silicon Graphics Iris GL graphics library and hence may only be run on Silicon Graphics 4D Series and IBM RS/6000 Series workstations.

2. GRIDED

GRIDED is a grid editing software package. This powerful code can do many manipulations to existing 2D and 3D grids. For the purpose of this thesis, this tool was used to interchange the J and K grid families of the single input grid generated from GRIDGEN, to change the orientation of the axis and to generate two additional planes that were supplied to OVERFLOW to solve the axisymmetric flow field.

3. OVERFLOW

OVERFLOW is a Navier-Stokes flow solver for structured grids. First-order implicit time stepping as well as local time stepping were used to accelerate convergence to a steady-state solution. The code solved the full Navier-Stokes equations and had a number of turbulence models available, which will be later discussed in more detail.

4. FAST

FAST is a software environment for analyzing Computational Fluid Dynamics data. FAST consists of a collection of separate programs (modules) that run simultaneously and allow the user to examine the results of numerical simulations by loading grid and solution data files. Calculations can be performed on the solution for flow visualization, which may be animated and recorded.

C. GRID GENERATION

The grids were created using the GRIDGEN code and edited by the GRIDDED code to be input to the OVERFLOW solver.

The main steps in designing the grids were:

- The construction of the grid outline using connectors (lines)
- The creation of domains among the connectors; in this step each connector was assigned a specific number of points.
- The distribution of the points on the connectors so as the grid to be finer near the walls, for example, and coarser at the freestream boundaries.
- The joining of the domains in a single one and the output of the grid as a PLOT3D, ASCII file.

One thing to be noted is that the assignment of the grid's axis was done automatically by the code and depended on the type of grid.

In order to overcome this problem, the GRIDDED code was used to interchange the J and K grid families (x- and y- axis) and change their orientation. FAST was used to check the correct appearance of the grids.

Several 2D computational grids were considered in modeling the engine, as follows:

- A small grid, in which part of the outer boundary was set as the ramjet shroud. This grid was similar to the one created by Piper (Ref. 1) but it was modified by replacing specific connectors and adding more nodes, for better accuracy.
- Two larger grids, which modeled the flow around the turbo-ramjet and had different radial dimensions.
 - A large grid, similar to the previous ones, in which the flame holders were modeled. This addition made the simulation more accurate and provided the potential of modeling the burning inside the afterburner. The two afterburner's configurations (short and long duct) were also modeled.

An example of the boundaries of a large grid, with the flameholders and the long afterburner duct is shown in Figure 33.

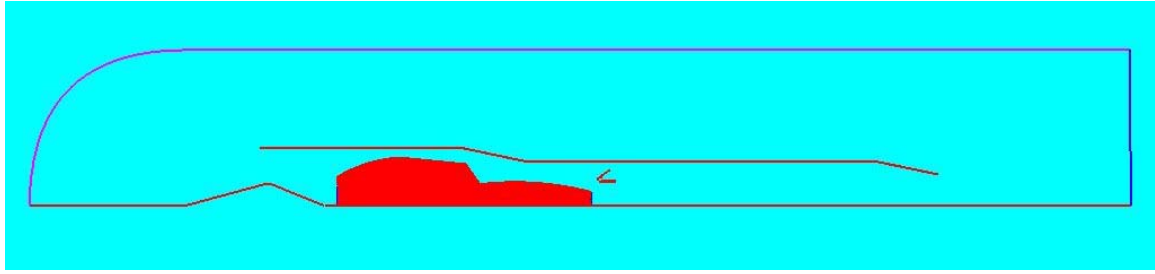


Figure 33. Grid Boundaries

D. TURBULENCE MODELS

1. Introduction

Turbulence modeling is one of the three key elements in Computational Fluid Dynamics, with the others being: grid generation and algorithm development. Little precision has been achieved in creating a mathematical model that approximates the physical behavior of turbulent flows, since turbulence is an extremely complicated phenomenon.

Four major categories of turbulence model exists:

- Algebraic (zero equation) Models
- One-Equation Models
- Two-Equation Models
- Second-Order Closure Models

All the existing models try to solve the “*fundamental problem of turbulence for the engineer*”, that is the computation of the Reynolds-stress tensor (Ref. 10),

$$\tau_{ij} = -\langle \rho u'_i u'_j \rangle \quad (1)$$

where ρ is the density of the fluid

u'_i, u'_j are the fluctuation velocities in all three directions.

This is done by computing the kinetic energy of the turbulent fluctuations (k),

$$k = \frac{1}{2} \langle u'_i u'_j \rangle^2 \quad (2)$$

A useful quantity, related to both k and τ_{ij} , is the eddy viscosity (μ_T). Each model uses different approaches to specify μ_T , k and finally τ_{ij} .

In the simulation of the turbo-ramjet engine, the k- ω two-equation model as well as the Baldwin-Barth and Spalart-Allmaras one-equation models were used and will be discussed briefly.

2. $k - \omega$ Turbulence Model

The k- ω turbulence model was the first one to be used in the simulation effort. This is a two-equation model which specifies the turbulence kinetic energy (k) and the rate of dissipation of turbulence energy (ω), using the following equations (Ref. 10):

Turbulence Kinetic Energy

$$\rho \frac{\partial k}{\partial t} + \rho U_j \frac{\partial k}{\partial x_j} = \tau_{ij} \frac{\partial U}{\partial x_j} - \beta^* \rho k \omega + \frac{\partial}{\partial x_j} \left[(\mu + \sigma^* \mu_T) \frac{\partial k}{\partial x_j} \right]$$

Dissipation of Energy

$$\rho \frac{\partial \omega}{\partial t} + \rho U_j \frac{\partial \omega}{\partial x_j} = a \frac{\omega}{k} \tau_{ij} \frac{\partial U}{\partial x_j} - \beta \rho \omega^2 + \frac{\partial}{\partial x_j} \left[(\mu + \sigma \mu_T) \frac{\partial \omega}{\partial x_j} \right]$$

where $\mu_T = \frac{\rho k}{\omega}$ is the eddy viscosity

U_j, ρ, x_j are the local velocity, density and x-coordinate

$a, \beta, \beta^*, \sigma, \sigma^*$ are constants

μ is the kinematic viscosity of the fluid

3. Baldwin-Barth Turbulence Model

The Baldwin-Barth turbulence model is a one-equation model, which introduces a transport equation for the kinematic eddy viscosity, $\nu_T = \frac{\mu_T}{\rho}$. The following equations are used to compute ν_T (Ref. 10):

Kinematic Eddy Viscosity

$$\nu_T = C_\mu \tilde{R}_T D_1 D_2$$

where \tilde{R}_T is the turbulence Reynolds number

$\nu = \frac{\mu}{\rho}$ is the kinematic molecular viscosity,

C_μ, D_1, D_2 are constants.

Turbulence Reynolds Number

$$\frac{\partial}{\partial t}(\nu \tilde{R}_T) + U_j \frac{\partial}{\partial x_j}(\nu \tilde{R}_T) = (C_{\varepsilon 2} f_2 - C_{\varepsilon 1}) \sqrt{\nu \tilde{R}_T P} + (\nu + \nu_T / \sigma_\varepsilon) \frac{\partial^2(\nu \tilde{R}_T)}{\partial x_k \partial x_k} - \frac{1}{\sigma_\varepsilon} \frac{\partial \nu_T}{\partial x_k} \frac{\partial(\nu \tilde{R}_T)}{\partial x_k}$$

$$\text{where } P = \nu_T \left[\left(\frac{\partial U_i}{\partial x_j} + \frac{\partial U_j}{\partial x_i} \right) \frac{\partial U_i}{\partial x_j} - \frac{2}{3} \frac{\partial U_k}{\partial x_k} \frac{\partial U_k}{\partial x_k} \right] \text{ and}$$

$f_2, C_{\varepsilon 1}, C_{\varepsilon 2}$ are constants.

4. Spalart-Allmaras Turbulence Model

The Spalart-Allmaras is a one-equation model, which is also written in terms of eddy viscosity. Its defining equations are as follows (Ref.10):

Kinematic Eddy Viscosity

$$\nu_T = \tilde{\nu} f_{u1}$$

$$\text{where } f_{u1} = \frac{\chi^3}{\chi^3 + c_{u1}^3}$$

$$\chi = \frac{\tilde{\nu}}{\nu} \text{ and}$$

$\tilde{\nu}$ is given by the following equation

Eddy Viscosity Equation

$$\frac{\partial \tilde{\nu}}{\partial t} + U_j \frac{\partial \tilde{\nu}}{\partial x_j} = c_{b1} \tilde{S} \tilde{\nu} - c_{w1} f_w \left(\frac{\tilde{\nu}}{d} \right)^2 + \frac{1}{\sigma} \frac{\partial}{\partial x_k} \left[(\nu + \tilde{\nu}) \frac{\partial \tilde{\nu}}{\partial x_k} \right] + \frac{c_{b2}}{\sigma} \frac{\partial^2 \tilde{\nu}}{\partial x_k^2}$$

$$\text{where } \tilde{S} = S + \frac{\tilde{\nu}}{\kappa^2 d^2} f_{u2},$$

d is the distance from the closest surface,

$c_{w1}, c_{b1}, c_{b2}, \sigma, f_w, f_{u2}, \kappa$ are constants,

$$S = \sqrt{2\Omega_{ij}\Omega_{ij}} \text{ and}$$

$$\Omega_{ij} = \frac{1}{2} \left(\frac{\partial U_i}{\partial x_j} - \frac{\partial U_j}{\partial x_i} \right) \text{ is the rotation tensor}$$

E. RESULTS

1. Overview

Several simulations were conducted in order to produce a realistic model that could be used to simulate the turbo-ramjet in various conditions and to estimate several properties such as: the velocity inside the afterburner duct and the bypass ratio of the engine.

The model created by Piper (Ref. 1) was further improved by adding the flameholder and expanding the grid around the turbo-ramjet engine.

The behavior of various turbulence models was also investigated and the results are discussed in the following paragraphs.

Finally, the turbojet engine was modeled such that the inlet flow into the compressor was extracted from the computational domain at conditions predicted by GASTURB. Likewise, the turbojet exhaust flow was reintroduced into the computational domain in conditions also predicted by GASTURB. This model was deemed to be more realistic than the model used by Piper (Ref. 1). He modeled the pressure rise through the engine as an actuator disk and the temperature rise by heating the internal walls of the engine. This model did not give realistic exhaust temperature profiles.

2. Ramjet Shroud with Nose Cone and Engine (Small Grid)

The first configuration was the small grid turbo-ramjet engine without flameholders. This model was based on the one created by Piper (Ref. 1) with a small modification of the connectors and the number of nodes.

The engine was modeled using a combination of constant temperature walls and an actuator disk.

The result at $M_\infty = 0.6$ were identical to the ones derived by Piper (Ref. 1) as shown in Figures 34, C1 and C2.

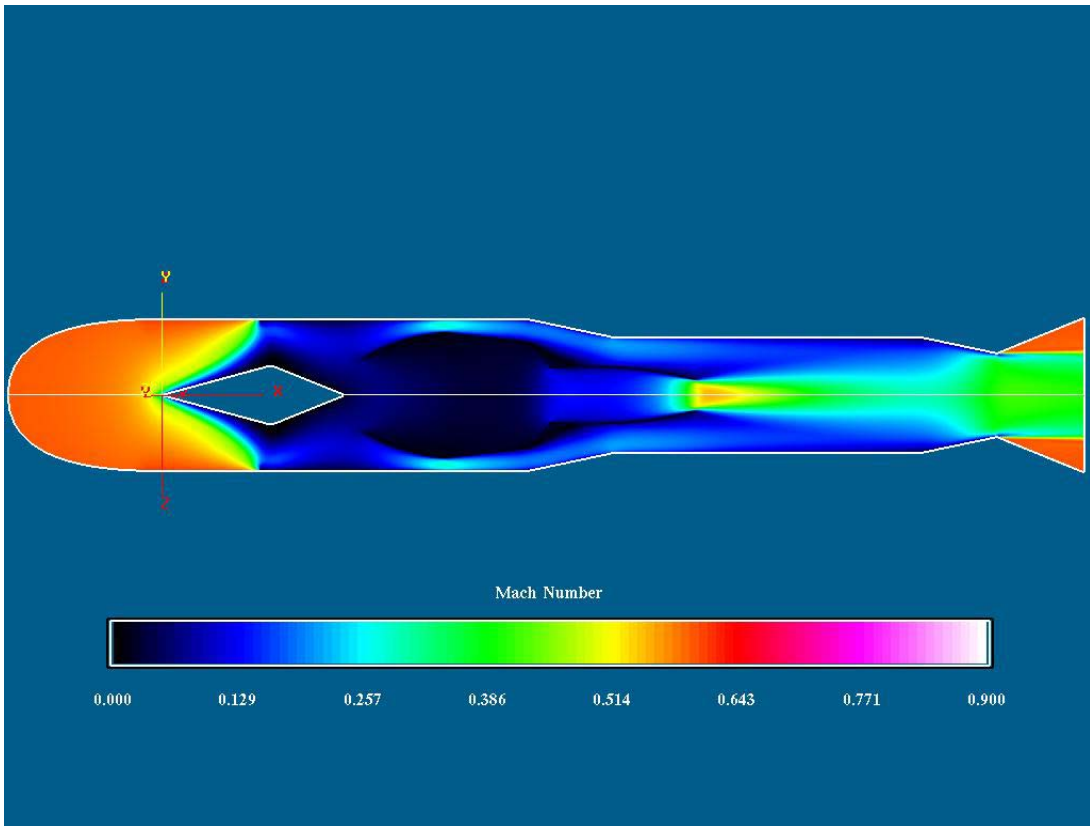


Figure 34. Mach Number Distribution at $M_\infty = 0.6$

Two additional simulations for $M_\infty = 1.5$ were run in order to examine the performance of this grid at supersonic speeds.

The first simulation was run considering a “Subsonic/Supersonic Inflow/Outflow condition” (# 32 in Ref. 9) for the freestream boundaries, which was also used in the subsonic solution. The results are presented in Figures 35, C4 and C5.

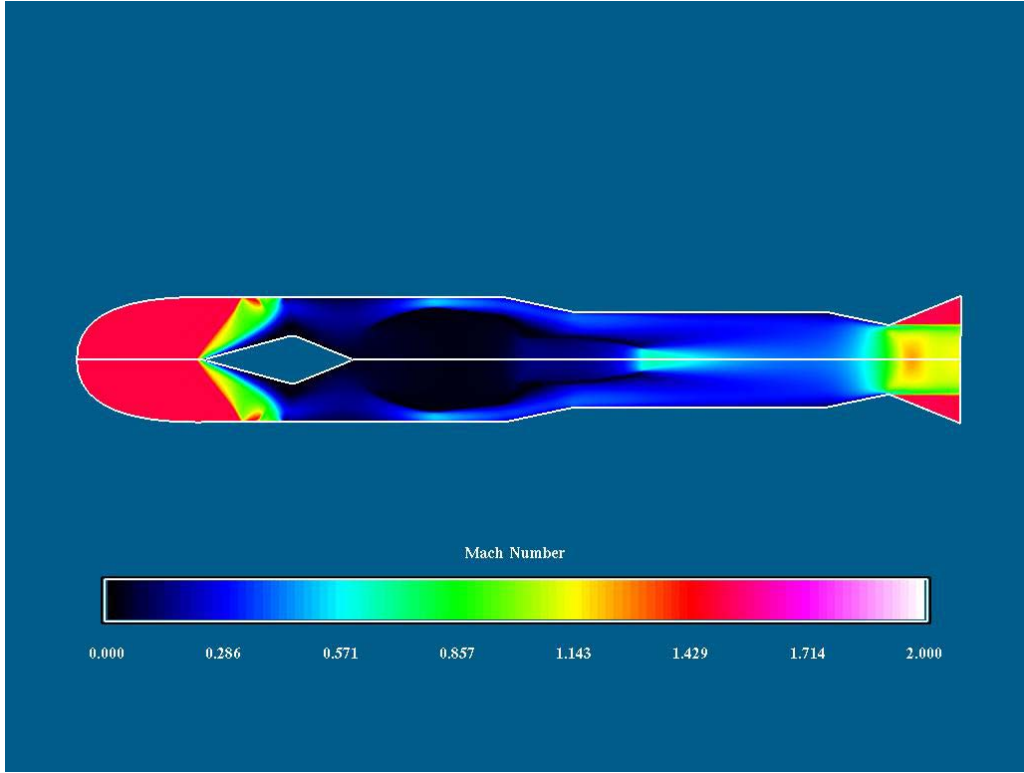


Figure 35. Mach Number Distribution for $M_\infty = 1.5$

Figure 35 shows the creation of an oblique shock wave, due to the presence of the shock cone. The flow inside the afterburner was low subsonic and an area of separated flow was created on the shock cone, which reduced the effective area of the inlet, causing spillage of the air around the engine.

On the boundary just in front of the engine's inlet, a small shock wave was created due to the reflection of the initial one from the grid's boundary. This made the solution grid depended, which was not valid and another solution with different boundary condition for the same grid was considered.

In the second approach, a “Characteristic condition based on Riemann invariants” (# 31 in Ref. 9) was considered instead of using a “Subsonic/Supersonic Inflow/Outflow condition” (# 32) for the inlet and exit freestream boundaries. The result in terms of Mach number distribution is presented in Figure 36.

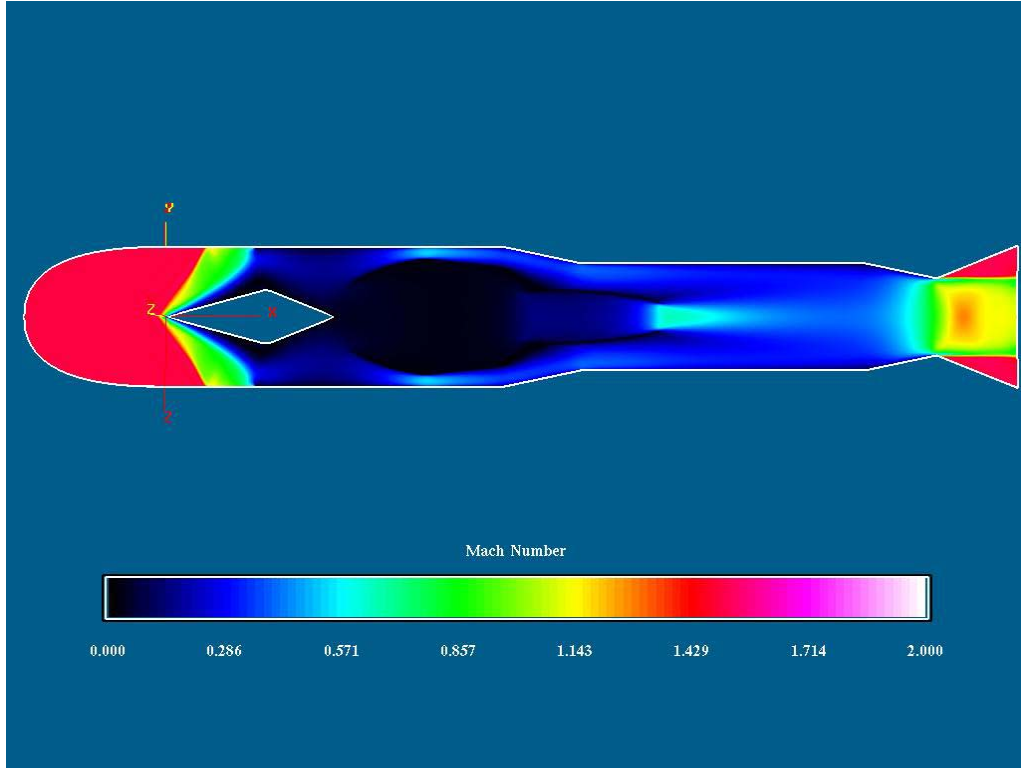


Figure 36. Mach Number Distribution for $M_{\infty} = 1.5$ (New Boundary Condition)

This solution was similar to the previous one, but the reflected shock strength was weaker. More results are presented in Figures C7 and C8.

3. Ramjet Shroud with Shock Cone and Engine (large grid)

In order to overcome the formation of reflected shocks as well as to investigate how the surrounding flow affected the solution, the previous grid was expanded radially. The new grid simulated an area of 8 inches around the turbo-ramjet engine and the previous boundary conditions for the simulation of the turbojet engine were used.

A solution at $M_{\infty} = 0.6$ was initially established, in order to compare the small grid solution to the new one. The results are presented in Figures 37, C10 and C11.

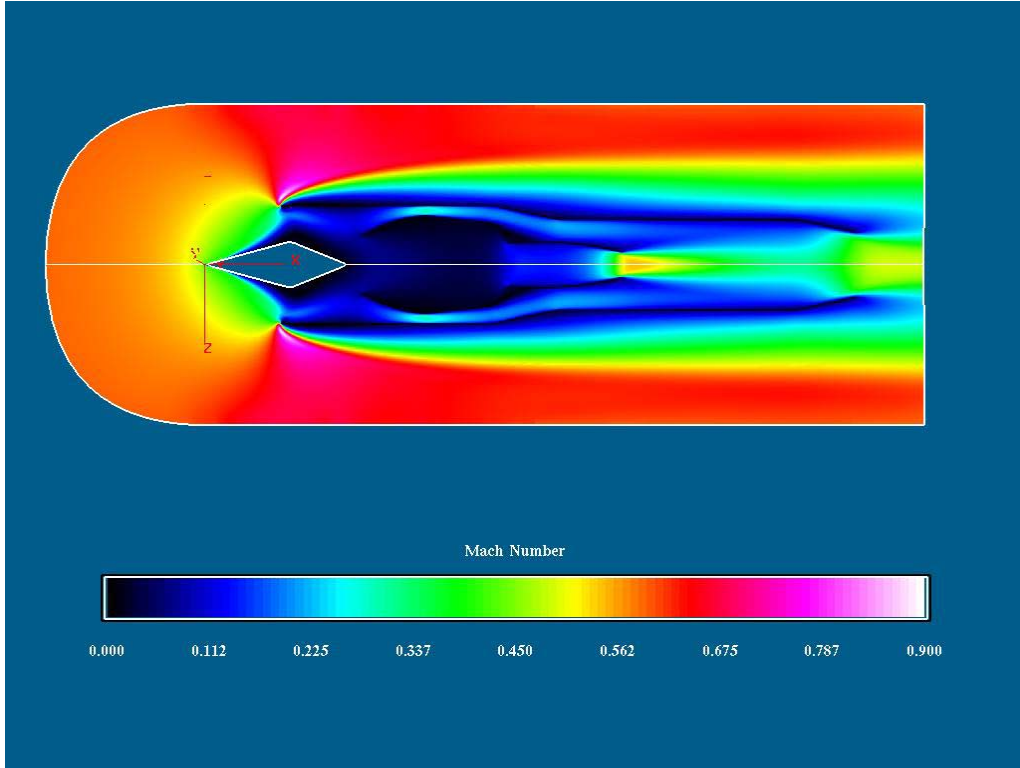


Figure 37. Mach Number Distribution for $M_\infty = 0.6$ (Large Grid)

The results were similar to the ones for the small grid, with the exception of the flow in the area in front of the inlet, where the spillage takes place. In the large-grid simulation and at subsonic speeds, the down stream geometry of the ramjet shroud affected the flow upstream. Hence the flow was adjusted to take account of the downstream conditions giving higher Mach numbers around the intake of the engine.

An additional solution at $M_\infty = 1.5$ was also considered, using initially the “Subsonic/Supersonic Inflow/Outflow condition” (# 32), as shown in Figure 38, C13 and C14.

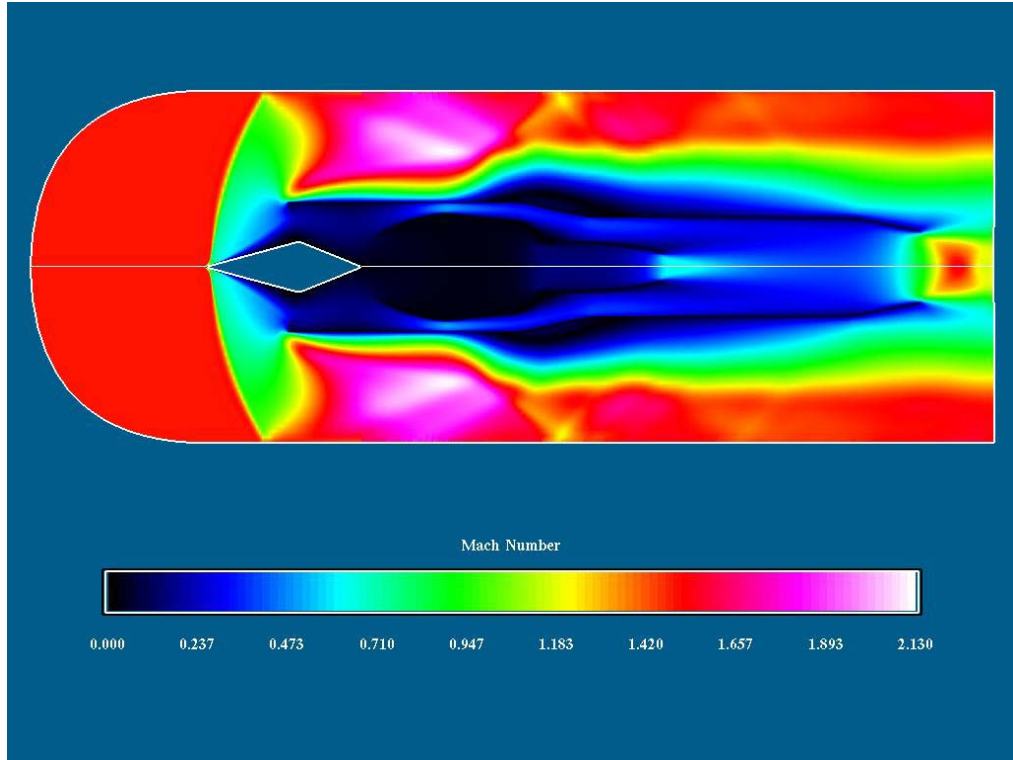


Figure 38. Mach Number Distribution for $M_{\infty} = 1.5$ (Boundary Condition # 32)

Figure 38 shows again the creation of a bow wave, which was normal in front of the intake, due to the fact that the turbojet engine operated at a condition that created a large back pressure, making the oblique shock captured in Figure 36 to move forward and become more normal.

Another observation is that waves were also reflected at the outer boundaries of the grid and propagated downstream inside the flow field. The result was the creation of a big separation bubble on the engine's wall due to the high pressure aft of these waves.

A new solution was then obtained, in which the outer boundary conditions were changed to “Characteristic condition based on Riemann invariants” (# 31). The results are presented in Figure 39.

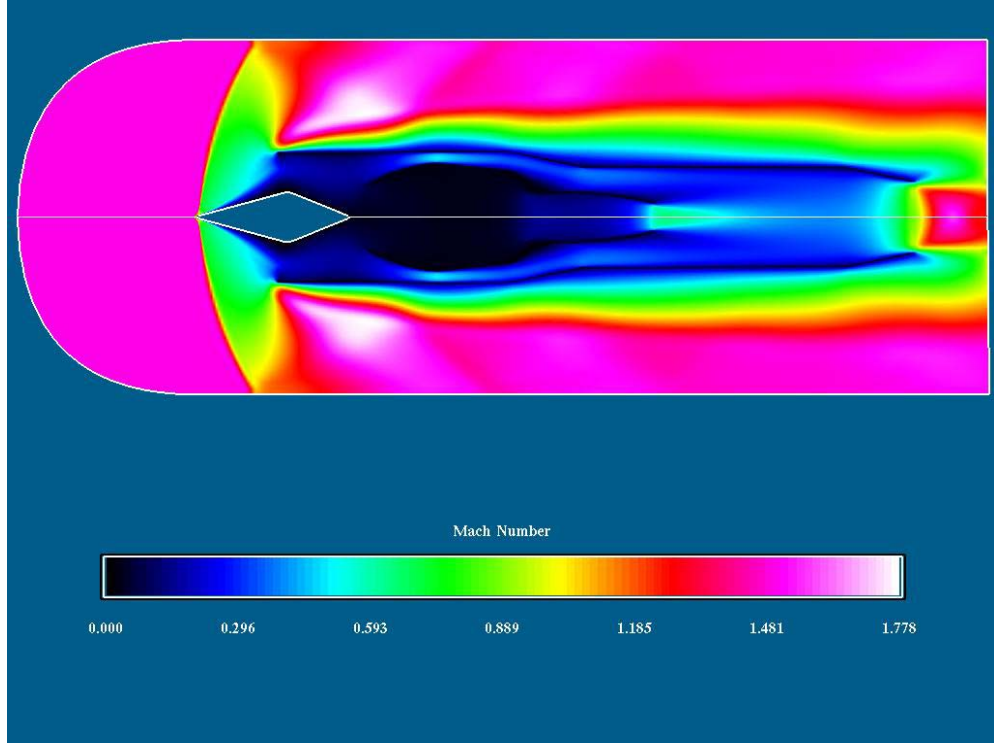


Figure 39. Mach Number Distribution for $M_{\infty} = 1.5$ (Boundary Condition # 31)

The solution of Figure 39 is clean, without the presence of the reflected shocks. Hence, there is no separation bubble on the outer wall of the turbo-ramjet and the maximum Mach number is smaller ($M_{\max} = 1.778$ compared to $M_{\max} = 2.13$ in the previous solution). The pressure and temperature distributions are presented in Figures C16 and C17.

4. Ramjet Shroud with Shock Cone, Engine and Flameholder

The next step in the simulation process was the modeling of the flameholder inside the afterburner duct, in order to investigate the effect of the additional area blockage, due to the presence of the flameholder, to the flow inside and around the turbo-ramjet engine. This blockage was designed to be 30 %, Ref. 1.

The large grid was used in this simulation, and the solutions for $M_{\infty} = 0.6$ and $M_{\infty} = 1.5$ using both types of boundary conditions (# 32 and 31) are presented in Figures 40, 41 and 42 respectively.

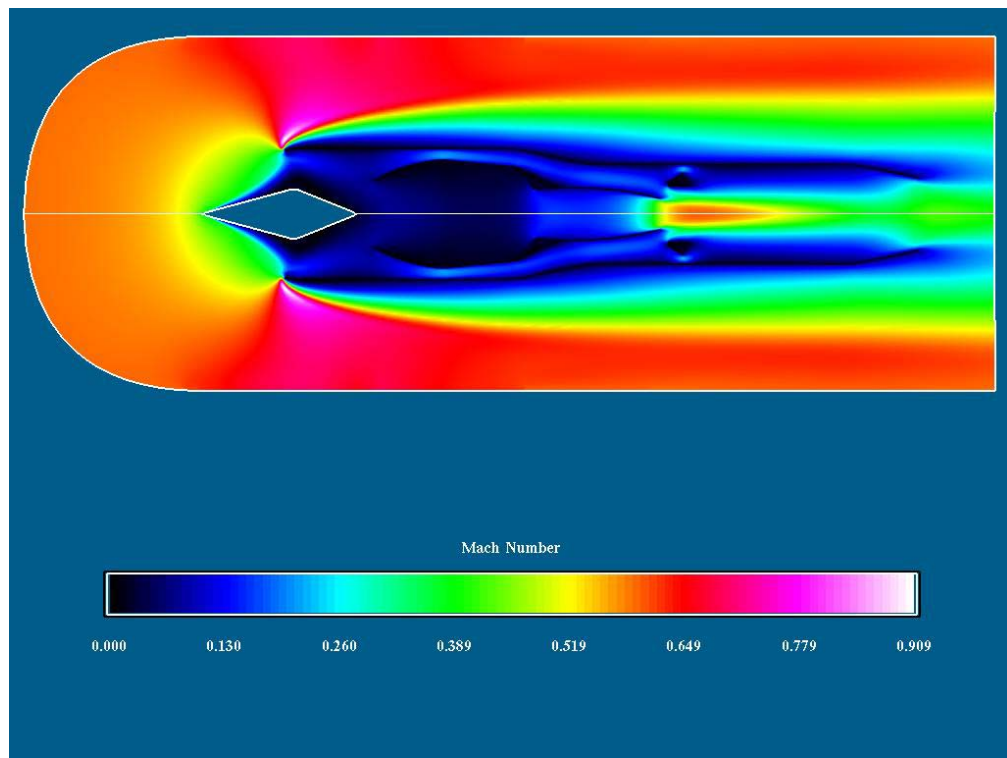


Figure 40. Mach Number Distribution for $M_{\infty} = 0.6$ (with Flameholder)

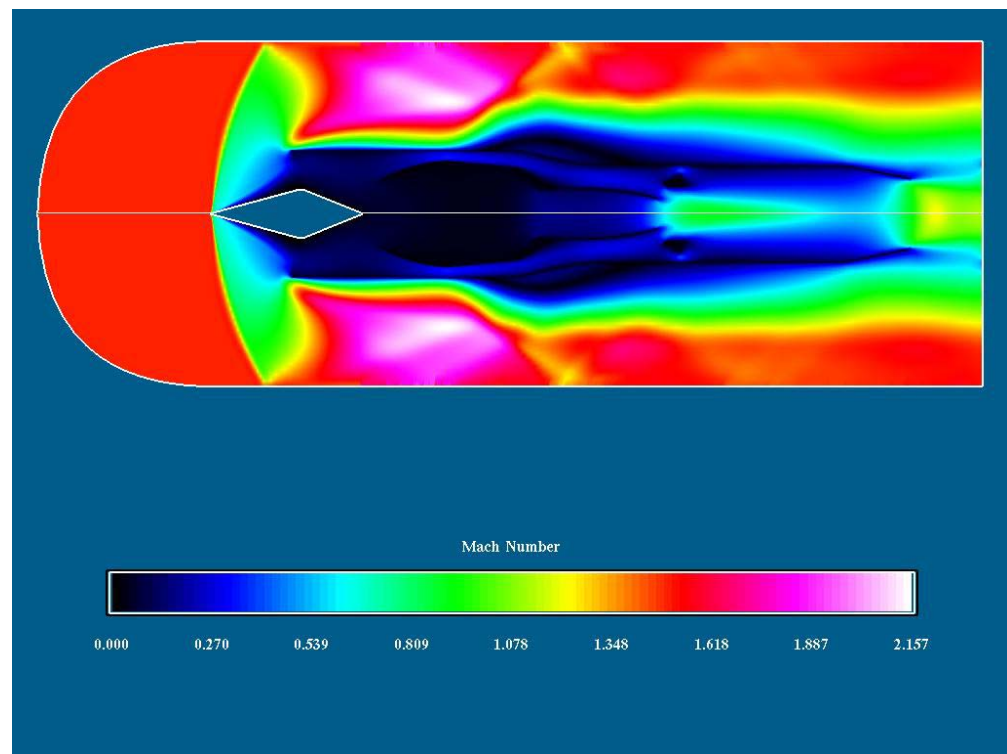


Figure 41. Mach Number Distribution for $M_{\infty} = 1.5$ (with Flameholder, BC #32)

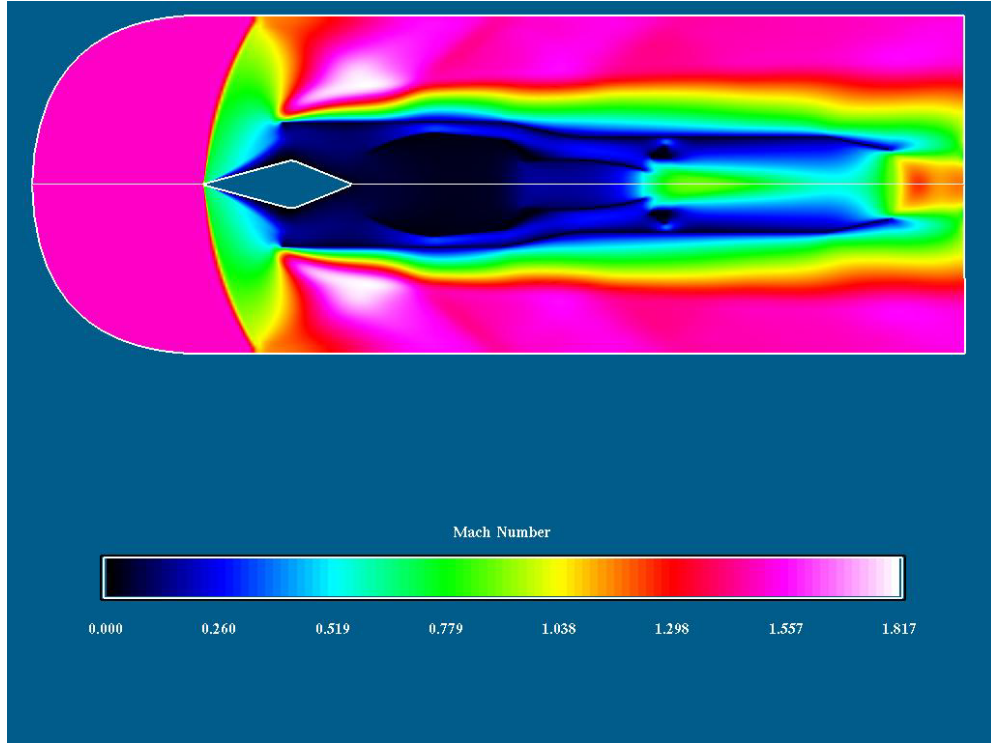


Figure 42. Mach Number Distribution for $M_{\infty} = 1.5$ (with Flameholder, BC #31)

The pressure and temperature distributions are shown in Figures C19, C20, C22, C23, C25 and C26. In Figure C20 (shown here as Figure 43), as well as in Figures C23 and C25, it is clear that the flameholder separated the flow in two regions: a high and a low pressure one. The pressure in the high-pressure region was higher than without the flameholder and in the low pressure region was lower. The results of this effect were:

- the increase of the amount of air that spills out, therefore the reduction of the air mass through the engine
- the induction of drag
- the acceleration of the flow, which produced higher Mach numbers inside the afterburner duct.

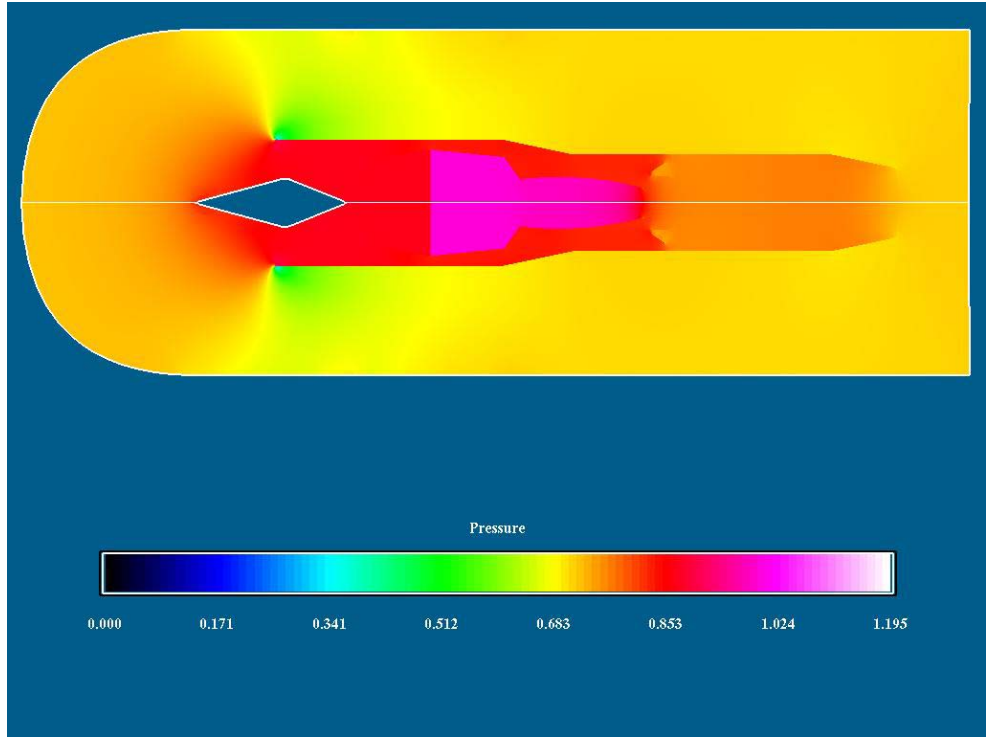


Figure 43. Pressure Distribution for the Turbo-Ramjet Engine at $M_{\infty} = 0.6$ (with Flameholder)

In Figures 44 and 45, the velocity vectors of the flameholder's wake is shown for $M_{\infty} = 0.6$ and $M_{\infty} = 1.5$. The recirculation zone is evident (region of dark blue color aft the flameholder). Two observations can be made:

- the length of the recirculation zone did not change significantly for different Mach numbers of the freestream.
- the recirculation zone was much smaller than what was expected according to Ref. 8 and Ref. 1. The latter computed the wake length to be 3.952 inches. This observation was the most significant one and led to the conclusion that the simulation was not accurate.

To solve the problem, the $k-\omega$, Baldwin-Barth and Spalart-Allmaras turbulence models were investigated.

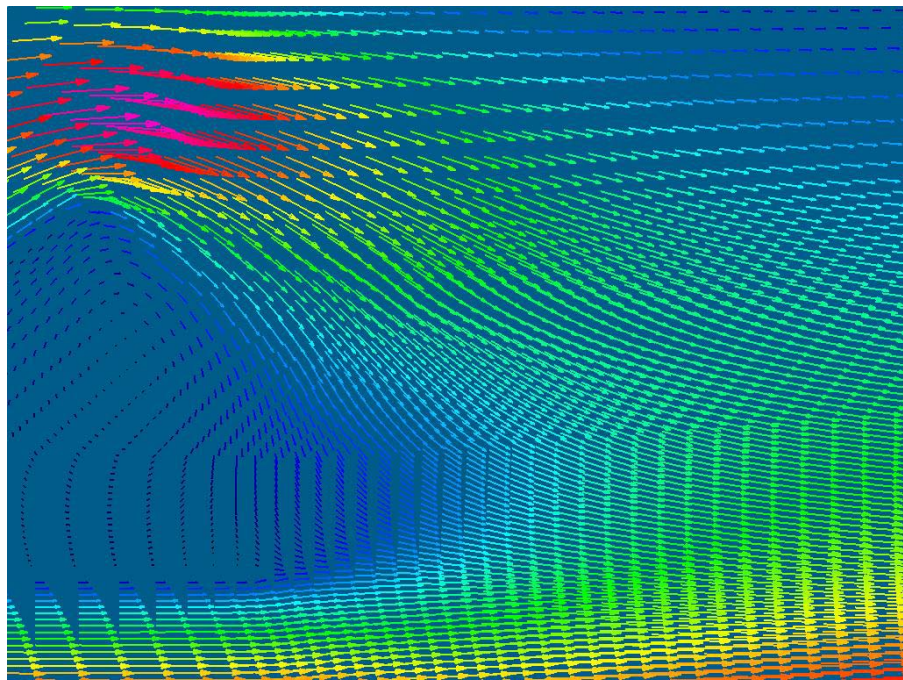


Figure 44. Velocity vectors aft from flameholder for $M_\infty = 0.6$

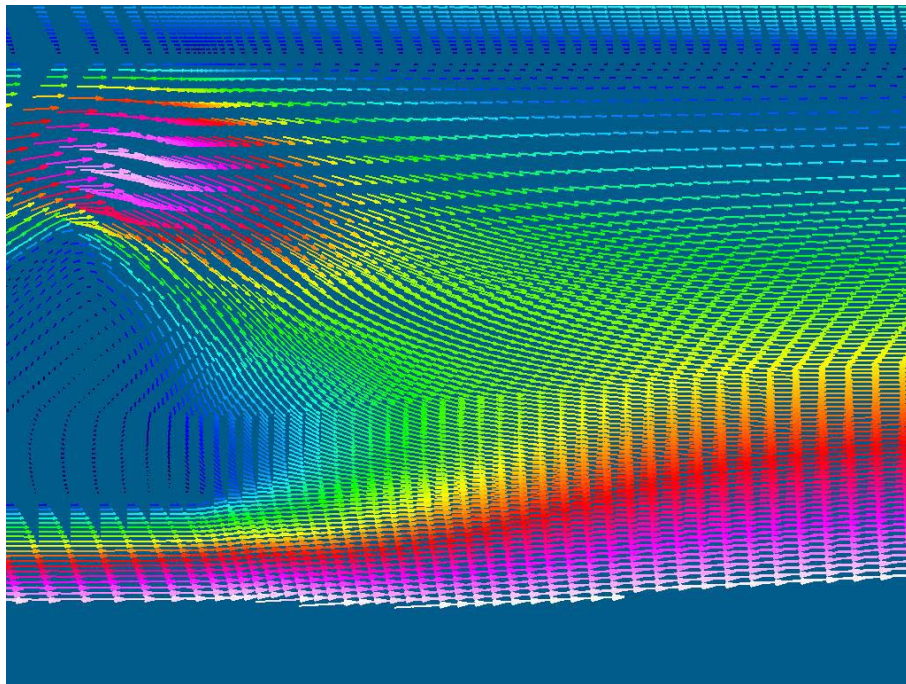


Figure 45. Velocity vectors aft from flameholder for $M_\infty = 1.5$

5. Investigation of Various Turbulence Models

a. *k-ω Turbulence Model*

The first turbulence model used was the $k-\omega$ model, which was considered to give realistic results for various engineering problems.

The implementation of this turbulence model in OVERFLOW used two user-defined parameters, $XKINF$ and $RETINF$, where $XKINF$ was the freestream turbulent kinetic energy and $RETINF$ was the freestream turbulence level, Ref. 9. The values of these parameters were changed from the default ones ($XKINF = 0.0001$ and $RETINF = 0.1$) to $XKINF = 0.00001$ and $RETINF = 0.001$, but the result didn't change significantly, giving a very small wake from the flameholder.

b. *Baldwin-Barth Turbulence Model*

The solution obtained with Baldwin-Barth turbulence model gave an unstable flow but a bigger flameholder wake and the engine's plume reached supersonic Mach number, Figure 46. Since the engine exhaust Mach number was 0.6, the supersonic plume was considered unrealistic and this solution was rejected.

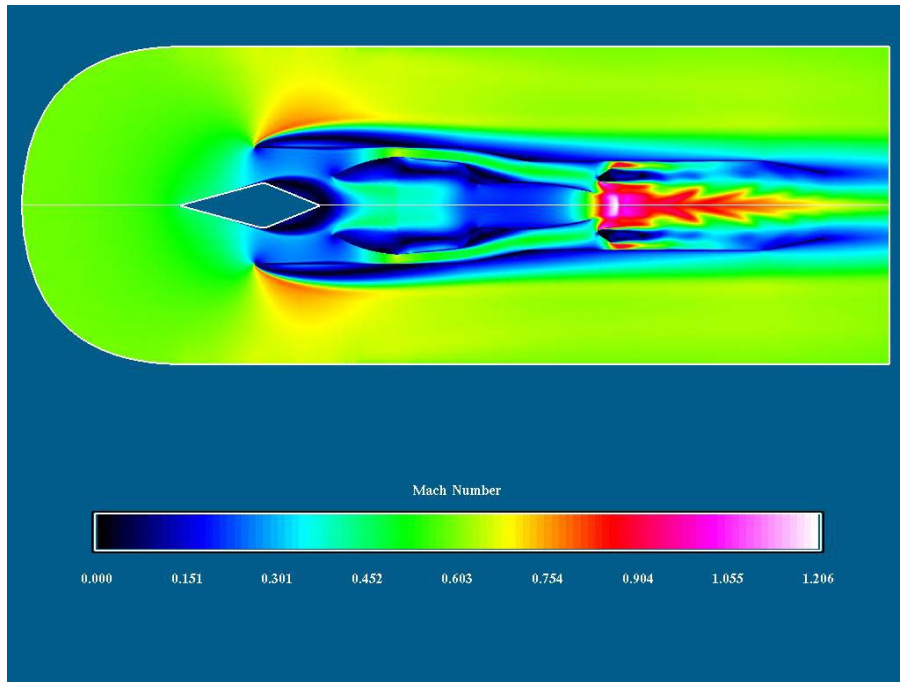


Figure 46. Mach distribution for $M_\infty = 0.6$ with Baldwin-Barth Model

c. Spalart-Allmaras Turbulence Model

The Spalart-Allmaras model gave the best results, regarding both the length of the flameholder wake and the stability of the flow, Figure 47.

A large-grid solution was obtained for $M_{\infty} = 0.6$, which revealed the creation of a separation bubble on the outer side of the turbo-ramjet's lip. This bubble was not created on the solution based on the $k-\omega$ model, Figure 36.

Additionally, a smaller separation bubble on the shock cone could be observed, which moved downstream. This increased the capture area of the engine that is the area through which the engine sucked air and consequently reduced the spillage.

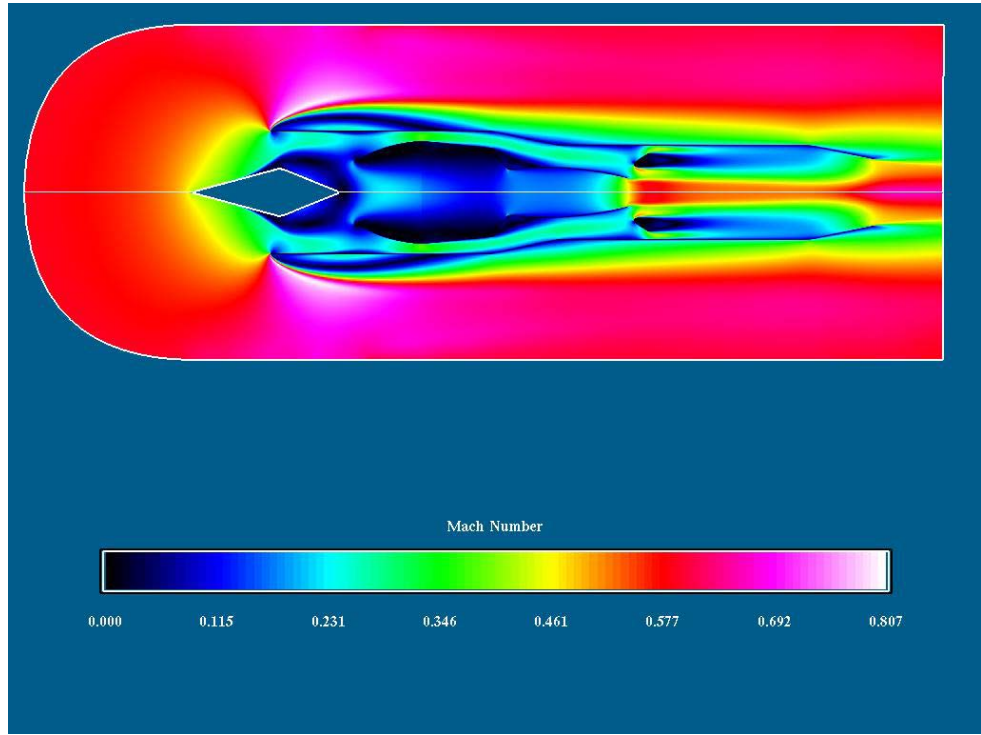


Figure 47. Mach distribution for $M_{\infty} = 0.6$ with Spalart-Allmaras Model

The velocity vectors in the flameholder's wake are shown in Figure 48. A larger recirculation zone was formed, which agreed with the theoretical computations made by Piper (Ref. 1).

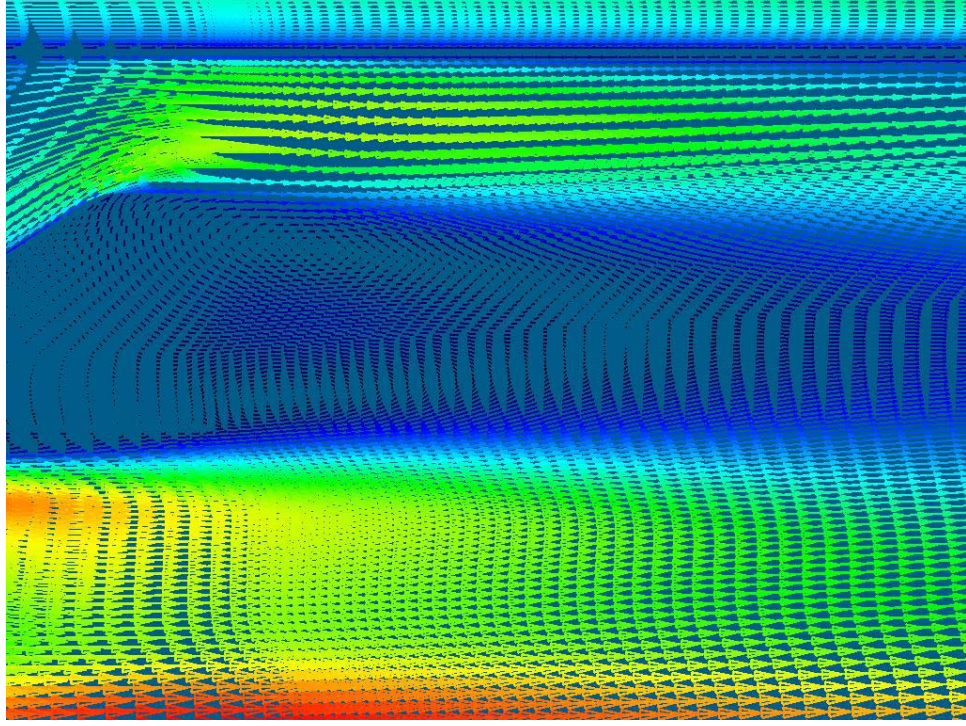


Figure 48. Velocity vectors aft from flameholder for $M_\infty = 0.6$

6. Simulations Using the Engine Model

a. *Creation of the Solution Files (Q files)*

In order to accurately simulate the turbojet engine, two solution files (Q files) were created: the *qinlet.dat* and *qexit.dat* files. These files contained user defined values for the Q-vector of the Navier-Stokes equations, as used by OVERFLOW code, Ref. 9:

$$Q = \begin{bmatrix} \rho \\ \rho u \\ \rho v \\ \rho w \\ e \end{bmatrix}$$

where ρ was the density,

u, v, w were the velocity components in the x-, y- and z-directions,
 e was the fluid's internal energy.

Additional properties were specified, as they were required by the turbulence models. The $k-\omega$ model required the values of $GAMINF$ (freestream ratio of specific heats), $XKINF$ and $RETINF$ as sixth, seventh and eighth rows of the Q file, while the Baldwin-Barth and the Spalart-Allmaras models required the input of the $GAMINF$ and the $RETINF$ only.

Two input files were created in order to specify the desired properties of the flow at the inlet and the exit of the engine: the *qinlet.inp* and the *qexit.inp*. These files contained the local Mach number, total pressure and temperature as well as the freestream Mach number, static pressure and temperature, plus the number of grid points of the solution files in the x-, y- and z-directions.

Finally, two Fortran programs were used to compute the Q-files, consisting of the Q-vector at the grid points designated as *makefileinlet.f* and *makefileexit.f*. These programs used the data contained in the input files to compute the solution variables as follows:

$$\begin{aligned}
 P &= P_0 \left(1 + \frac{\gamma-1}{2} M^2 \right)^{\frac{\gamma-1}{\gamma}} \\
 T &= T_0 \left(1 + \frac{\gamma}{\gamma-1} M^2 \right)^{-1} \\
 a &= \sqrt{\gamma RT} \\
 a_\infty &= \sqrt{\gamma RT_\infty} \\
 \rho &= \gamma \frac{P}{a^2} \\
 \rho_\infty &= \gamma \frac{P_\infty}{a_\infty^2} \\
 u &= Ma \\
 u_\infty &= M_\infty a_\infty \\
 v &= 0 \\
 w &= 0 \\
 e &= \frac{P}{\rho(\gamma-1)} + \frac{1}{2} (u^2 + v^2 + w^2)
 \end{aligned}$$

where $P, T, \rho, a, M, u, v, w$ were the local static pressure, static temperature, density, speed of sound, Mach number and velocity components in all directions

P_0, T_0 were the local stagnation pressure and temperature
 $P_\infty, T_\infty, \rho_\infty, \gamma, a_\infty, M_\infty$ were the freestream static pressure, static temperature, density, ratio of specific heats ($\gamma = \frac{C_p}{C_v}$), speed of sound and Mach number.

The results were saved in the *qinlet.dat* and *qexit.dat* files. The listing of each program and input files are presented in Appendix D.

b. Results

The Q-files were defined at the inlet and exit planes of the turbojet engine using the “Prescribed Q with slow-start (read from file)” boundary condition (#43 in the OVERFLOW code manual). This boundary condition required the designation of the iteration number at which the Q-file would be used by OVERFLOW and the name of the Q-file.

Two grids were tried and two turbulence models (k- ω and Spalart-Allmaras models) for the simulation of the turbo-ramjet engine. The difference between the two grids was that the first one did not have any grid points inside the turbojet, Figure 49, while the second one had a full grid but it was blanked out using the “Blank-out Region” boundary condition (#61 in Ref. 9), Figure 50.

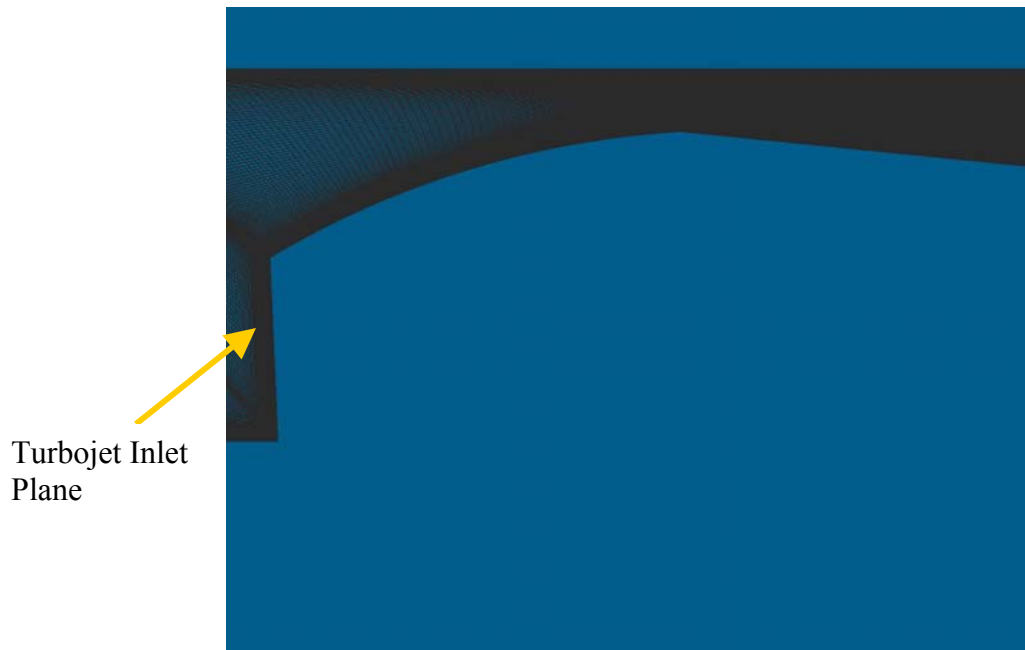


Figure 49. Detail of first grid without any grid points inside the turbojet engine

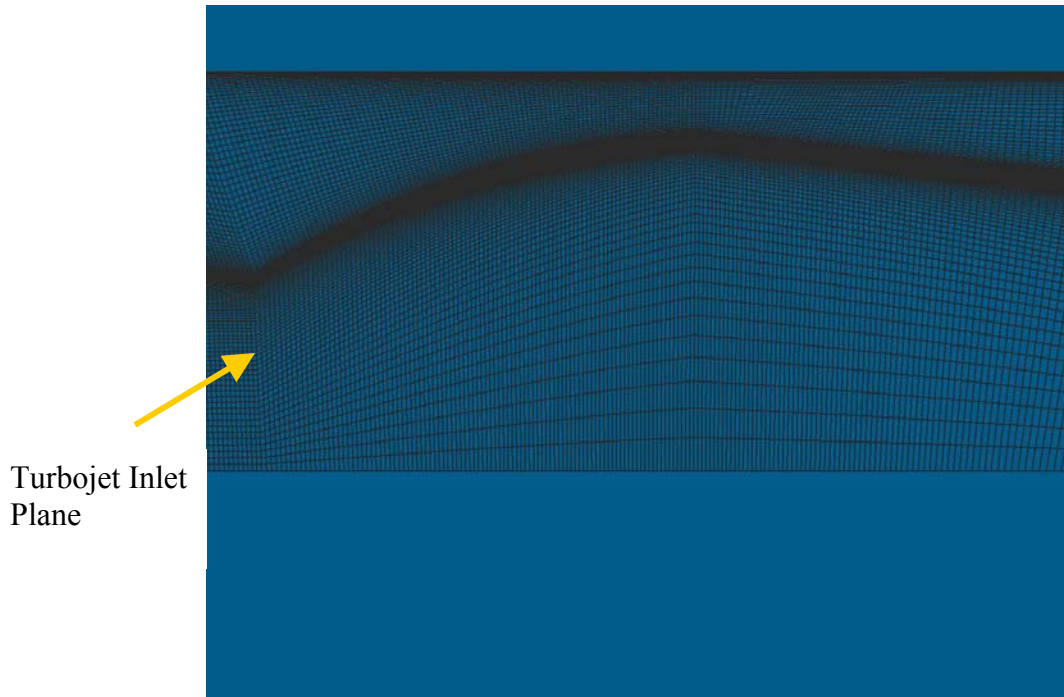


Figure 50. Detail of the second grid with grid points inside the turbojet engine

The $k-\omega$ model did not give reasonable results in either grid. It returned negative pressures and densities at the lips of the inlet and exhaust of the turbojet engine. When the values of the parameters DT (time increment) and $CFLMIN$ (minimum value for $CFL = \frac{dt}{c \cdot dx}$, where dt is the time step, dx is the space step and c is the local speed of sound) were reduced to 0.00001 and 0.0001 respectively, the problem was fixed but the convergence was too slow and the simulation was interrupted.

The Spalart-Allmaras model was able to converge only with the second grid (blanked out region). With the first grid, the convergence was again very slow, although higher values for DT and $CFLMIN$ were accepted. The result for $M_\infty = 0.6$ and the engine simulated for operation at $M_{inlet} = 0.2$ is presented in Figure 51. It has to be noted that specific attention was paid in order to satisfy that the mass flow rate at the inlet of the engine be equal to the mass flow rate at the exit, thus justifying the continuity through the engine.

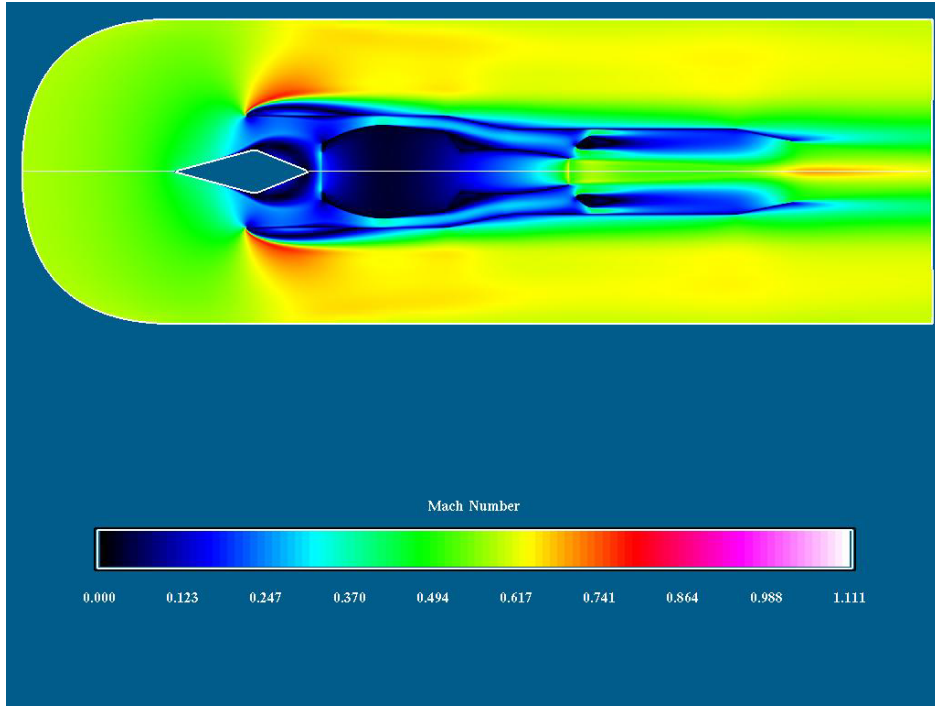


Figure 51. Mach distribution for $M_{\infty} = 0.6$ with Spalart-Allmaras Model and Engine Modeling with Q-files

An additional solution for a long afterburner duct, which was the case of the last configuration of the turbo-ramjet engine, was also obtained as presented in Figure 52. The solution is similar to the previous one, but the Mach number inside the duct is smaller, contributing to the better combustion evidenced during the runs.

The bypass ratio of the engine, that is the ratio of the mass flow rate bypassing the turbojet to the mass flow rate passing through the turbojet, was estimated to be 1.66 for the short duct configuration. This is an initial estimate, because the actual conditions at the inlet and exit of the turbojet were unknown at this point. Actual measurements and further investigation are required in order to come to a more accurate prediction.

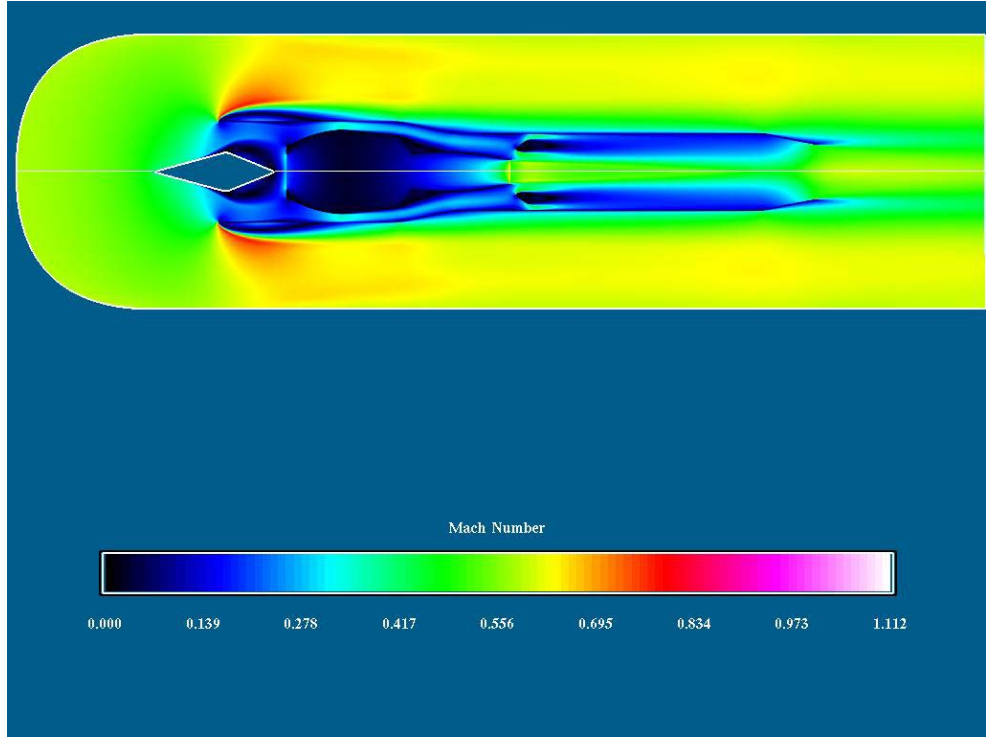


Figure 52. Mach distribution for $M_{\infty} = 0.6$ with Spalart-Allmaras Model and Long Afterburner Duct

7. Limiting Factors of the Models

The main limiting factors of the simulations were the following:

- OVERFLOW could not be used to solve combustion problems. All the solutions obtained were valid only for “cold” operation of the ramjet. They provided a good idea of the flow inside the afterburner, such as the form and size of the flameholder’s wake, the chocking areas, the bypass ratio and the spillage. They could not provide accurate results for the flow velocity in the combustion area which depends on the temperature of the plume.
- The implementation of the $k-\omega$ model in OVERFLOW was questioned, as it could not give a valid solution. This model gives generally good results for many engineering problems but it could not accurately predict the size of the flameholder’s wake. Additionally, it could not give a converged solution for the modeling of the turbojet engine with Q-files, as regions of very high Mach number at the inlet and engine lips of the turbojet were formed.

THIS PAGE INTENTIONALY LEFT BLANK

V. CONCLUSIONS AND RECOMMENDATIONS

The turbo-ramjet's fuel system was upgraded by using a new more powerful pump, which was able to provide the fuel flow rate required for the operation at freestream Mach numbers close to 0.3.

Various configurations of the fuel spray set up were also investigated. The existing spray rings were redesigned with smaller diameter injector ports resulting in a finer spray. The replacement of the flexible fuel lines by rigid ones gave the opportunity to design and construct a fuel preheating system that improved the vaporization of the fuel and minimized the draining of unburned fuel, thus increasing the combustion's efficiency. This design reached its limits when the vast preheating resulted in instability of the fuel flow and consequently of the combustion.

A second design consisting of fuel injectors were also tried, in an effort to create a fine and controlled atomized fuel. The results were very encouraging especially for the configuration with the twelve M1 injectors, which created a smooth, stable and controllable combustion. Although the drainage of unburned fuel was reduced, compared to the initial designs, it remained a significant amount and revealed the poor atomization of the fuel.

The afterburner duct was elongated by 6 inches, which was beneficial to the stability of the flame and the restriction of the combustion inside the afterburner.

The maximum operating Mach number of 0.3 was easily achieved, but it could not be exceeded. The main reasons for this are:

- The design of the flameholders, which create a mixing zone of higher velocity than the one required for the combustion.
- The poor vaporization of the fuel, which liquefies when it contacts the cold afterburner skin.
- The inability of the fuel pump to provide the required fuel flow rate for operation at higher Mach number.

In order to improve the performance of the engine, further testing is needed. This can incorporate the combination of the fuel preheating and fuel injectors. In this case the higher pressure in the fuel lines may prohibit the vaporization of the fuel inside the lines,

thus avoiding the instability occurred in the spray ring configuration. The modification of the flameholders can also be considered in order to reduce the flow velocity in the afterburner. The use of a wider afterburner duct will also contribute in this direction and is a potential solution. Finally, the redesign of the engine's nozzle can increase the thrust by correctly expanding the flow throughout the range of operating freestream Mach numbers.

The computational tools investigated in this research can be used to predict the turbo-ramjet engine's performance at different Mach numbers. The ability to combine a CFD solver, like OVERFLOW, and a gas turbine prediction program, like GASTURB, was demonstrated and both programs can be used to predict the turbojet/ramjet bypass ration, which will assist in the design, development and testing process.

The inability of OVERFLOW to model combustion problems was a limiting factor of the created models. Thus, other solvers, like FASTRAN or ACE, may be used and compared to the solutions given by OVERFLOW in order to create a more complete and accurate model.

APPENDIX A. SOPHIA J450 ENGINE AND FUEL PUMP SPECIFICATIONS

SOPHIA J450 ENGINE SPECIFICATIONS

Length/Diameter:	13.19/4.72 in
Total weight:	4 lbf
Fuel:	Coleman/Kerosene
Starting System:	Compressed Air
Ignition System:	Spark Plug
Lubrication:	6V pulsed oil pump
Fuel Feed System:	12V turbine fuel pump
Compressor:	Single stage centrifugal
Thrust :	11 lbf at 123000 RPM
Fuel consumption:	19.98 lbm/hr
Throttle system:	Manual control

Table A1. Sophia J450 Engine Specifications

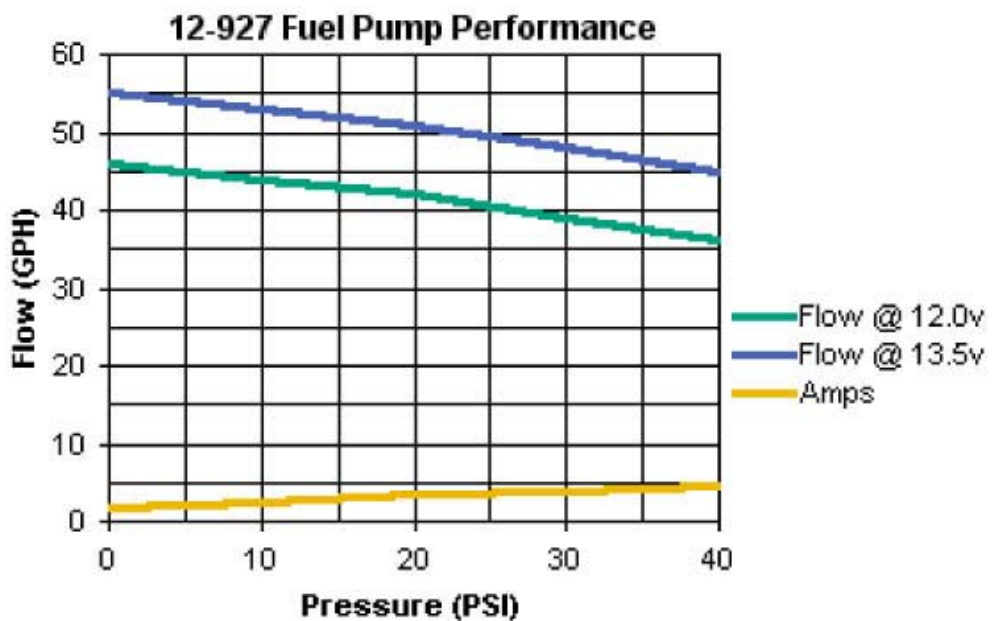


Figure A1. Fuel Pump Characteristics

THIS PAGE INTENTIONALLY LEFT BLANK

APPENDIX B. INSTRUMENTATION CALIBRATION RESULTS AND THRUST MEASUREMENTS

ΔP	M								
0.10	0.10	0.65	0.25	1.20	0.34	1.75	0.40	2.30	0.46
0.15	0.12	0.70	0.26	1.25	0.34	1.80	0.41	2.35	0.47
0.20	0.14	0.75	0.27	1.30	0.35	1.85	0.42	2.40	0.47
0.25	0.16	0.80	0.28	1.35	0.36	1.90	0.42	2.45	0.48
0.30	0.17	0.85	0.29	1.40	0.36	1.95	0.43	2.50	0.48
0.35	0.18	0.90	0.29	1.45	0.37	2.00	0.43	2.55	0.48
0.40	0.20	0.95	0.30	1.50	0.38	2.05	0.44	2.60	0.49
0.45	0.21	1.00	0.31	1.55	0.38	2.10	0.44	2.65	0.49
0.50	0.22	1.05	0.32	1.60	0.39	2.15	0.45	2.70	0.50
0.55	0.23	1.10	0.32	1.65	0.39	2.20	0.45	2.75	0.50
0.60	0.24	1.15	0.33	1.70	0.40	2.25	0.46	2.80	0.51

Table B1. Plume's Static Differential Pressure and Corresponding Mach Numbers

THRUST BEAM CALIBRATION

WEIGHT	VOLTAGE (mV)	VOLTAGE (V)
-31.3	0.112	0.000112
-26.3	0.166	0.000166
-21.3	0.215	0.000215
-16.3	0.263	0.000263
-11.3	0.313	0.000313
-6.3	0.358	0.000358
-1.3	0.396	0.000396
0	0.415	0.000415
1.3	0.43	0.00043
6.3	0.472	0.000472
11.3	0.522	0.000522
16.3	0.563	0.000563
21.3	0.613	0.000613
26.3	0.665	0.000665
31.3	0.711	0.000711

Table B2. Thrust Beam Calibration Values

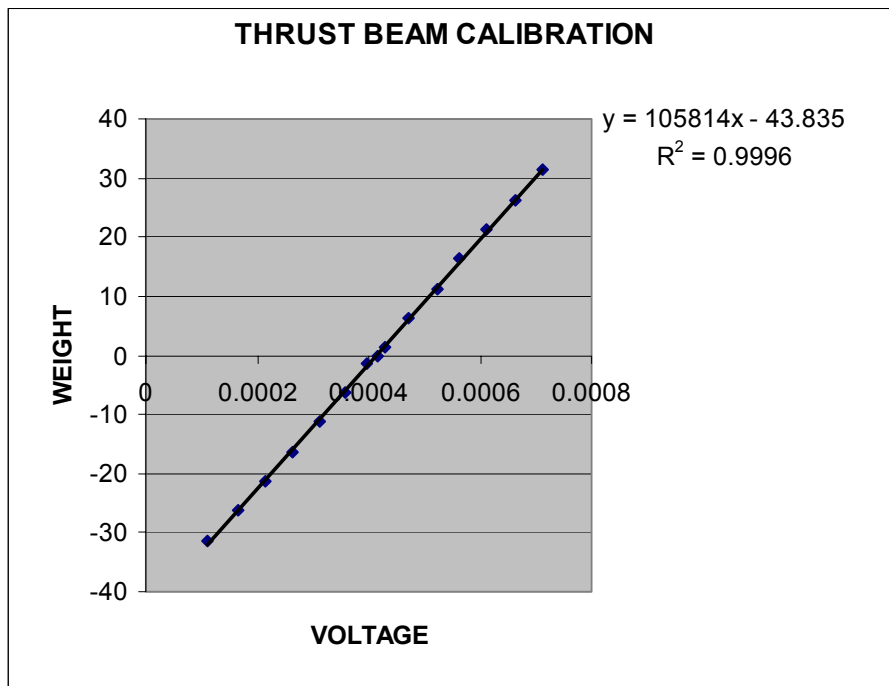


Figure B1. Thrust Beam Calibration

**THRUST MEASUREMEANTS FOR SMALL AFTERBURNER DUCT
CONFIGURATION WITH FUEL PREHEATING**

THRUST (lbf)	STATIC PRESSURE (psi)	STAGNATION PRESSURE (psi)	FREESTREAM MACH NUMBER
5.584832973	0.00769775	0.01407925	0.027
5.671751643	0.00768875	0.014064	0.027
5.71109832	0.00779225	0.01407625	0.028
5.744862568	0.0076765	0.0138145	0.027
5.776712072	0.007707	0.013839	0.027
5.861311472	0.0076125	0.0138055	0.027
5.940031794	0.007391	0.0138695	0.027
5.939357587	0.00749425	0.01395425	0.027
5.829165318	0.0075095	0.01385725	0.027
5.844564189	0.00723275	0.01407625	0.027
5.921936098	0.00720225	0.0138785	0.027
5.792758181	0.007412	0.26740575	0.027
2.837523409	0.27171675	0.26571525	0.162
3.025114556	0.26352325	0.258218	0.16
3.151056283	0.25654275	0.252019	0.158
3.081181548	0.25065125	0.245519	0.156
3.099546926	0.24438475	0.2402625	0.154
3.236977128	0.23851125	0.23459525	0.152
3.220931019	0.2333825	0.2296825	0.15
3.222198527	0.228132	0.22497925	0.149
0.699237835	0.42965	0.41794225	0.204
0.955382273	0.41682325	0.404179	0.201
1.128869025	0.40368025	0.39331325	0.198
1.270910798	0.39181725	0.38095175	0.195
1.224013012	0.3801705	0.3693165	0.192
1.348606326	0.36995225	0.3599405	0.189
1.454510644	0.35854825	0.3497895	0.186
1.627350159	0.50410175	0.4936345	0.22
-0.22593495	0.4928045	0.4777035	0.218
0.076460037	0.47690725	0.4617545	0.215
0.266990724	0.4608455	0.4452795	0.211
0.332837093	0.44343425	0.01396975	0.207
5.529440188	0.00646675	0.0128085	0.025
0.75139443	0.0064605	0.01394275	0.025
0.700882898	0.0067435	0.0131185	0.026
0.69761974	0.006734	0.01402725	0.026

Table B3. Run 2, 20 Oct. 2003

THRUST (lbf)	STATIC PRESSURE (psi)	STAGNATION PRESSURE (psi)	FREESTREAM MACH NUMBER
7.867678	0.000842	-0.0051745	0.009
7.810509	0.00072025	-0.0052655	0.008
8.03286	0.000763	-0.00511375	0.009
7.960611	0.00096975	-0.00512575	0.01
7.99516	0.000836	-0.004986	0.009
8.041949	0.00074175	-0.0051075	0.009
8.006806	0.00083	-0.00479125	0.009
7.875192	0.00074175	-0.004977	0.009
7.76403	0.00049875	-0.0051925	0.007
7.31029	0.041493	0.034008	0.064
7.628078	0.0407355	0.0330835	0.063
7.775365	0.0397935	0.03248475	0.062
7.783215	0.0388295	0.03154525	0.062
7.684912	0.038079	0.03121075	0.061
7.540801	0.03774775	0.03097375	0.061
7.559934	0.0372095	0.03046625	0.06
7.287024	0.03683225	0.03023475	0.06
7.255651	0.03633675	0.03010125	0.06
7.305255	0.0358685	0.02937125	0.059
7.297431	0.03524525	0.029165	0.059
7.331334	0.03492625	0.02842275	0.058
7.261306	0.03482875	0.02942625	0.058
7.28798	0.0343755	0.02828025	0.058
7.201012	0.03385275	0.02745625	0.057
7.090469	0.03417825	0.027885	0.058
6.948553	0.03399575	0.02713425	0.058
5.724215	0.34205225	0.4327025	0.182
1.723005	0.4472225	0.42186675	0.208
1.928392	0.434125	0.40949925	0.205
1.993075	0.421554	0.3968365	0.202
2.043634	0.410314	0.386451	0.199
2.194975	0.3987185	0.56724425	0.196
-3.35525	0.822136	0.778281	0.28
-3.23968	0.7878215	0.7481555	0.275
-2.78372	0.756498	0.7160205	0.269
-2.45619	0.72724175	0.689023	0.264
-2.0119	0.69994675	0.66299	0.259
6.289401	0.0016965	-0.0016205	0.013
6.583666	0.001584	-0.00091525	0.012
6.160396	0.00182125	-0.00130425	0.013
2.273499	0.00171475	-0.0012005	0.013
2.177391	0.0017635	-0.0010155	0.013
2.073122	0.00198225	-0.00089075	0.014
2.119937	0.00136225	-0.0013225	0.012

Table B4. Run 4, 22 Oct. 2003

THRUST (lbf)	STATIC PRESSURE (psi)	STAGNATION PRESSURE (psi)	FREESTREAM MACH NUMBER
6.127395	0.00224675	-0.0027695	0.015
6.192415	0.0025265	-0.00266025	0.016
6.334951	0.00256625	-0.0023895	0.016
6.481928	0.00266325	-0.0022955	0.016
6.665598	0.00292775	-0.002271	0.017
6.689793	0.0031465	-0.00176325	0.018
6.714014	0.003624	-0.0008575	0.019
7.118434	0.00351775	-0.00122225	0.019
6.58741	0.003493	-0.00124025	0.018
5.930814	0.25539025	0.24406275	0.157
3.847051	0.25382775	0.23728275	0.157
5.479579	0.24706025	0.2314245	0.155
5.501554	0.2415395	0.22512225	0.153
5.456366	0.655146	0.6275255	0.251
8.21999	0.002952	-0.00103375	0.017
8.247309	0.00300075	-0.0013135	0.017

Table B5. Run 5, 22 Oct. 2003

THRUST (lbf)	STATIC PRESSURE (psi)	STAGNATION PRESSURE (psi)	FREESTREAM MACH NUMBER
6.61034	0.00479125	0.00062625	0.020
6.6697	0.004694	0.000614	0.020
6.72938	0.004685	0.00041975	0.020
6.75732	0.00436875	0.00029825	0.020
6.78998	0.00444775	0.000304	0.020
6.86879	0.0046635	0.00041675	0.020
6.93254	0.0047155	0.000298	0.020
6.8534	0.00466075	0.00031	0.020
6.72372	0.00478525	0.00037675	0.020
6.62322	0.0050525	0.03216575	0.020
4.02819	0.56292375	0.54732475	0.230
0.31621	0.56048875	0.52918975	0.230
0.56118	0.54139625	0.5110975	0.230
0.80267	0.52405775	0.4949265	0.220
1.70137	0.50729425	0.48025125	0.220
2.3096	0.491643	0.464582	0.220
2.54636	0.66259475	0.89015175	0.250
-3.10778	0.9176325	0.86929925	0.300
-2.73538	0.878888	0.83270075	0.290
-2.39967	0.84354225	0.79956575	0.280
-1.87306	0.8095255	0.76792	0.280
-1.51855	0.77669425	0.88533025	0.270
7.11936	0.00660925	0.00332	0.030
7.83597	0.005983	0.00348725	0.020
2.83339	0.0061655	0.003408	0.020
2.64624	0.00586125	0.00345975	0.020
2.64874	0.0062385	0.00324975	0.020
2.58974	0.00592875	0.0031955	0.020
2.45781	0.005816	0.0029855	0.020
2.51498	0.00575225	0.00270275	0.020

Table B6. Run 6, 22 Oct. 2003

THRUST (lbf)	STATIC PRESSURE (psi)	STAGNATION PRESSURE (psi)	FREESTREAM MACH NUMBER
2.835	0.246	0.327	0.154
3.587	0.292	0.420	0.168
0.490	0.349	0.450	0.183
0.437	0.358	0.348	0.186
0.364	0.368	0.357	0.188
-1.291	0.375	0.365	0.190
-0.052	0.377	0.367	0.190
-0.477	0.384	0.373	0.192
-0.108	0.387	0.376	0.193
-0.463	0.393	0.381	0.194
-0.169	0.397	0.386	0.195
-0.535	0.401	0.389	0.196
-0.311	0.408	0.396	0.198
-0.660	0.412	0.399	0.199
-0.782	0.421	0.408	0.201
-0.447	0.422	0.408	0.201
-0.867	0.431	0.418	0.203
-0.966	0.441	0.428	0.206
-1.077	0.451	0.439	0.208
-1.184	0.464	0.449	0.211
-1.322	0.476	0.461	0.213
-1.473	0.489	0.473	0.216
-1.590	0.502	0.485	0.219
-1.740	0.517	0.500	0.223
-2.335	0.572	0.280	0.234

Table B7. Thrust Measurements for Configuration with Six M1 Injectors Spraying Axially

THRUST (lbf)	STATIC PRESSURE (psi)	STAGNATION PRESSURE (psi)	FREESTREAM MACH NUMBER
-5.232	0.969	1.123	0.303
-5.162	0.872	0.839	0.288
-4.774	0.844	0.812	0.283
-4.469	0.820	0.788	0.279
-4.233	0.795	0.766	0.275
-4.140	0.848	0.968	0.284
-3.864	0.897	0.865	0.292
-1.880	0.600	0.579	0.240
-1.829	0.580	0.559	0.236
-1.616	0.564	0.543	0.232
-1.449	0.546	0.528	0.229
-0.865	0.486	0.468	0.216
-0.846	0.499	0.481	0.219
-0.615	0.472	0.455	0.213
-0.528	0.477	0.458	0.214
-0.473	0.490	0.472	0.217
-0.435	0.462	0.705	0.210
-0.419	0.465	0.448	0.211
-0.269	0.455	0.438	0.209
-0.150	0.445	0.449	0.207
4.086	0.215	0.540	0.144
4.512	0.289	0.404	0.167

Table B8. Thrust Measurements for Configuration with Six M2 Injectors Spraying at 45° Relative to the Flow

THRUST (lbf)	STATIC PRESSURE (psi)	STAGNATION PRESSURE (psi)	FREESTREAM MACH NUMBER
-5.509	0.900	0.872	0.292
-5.468	0.900	0.872	0.292
-5.046	0.869	0.842	0.287
-4.584	0.841	0.814	0.283
-4.187	0.813	0.789	0.278
-3.876	0.788	0.763	0.274
-3.739	0.763	0.739	0.270
-3.527	0.780	0.754	0.272
-3.524	0.756	0.729	0.268
-3.264	0.732	0.709	0.264
-3.052	0.710	0.688	0.260
-2.816	0.688	0.668	0.256
-2.540	0.670	0.861	0.253
-1.755	0.607	0.586	0.241
-1.686	0.589	0.570	0.237
-1.556	0.573	0.553	0.234
-1.432	0.559	0.540	0.231
-1.414	0.892	0.926	0.291
-1.285	0.545	0.526	0.228
-1.134	0.531	0.513	0.225
0.930	0.387	0.373	0.193
0.932	0.377	0.364	0.190
1.074	0.367	0.355	0.188
1.203	0.352	0.385	0.184

Table B9. Thrust Measurements for Configuration with Twelve M2 Injectors

THRUST MEASUREMENTS DONE BY PIPER (Ref 1)

P total	P1	P2	FF	Thrust	Mach
0.0000	0.0715	0.0532	NA	5.08	0.000
0.0000	0.0743	0.0551	0.00313	5.33	0.000
0.0000	0.0763	0.0565	0.00339	5.44	0.000
0.0000	0.0777	0.0580	0.00319	5.53	0.000
0.0000	0.0777	0.0586	0.00281	5.65	0.000
0.0000	0.0774	0.0521	0.00342	5.65	0.000
0.0000	0.0556	0.0405	0.00290	5.82	0.000
0.0000	0.0447	0.0311	0.00486	5.82	0.000
0.0000	0.0285	0.0166	0.00489	5.87	0.000
0.0000	0.0186	0.0119	0.00538	5.72	0.000
0.0000	0.0165	0.0083	0.00525	5.60	0.000
0.0000	0.0117	0.0055	0.00467	5.39	0.000
0.0000	0.0088	0.0056	0.00508	5.33	0.000
0.0000	0.0098	0.0048	0.00502	5.17	0.000
0.0000	0.0123	0.0068	0.00503	5.29	0.000
0.0000	0.0107	0.0072	0.00512	5.37	0.000
0.0000	0.0131	0.0064	0.00469	5.41	0.000
0.1533	0.0124	0.0243	0.00459	4.94	0.122
0.1521	0.0591	0.0683	0.00556	4.26	0.121
0.2786	0.1713	0.1721	0.00505	3.47	0.164
0.2720	0.1702	0.1708	0.00463	3.50	0.162
0.2365	0.1486	0.1464	0.00518	3.98	0.151
0.2344	0.1549	0.1485	0.00507	4.00	0.150
0.2301	0.1527	0.1558	0.00493	4.11	0.149
0.2245	0.1488	0.1483	0.00509	4.31	0.147
0.2228	0.1433	0.1433	0.00492	4.38	0.147
0.3054	0.1275	0.1331	0.00416	3.29	0.171
0.3017	0.1226	0.1310	NA	3.40	0.170
0.2959	0.1098	0.1216	0.00494	3.48	0.169
0.2869	0.1008	0.1232	0.00498	3.61	0.166
0.1636	0.0964	0.0916	0.00632	4.72	0.126
0.1601	0.0898	0.0900	0.00521	4.41	0.124
0.1554	0.0888	0.0886	0.00482	4.33	0.122
0.1501	0.0845	0.0843	0.00579	4.51	0.120
0.1477	0.0831	0.0843	0.00513	4.80	0.119
0.1446	0.0817	0.0819	0.00536	5.08	0.118
0.1443	0.0793	0.0807	0.00553	5.24	0.118
0.1421	0.0785	0.0816	0.00524	5.41	0.117

Table B10. Measurements with AB ON (Ref. 1)

THRUST MEASUREMENTS DONE BY GARCIA (Ref 6)

Mach No	lbf
0.1962	-2.13
0.1869	-1.88
0.1770	-1.49
0.1666	-1.11
0.1554	-0.675
0.2436	-5.35
0.2397	-5.04
0.2358	-4.83
0.2317	-4.61
0.2276	-4.45
0.2378	-5.08
0.2373	-5.15
0.2368	-5.28
0.2363	-5.12
0.2358	-5.05

Table B11. Measurements with AB OFF (Ref. 6)

THIS PAGE INTENTIONALLY LEFT BLANK

APPENDIX C. RESULTS AND INPUT FILES TO OVERFLOW

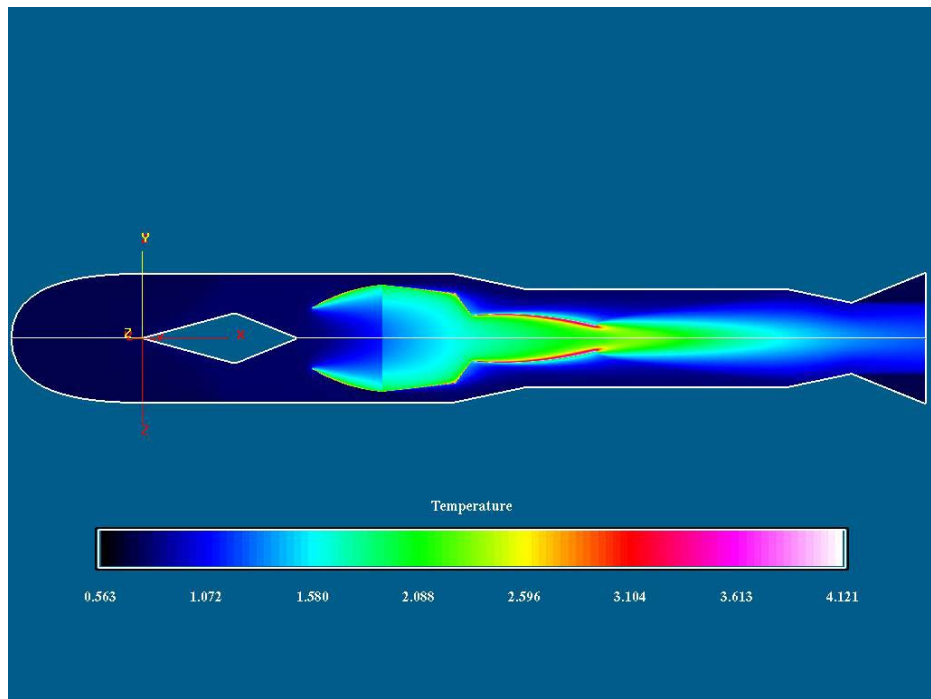


Figure C1. Temperature Distribution for the Turbo-Ramjet Engine at $M_{\infty} = 0.6$
(Inflow/Outflow BC)

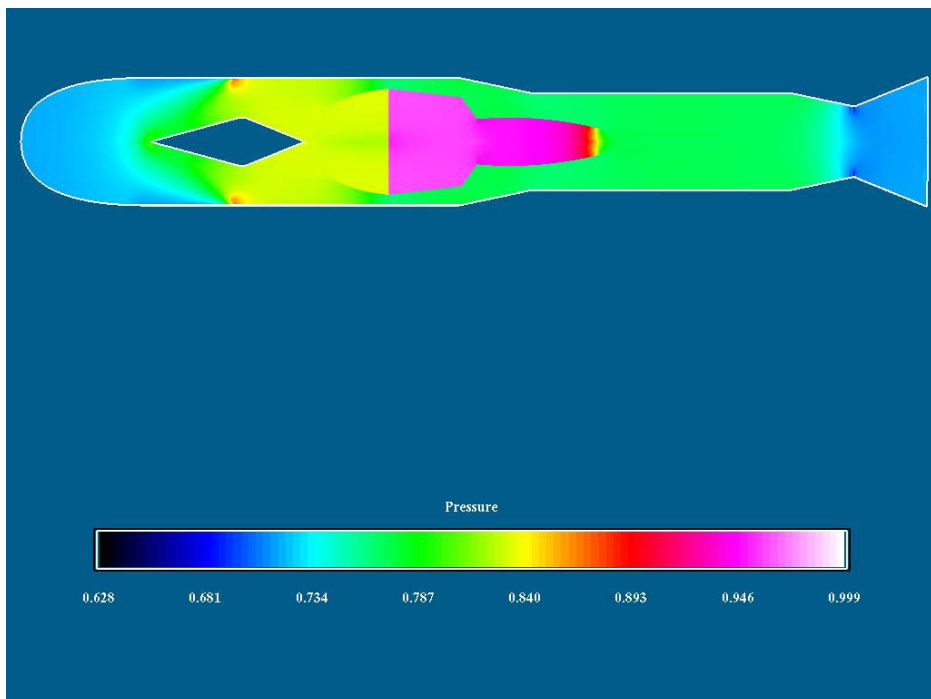


Figure C2. Pressure Distribution for the Turbo-Ramjet Engine at $M_{\infty} = 0.6$
(Inflow/Outflow B.C.)

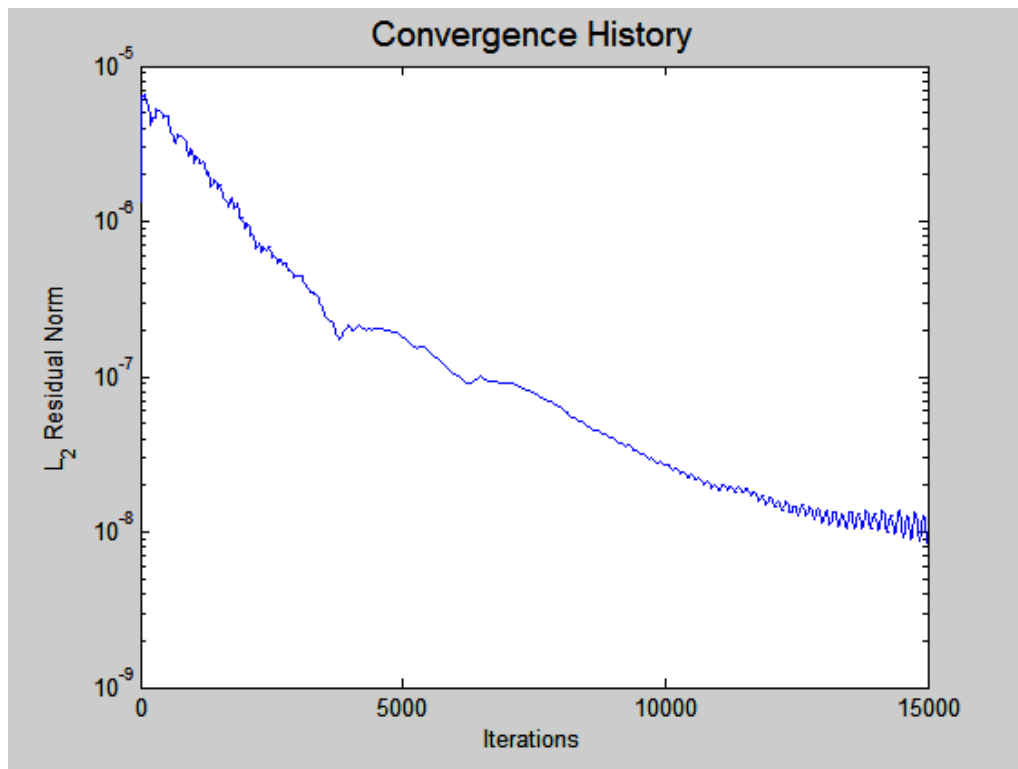


Figure C3. Convergence History for Turbo-Ramjet Engine at $M_{\infty} = 0.6$ (Small Grid - Inflow/Outflow B.C.)

Overflow.in Input File for Turbo-Ramjet at $M_\infty = 0.6$ (Small Grid-Inflow/Outflow B.C.)

```

$GLOBAL
    CHIMRA= .F.,      NSTEPS=30000,      RESTRT= .F.,      NSAVE =100,
    NQT    = 202,
    $END
$FLOINP
    ALPHA =0,    FSMACH= 0.600,    REY    = 1.0420E7,    TINF   = 520.000,
    XKINF=.0001, RETINF=0.1, GAMINF=1.4,
    $END
$VARGAM
    IGAM=0,
    $END
$GRDNAM
    NAME = 'Axi-symmetric shroud with nose cone for bypass ratio
computation',
    $END
$NITERS
    $END
$METPRM
    $END
$TIMACU
    ITIME=1,
    CFLMIN=1,
    CFLMAX=10,
    $END
$SMOACU
    $END
$VISINP
    VISC =.T.,
    CFLT = 1,
    ITERT = 3,
    $END
$BCINP
    NBC    =    13,
    IBTYP =    5,    5,    5,    7,    7,    7,    44,    32,    32,    31,    22,    16,
16,
    IBDIR =    2,    2,   -2,    2,    2,   -2,    1,    1,    2,   -2,    3,    1,
2,
    JBCS  = 191,    1, 105, 296, 382, 191, 290,   -1, 559,    1,    1,    1,
174,
    JBCE  = 295, 173, 558, 381, 437, 437, 291,   -1,   -1, 104,   -1,    1,   -
1,
    KBCS  = 49,    1,   -1,    49,    49,    48,    1,    1,   -1,   -1,    1,    1,
1,
    KBCE  = 49,    1,   -1,    49,    49,    48,    47,   -1,   -1,   -1,   -1,   -1,
1,
    LBCS  =    1,    1,    1,    1,    1,    1,    1,    1,    1,    1,    1,    1,
1,
    LBCE  =   -1,   -1,   -1,   -1,   -1,   -1,   -1,   -1,   -1,   -1,   -1,   -1,
1,
    BCPAR1(4)=1000,
    BCPAR1(5)=1500,
    BCPAR1(6)=3000,
    BCPAR1(7)=0.18,

```

\$END
\$SCEINP
\$END

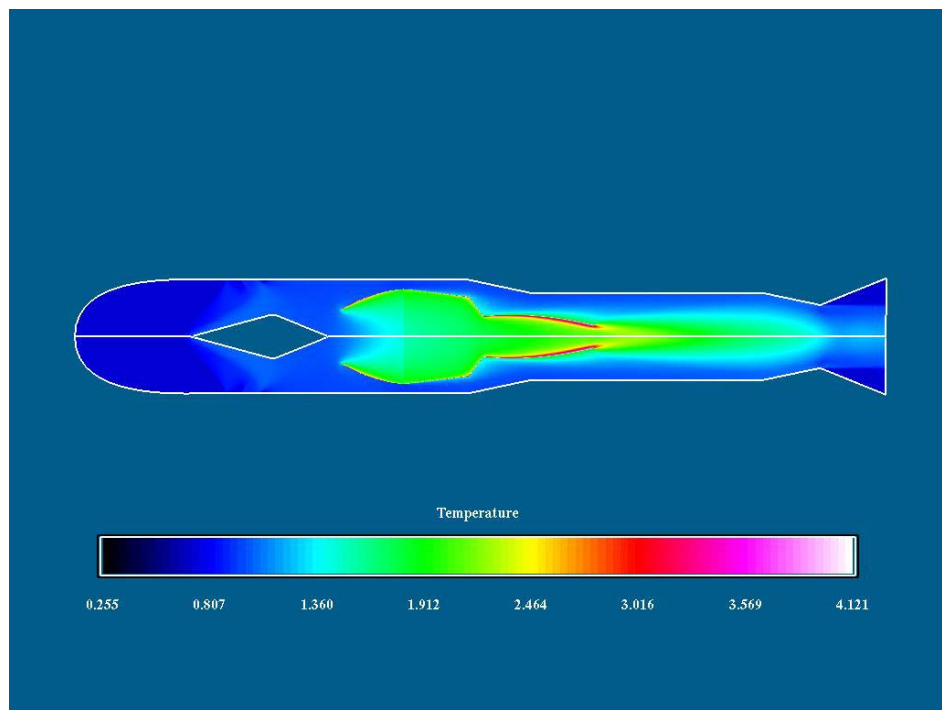


Figure C4. Temperature Distribution for the Turbo-Ramjet Engine at $M_{\infty} = 1.5$ (Small Grid - Inflow/Outflow B.C.)

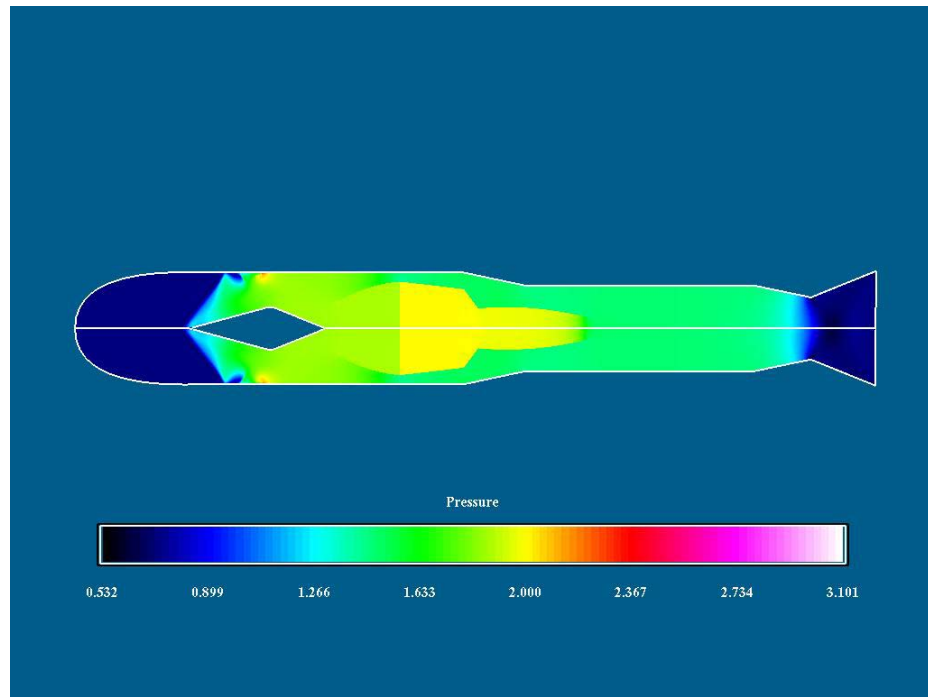


Figure C5. Pressure Distribution for the Turbo-Ramjet Engine at $M_{\infty} = 1.5$ (Small Grid - Inflow/Outflow B.C.)

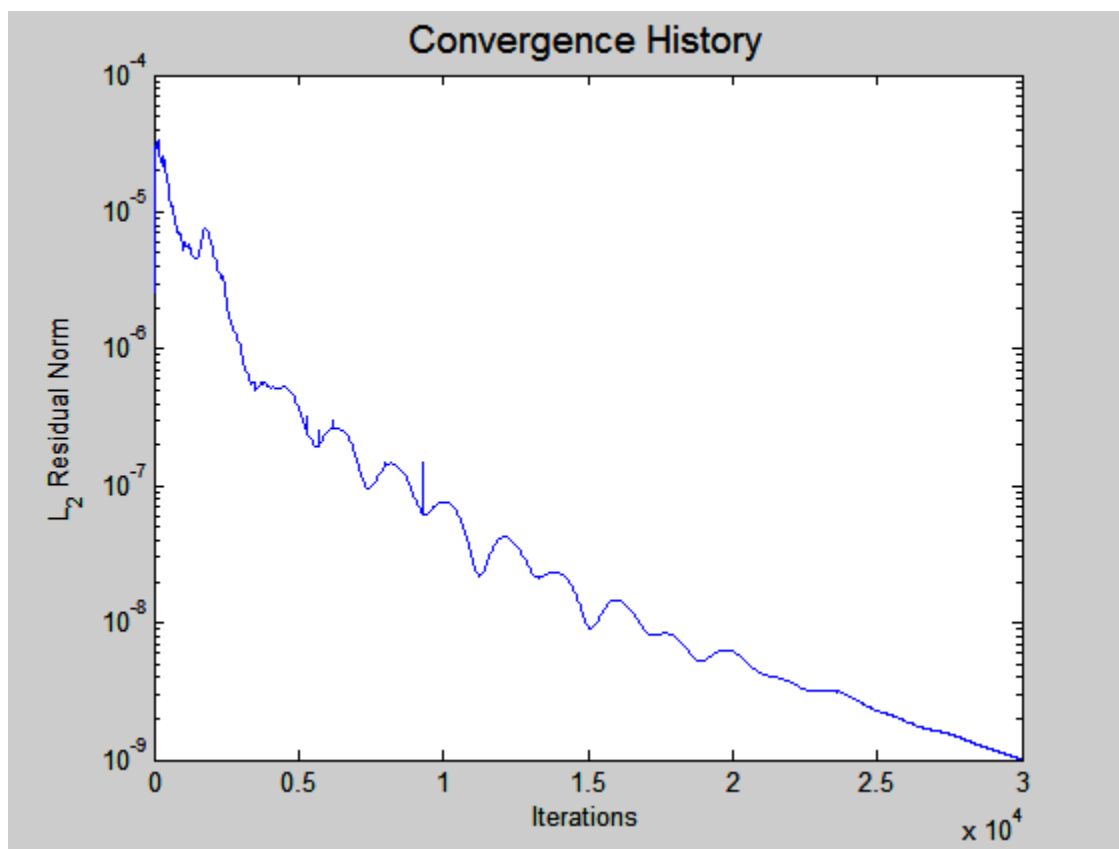


Figure C6. Convergence History for Turbo-Ramjet Engine at $M_\infty = 1.5$ (Small Grid - Inflow/Outflow B.C.)

Overflow.in Input File for Turbo-Ramjet at $M_\infty = 1.5$ (Small Grid – Inflow/Outflow Boundary Condition)

```

$GLOBAL
    CHIMRA= .F.,      NSTEPS=30000,      RESTRT= .F.,      NSAVE =100,
    NQT    = 202,
    $END
$FLOINP
    ALPHA =0,    FSMACH= 1.500,    REY    = 1.0420E7,    TINF   = 520.000,
    XKINF=.0001, RETINF=0.1, GAMINF=1.4,
    $END
$VARGAM
    IGAM=0,
    $END
$GRDNAM
    NAME = 'Axi-symmetric shroud with nose cone for bypass ratio
computation',
    $END
$NITERS
    $END
$METPRM
    $END
$TIMACU
    ITIME=1,
    CFLMIN=1,
    CFLMAX=10,
    $END
$SMOACU
    $END
$VISINP
    VISC =.T.,
    CFLT = 1,
    ITERT = 3,
    $END
$BCINP
    NBC    =    13,
    IBTYP =    5,    5,    5,    7,    7,    7,    44,    32,    32,    31,    22,    16,
16,
    IBDIR =    2,    2,   -2,    2,    2,   -2,    1,    1,    2,   -2,    3,    1,
2,
    JBCS  = 191,    1, 105, 296, 382, 191, 290,   -1, 559,    1,    1,    1,
174,
    JBCE  = 295, 173, 558, 381, 437, 437, 291,   -1,   -1, 104,   -1,    1,
-1,
    KBCS  = 49,    1,   -1,    49,    49,    48,    1,    1,   -1,   -1,    1,    1,
1,
    KBCE  = 49,    1,   -1,    49,    49,    48,    47,   -1,   -1,   -1,   -1,   -1,
1,
    LBCS  =    1,    1,    1,    1,    1,    1,    1,    1,    1,    1,    1,    1,
1,
    LBCE  =   -1,   -1,   -1,   -1,   -1,   -1,   -1,   -1,   -1,   -1,    1,   -1,
-1,
    BCPAR1(4)=1000,
    BCPAR1(5)=1500,
    BCPAR1(6)=3000,
    BCPAR1(7)=0.18,

```

\$END
\$SCEINP
\$END

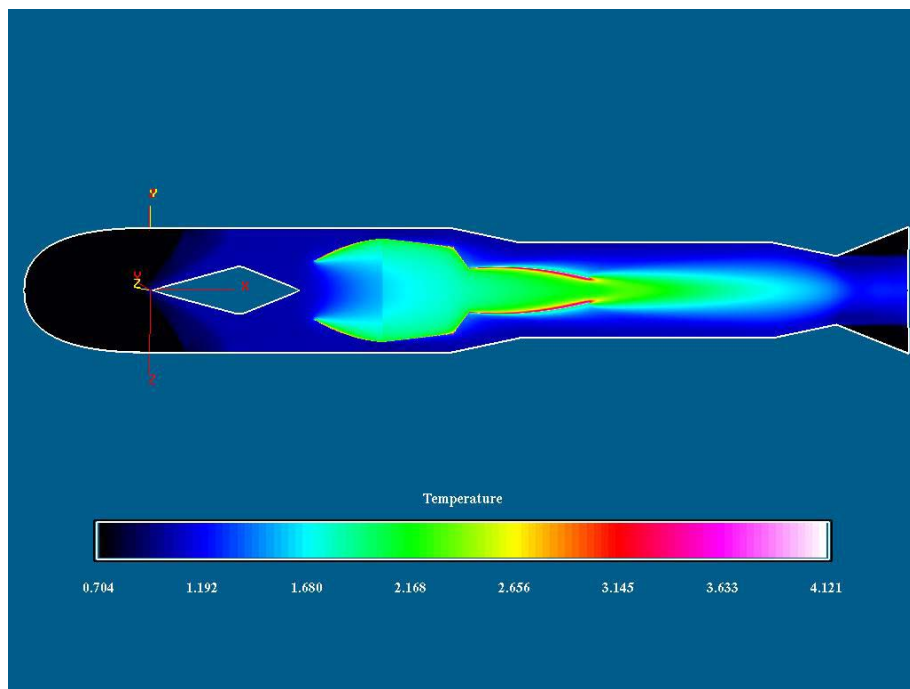


Figure C7. Temperature Distribution for the Turbo-Ramjet Engine at $M_{\infty} = 1.5$
(Riemann Invariants B.C.)

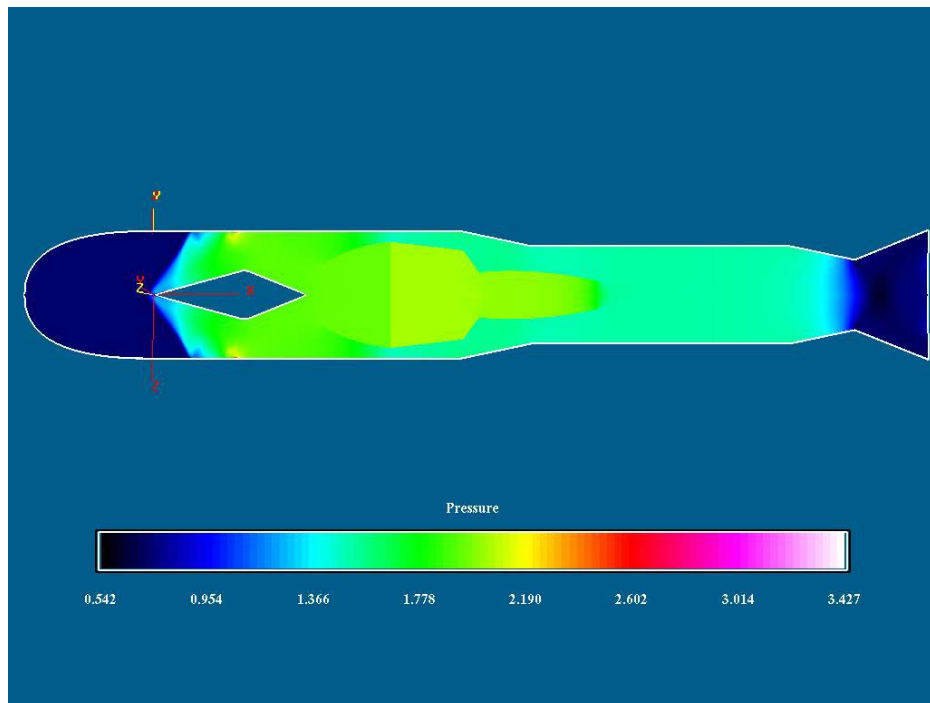


Figure C8. Pressure Distribution for the Turbo-Ramjet Engine at $M_{\infty} = 1.5$ (Riemann Invariants B.C.)

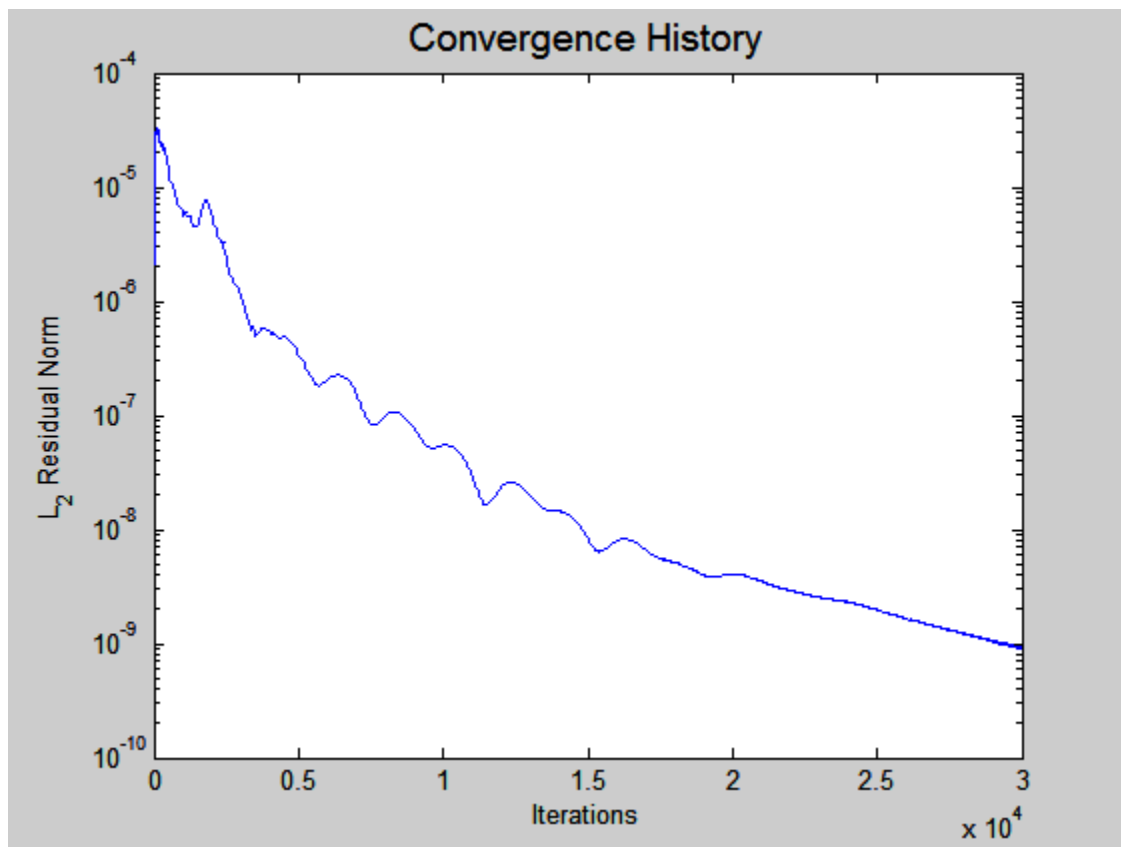


Figure C9. Convergence History for Turbo-Ramjet Engine at $M_{\infty} = 1.5$ (Small Grid - Riemann Invariants B.C.)

Overflow.in Input File for Turbo-Ramjet at $M_\infty = 1.5$ (Small Grid – Riemann Invariants Boundary Condition)

```

$GLOBAL
    CHIMRA= .F.,      NSTEPS=30000,      RESTRT= .F.,      NSAVE =100,
    NQT   = 202,
    $END
$FLOINP
    ALPHA =0,    FSMACH= 1.500,    REY    = 1.0420E7,    TINF   = 520.000,
    XKINF=.0001, RETINF=0.1, GAMINF=1.4,
    $END
$VARGAM
    IGAM=0,
    $END
$GRDNAM
    NAME = 'Axi-symmetric shroud with nose cone for bypass ratio
computation',
    $END
$NITERS
    $END
$METPRM
    $END
$TIMACU
    ITIME=1,
    CFLMIN=1,
    CFLMAX=10,
    $END
$SMOACU
    $END
$VISINP
    VISC =.T.,
    CFLT = 1,
    ITERT = 3,
    $END
$BCINP
    NBC    = 13,
    IBTYP = 5,   5,   5,   7,   7,   7,   44,   31,   31,   31, 22, 16,
16,
    IBDIR = 2,   2,  -2,   2,   2,  -2,   1,   1,   2,  -2,   3,   1,
2,
    JBCS  = 191,  1, 105, 296, 382, 191, 290,  -1, 559,   1,   1,   1,
174,
    JBCE  = 295, 173, 558, 381, 437, 437, 291,  -1,  -1, 104,  -1,   1,
-1,
    KBCS  = 49,   1,  -1,   49,   49,   48,   1,   1,  -1,  -1,   1,   1,
1,
    KBCE  = 49,   1,  -1,   49,   49,   48,   47,  -1,  -1,  -1,  -1,  -1,
1,
    LBCS  = 1,    1,   1,   1,   1,   1,   1,   1,   1,   1,   1,   1,
1,
    LBCE  = -1,  -1,  -1,  -1,  -1,  -1,  -1,  -1,  -1,  -1,  -1,  -1,
-1,
    BCPAR1(4)=1000,
    BCPAR1(5)=1500,
    BCPAR1(6)=3000,

```

```
BCPAR1(7)=0.18,  
$END  
$SCEINP  
$END
```

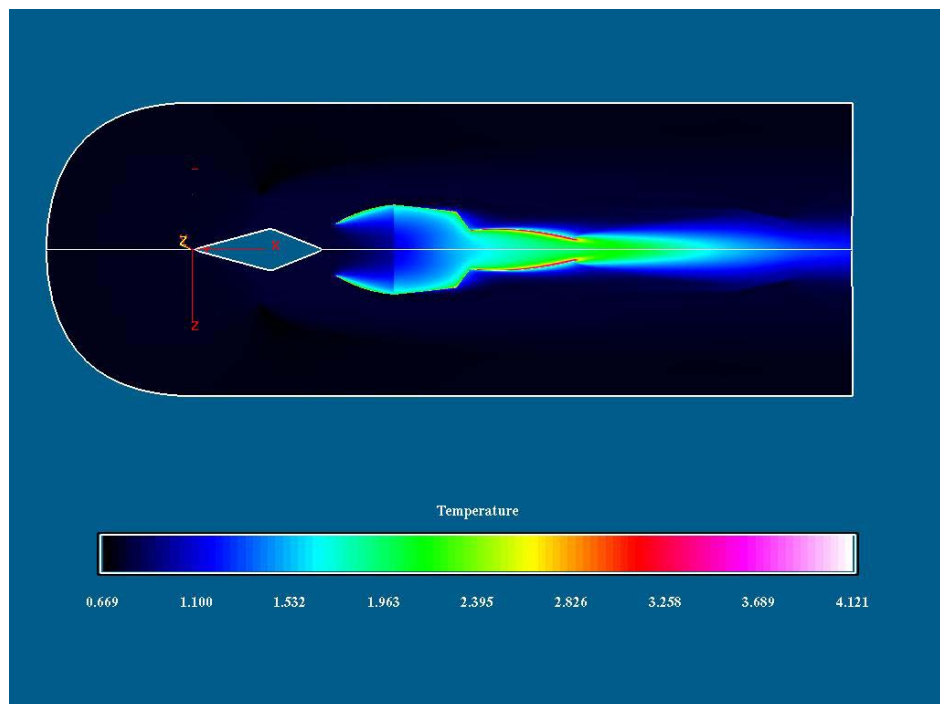


Figure C10. Temperature Distribution for the Turbo-Ramjet Engine at $M_{\infty} = 0.6$ (Large Grid – Inflow/Outflow B.C.)

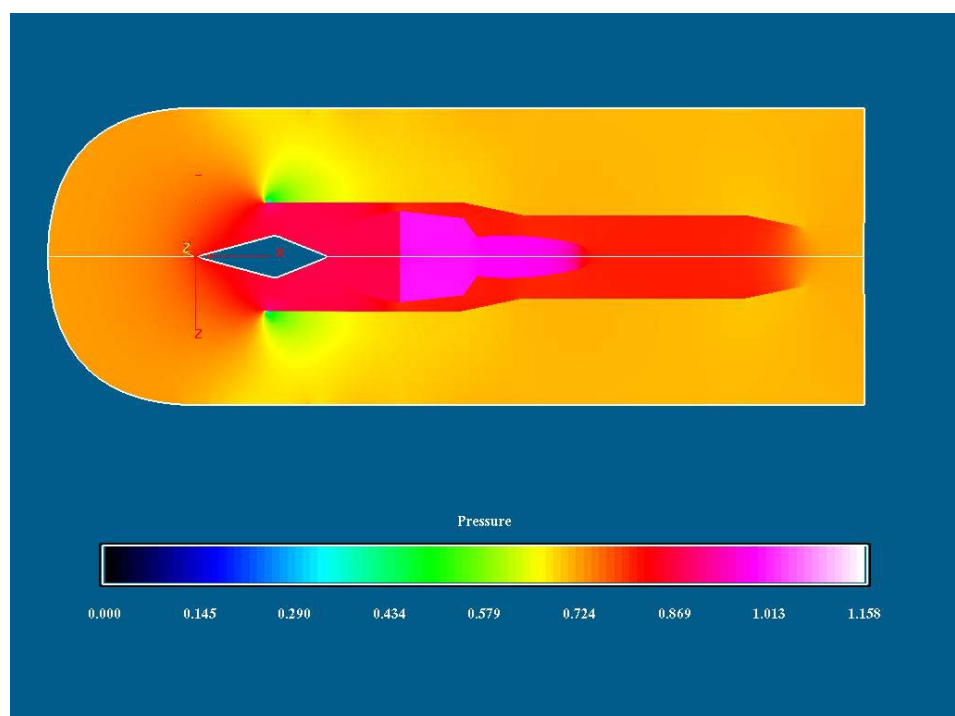


Figure C11. Pressure Distribution for the Turbo-Ramjet Engine at $M_{\infty} = 0.6$ (Large Grid - Inflow/Outflow B.C)

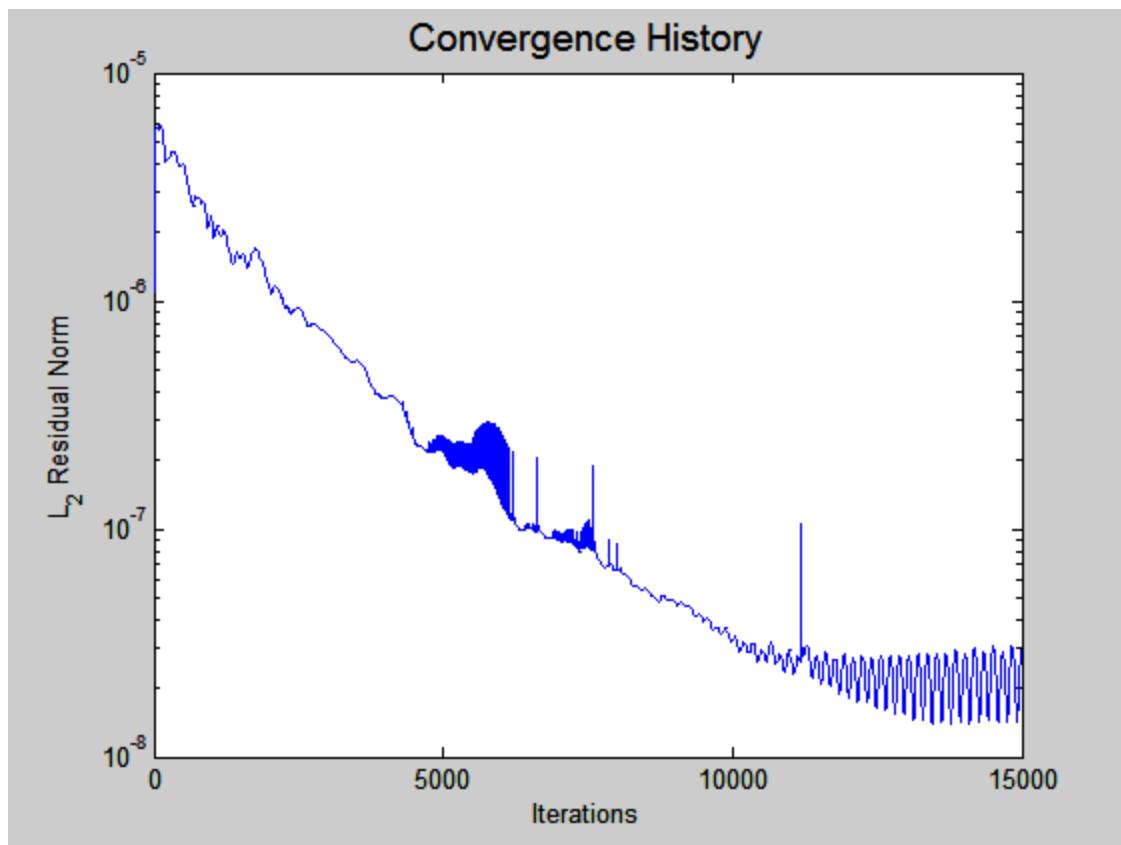


Figure C12. Convergence History for Turbo-Ramjet Engine at $M_{\infty} = 0.6$ (Large Grid - Inflow/Outflow B.C.)

Overflow.in Input File for Turbo-Ramjet at $M_\infty = 0.6$ (Large Grid - Inflow/Outflow Boundary Condition)

```

$GLOBAL
    CHIMRA= .F.,      NSTEPS=20000,      RESTRT= .F.,      NSAVE =100,
    NQT    = 202,
    $END
$FLOINP
    ALPHA =0,    FSMACH=0.6000,    REY    = 1.0420E7,    TINF   = 520.000,
    XKINF=.0001, RETINF=0.1,    GAMINF=1.4,
    $END
$VARGAM
    IGAM=0,
    $END
$GRDNAM
    NAME = 'Throughflow into engine heating grid TEMP change for mass
computation',
    $END
$NITERS
    $END
$METPRM
    $END
$TIMACU
    ITIME=1,
    CFLMIN=1,
    CFLMAX=10,
    $END
$SMOACU
    $END
$VISINP
    VISC =.T.,
    CFLT = 1,
    ITERT = 3,
    $END
$BCINP
    NBC    = 15,
    IBTYP = 5,    5,    5,    5,    7,    7,    7,    44,    31,    31,    31,
22, 16, 16, 44,
    IBDIR = 2,    -2,    2,    2,    2,    2,    -2,    1,    1,    1,    -2,
3,  1,  2,  1,
    JBCS = 81,    81,    1,  167,  296,  358,  167,  265,  -1,  -1,  1,
1,  1,  168, 534,
    JBCE = 534,  534,  167,  295,  357,  413,  413,  266,  -1,  -1,  -1,
1,  1,  -1, 534,
    KBCS = 109,  108,    1,    52,    52,    52,    51,    1,    1,  109,  -1,
1,  1,  1,  1,
    KBCE = 109,  108,    1,    52,    52,    52,    51,    50,  108,  -1,  -1,  -
1,  -1,  1, 107,
    LBCS = 1,    1,    1,    1,    1,    1,    1,    1,    1,    1,    1,
1,  1,  1,  1,
    LBCE = -1,   -1,   -1,   -1,   -1,   -1,   -1,   -1,   -1,   -1,   -1,
1,  -1,  -1,  -1,
    BCPAR1(5)=1000,
    BCPAR1(6)=1500,
    BCPAR1(7)=3000,
    BCPAR1(8)=.18,

```

```
BCPAR1(15)=0,  
$END  
$SCEINP  
$END
```

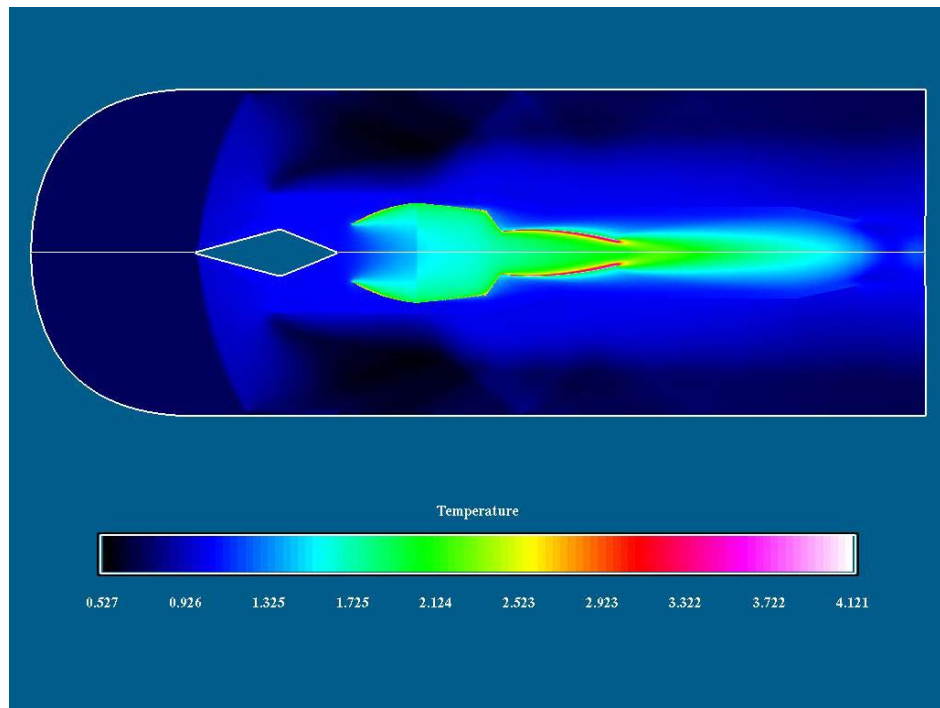


Figure C13. Temperature Distribution for the Turbo-Ramjet Engine at $M_{\infty} = 1.5$ (Large Grid - Inflow/Outflow B.C.)

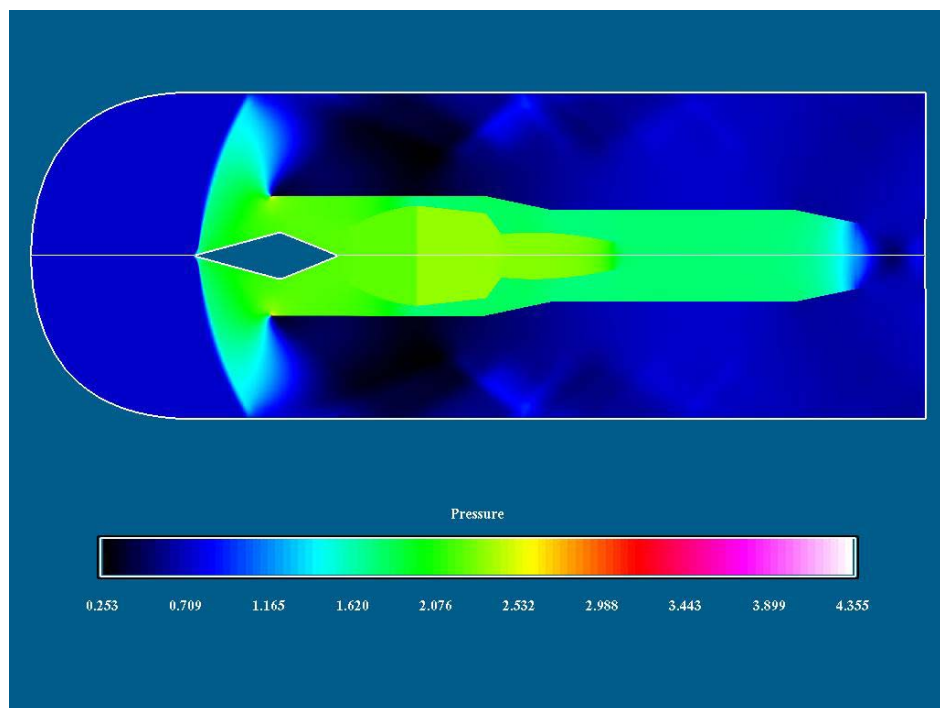


Figure C14. Pressure Distribution for the Turbo-Ramjet Engine at $M_{\infty} = 1.5$ (Large Grid - Inflow/Outflow B.C.)

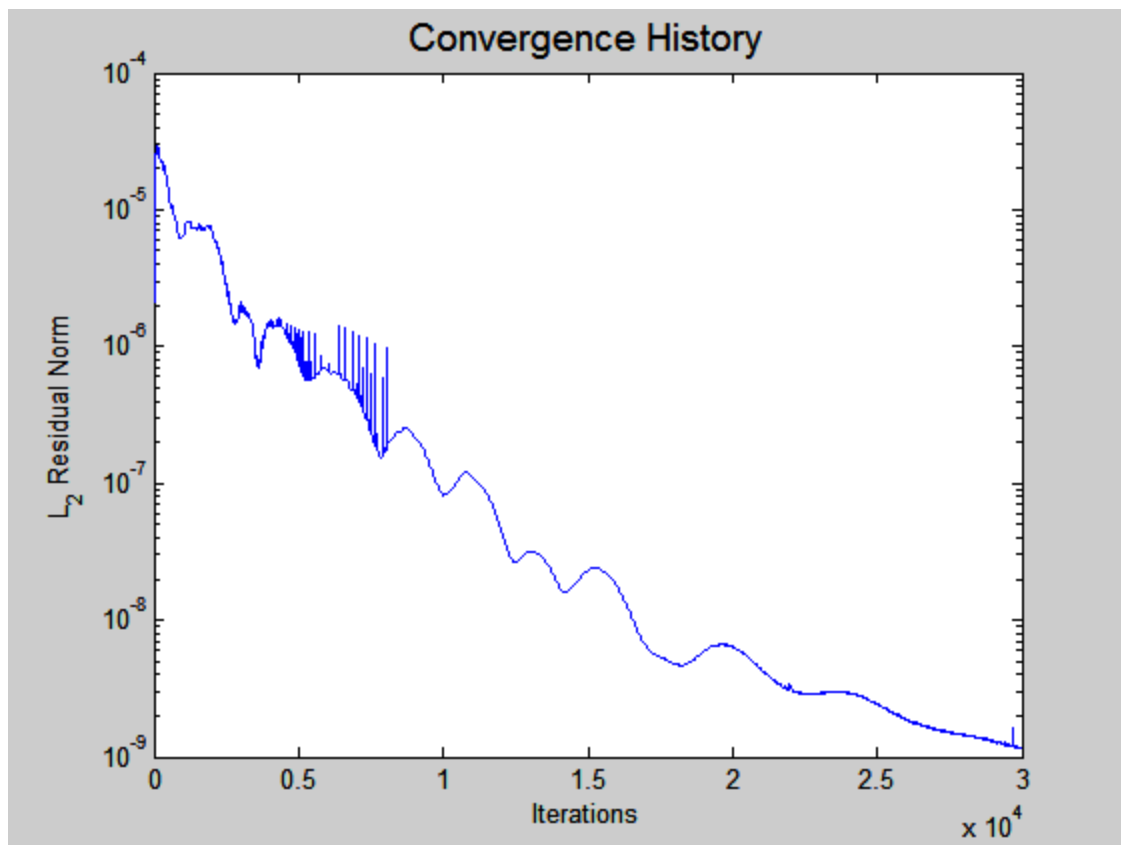


Figure C15. Convergence History for Turbo-Ramjet Engine at $M_{\infty}=1.5$ (Large Grid - Inflow/Outflow B.C)

Overflow.in Input File for Turbo-Ramjet at $M_\infty = 1.5$ (Large Grid - Inflow/Outflow Boundary Condition)

```

$GLOBAL
    CHIMRA= .F.,      NSTEPS=30000,      RESTRT= .F.,      NSAVE =100,
    NQT     = 202,
    $END
$FLOINP
    ALPHA =0,      FSMACH=1.5000,      REY     = 1.0420E7,      TINF    = 520.000,
    XKINF=.0001,    RETINF=0.1,      GAMINF=1.4,
    $END
$VARGAM
    IGAM=0,
    $END
$GRDNAM
    NAME = 'Throughflow into engine heating grid for mass
computation',
    $END
$NITERS
    $END
$METPRM
    $END
$TIMACU
    ITIME=1,
    CFLMIN=1,
    CFLMAX=10,
    $END
$SMOACU
    $END
$VISINP
    VISC =.T.,
    CFLT = 1,
    ITERT = 3,
    $END
$BCCINP
    NBC     = 15,
    IBTYP   = 5,      5,      5,      5,      7,      7,      7,      44,      32,      32,      32,
22, 16, 16, 44,
    IBDIR   = 2,      -2,      2,      2,      2,      2,      -2,      1,      1,      1,      -2,
3, 1, 2, 1,
    JBCS    = 81,      81,      1,      167,      296,      358,      167,      265,      -1,      -1,      1,
1, 1, 168, 534,
    JBCE    = 534,      534,      167,      295,      357,      413,      413,      266,      -1,      -1,      -1,
1, 1, -1, 534,
    KBCS    = 109,      108,      1,      52,      52,      52,      51,      1,      1,      109,      -1,
1, 1, 1, 1,
    KBCE    = 109,      108,      1,      52,      52,      52,      51,      50,      108,      -1,      -1,      -
1, -1, 1, 107,
    LBCS    = 1,      1,      1,      1,      1,      1,      1,      1,      1,      1,      1,      1,
1, 1, 1, 1,
    LBCE    = -1,      -1,      -1,      -1,      -1,      -1,      -1,      -1,      -1,      -1,      -1,      -1,
1, -1, -1, -1,
    BCPAR1(5)=1000,
    BCPAR1(6)=1500,
    BCPAR1(7)=3000,
    BCPAR1(8)=.18,
    BCPAR1(15)=0,

```

\$END
\$SCEINP
\$END

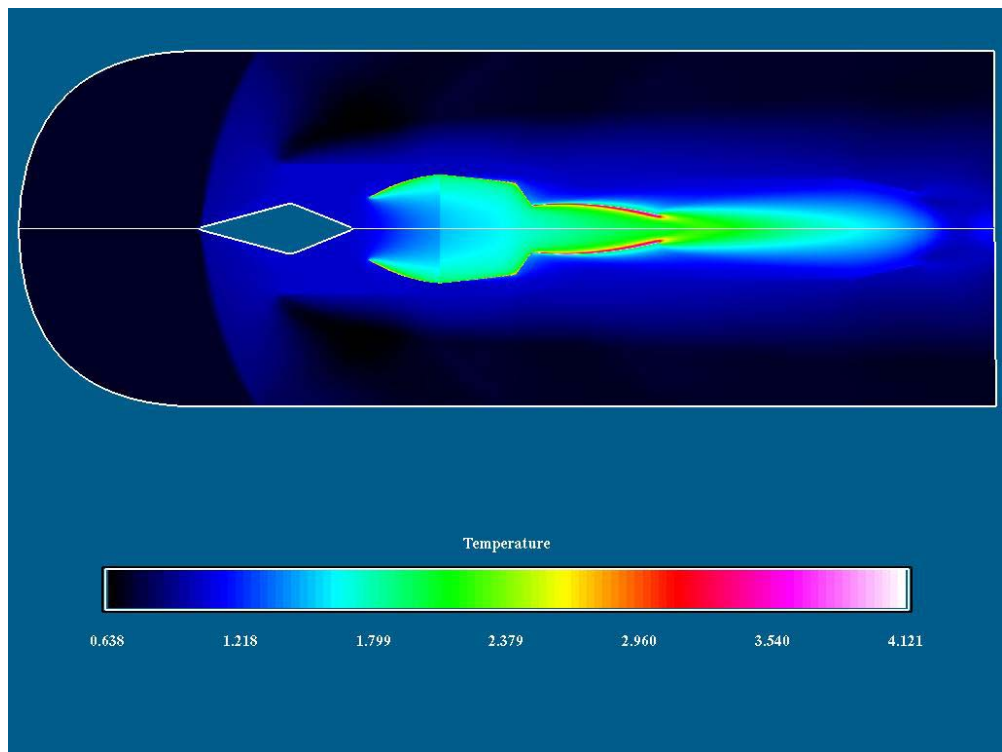


Figure C16. Temperature Distribution for the Turbo-Ramjet Engine at $M_{\infty} = 1.5$ (Large Grid – Riemann Invariants B.C.)

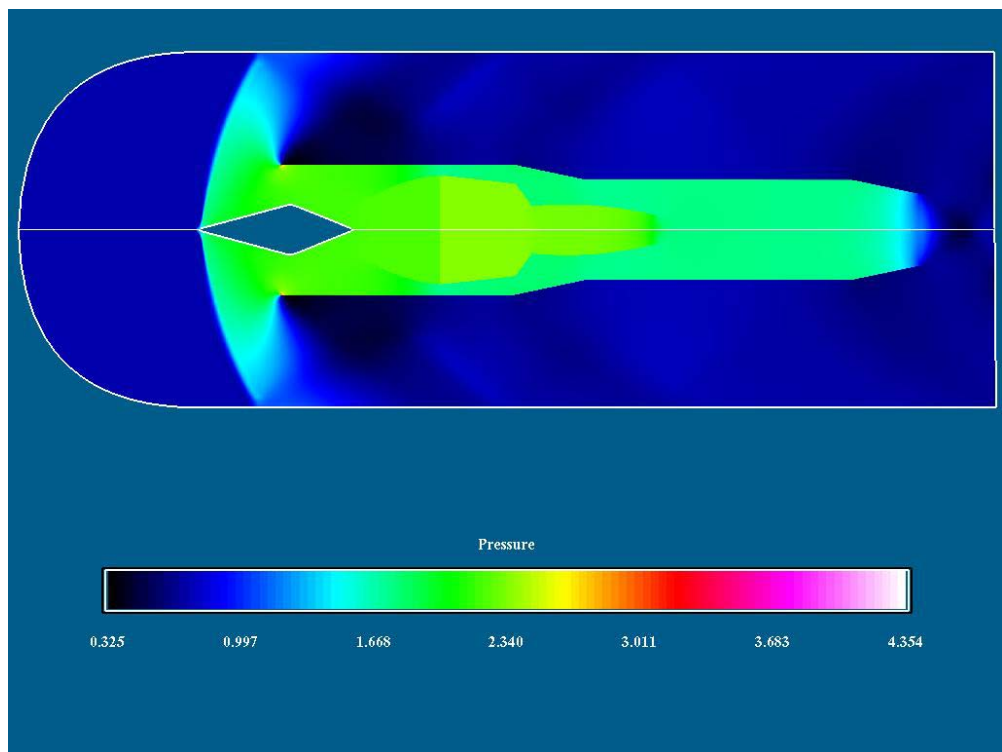


Figure C17. Pressure Distribution for the Turbo-Ramjet Engine at $M_{\infty} = 1.5$ (Large Grid - Riemann Invariants B.C.)

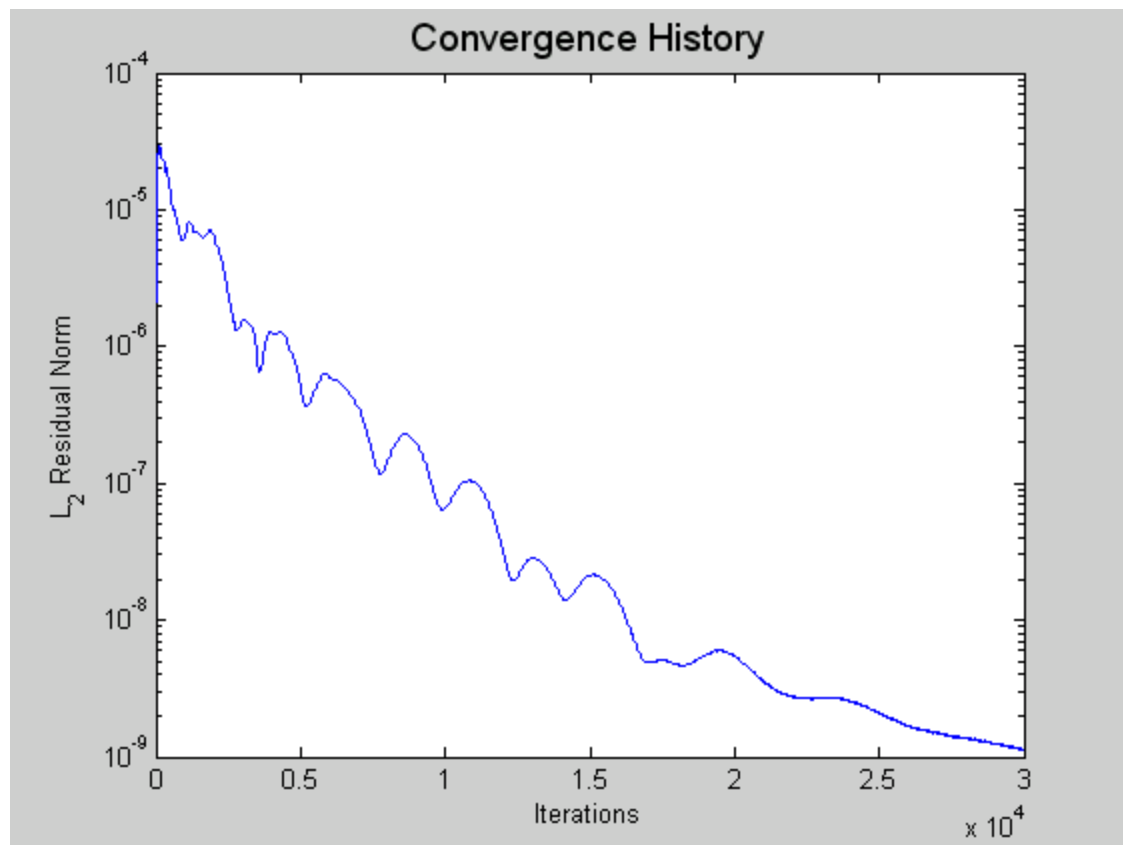


Figure C18. Convergence History for Turbo-Ramjet Engine at $M_{\infty}=1.5$ (Large Grid - Riemann Invariants B.C.)

Overflow.in Input File for Turbo-Ramjet at $M_\infty = 1.5$ (Large Grid - Riemann Invariants Boundary Condition)

```

$GLOBAL
    CHIMRA= .F.,      NSTEPS=30000,      RESTRT= .F.,      NSAVE =100,
    NQT     = 202,
    $END
$FLOINP
    ALPHA =0,      FSMACH=1.5000,      REY     = 1.0420E7,      TINF    = 520.000,
    XKINF=.0001,    RETINF=0.1,      GAMINF=1.4,
    $END
$VARGAM
    IGAM=0,
    $END
$GRDNAM
    NAME = 'Throughflow into engine heating grid for mass
computation',
    $END
$NITERS
    $END
$METPRM
    $END
$TIMACU
    ITIME=1,
    CFLMIN=1,
    CFLMAX=10,
    $END
$SMOACU
    $END
$VISINP
    VISC =.T.,
    CFLT = 1,
    ITERT = 3,
    $END
$BCCINP
    NBC     = 15,
    IBTYP  = 5,      5,      5,      5,      7,      7,      7,      44,      32,      32,      32,
22, 16, 16, 44,
    IBDIR  = 2,      -2,      2,      2,      2,      2,      -2,      1,      1,      1,      -2,
3, 1, 2, 1,
    JBCS   = 81,     81,     1,     167,     296,     358,     167,     265,     -1,     -1,     1,
1, 1, 168, 534,
    JBCE   = 534,    534,    167,    295,    357,    413,    413,    266,    -1,    -1,    -1,    -
1, 1, -1, 534,
    KBCS   = 109,    108,    1,     52,     52,     52,     51,      1,      1,     109,    -1,
1, 1, 1, 1,
    KBCE   = 109,    108,    1,     52,     52,     52,     51,     50,     108,    -1,    -1,    -
1, -1, 1, 107,
    LBCS   = 1,      1,      1,      1,      1,      1,      1,      1,      1,      1,      1,
1, 1, 1, 1,
    LBCE   = -1,     -1,     -1,     -1,     -1,     -1,     -1,     -1,     -1,     -1,     -1,
1, -1, -1, -1,
    BCPAR1(5)=1000,
    BCPAR1(6)=1500,
    BCPAR1(7)=3000,
    BCPAR1(8)=.18,
    BCPAR1(15)=0,

```

\$END
\$SCEINP
\$END

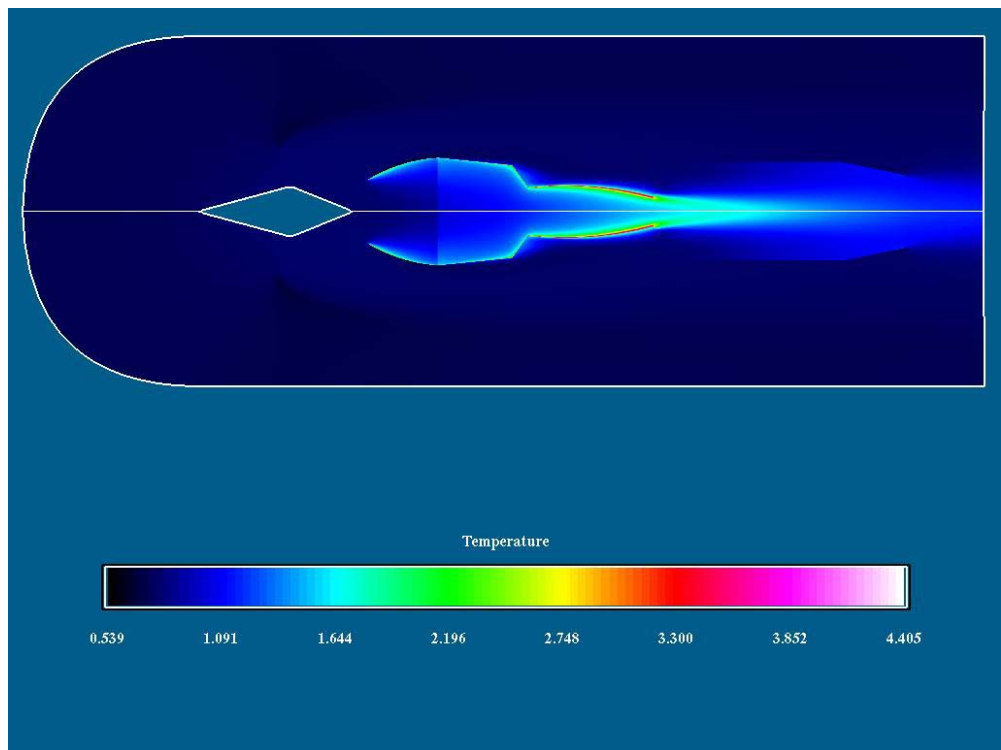


Figure C19. Temperature Distribution for the Turbo-Ramjet Engine at $M_{\infty} = 0.6$ (with Flameholder – Inflow/Outflow B.C.)

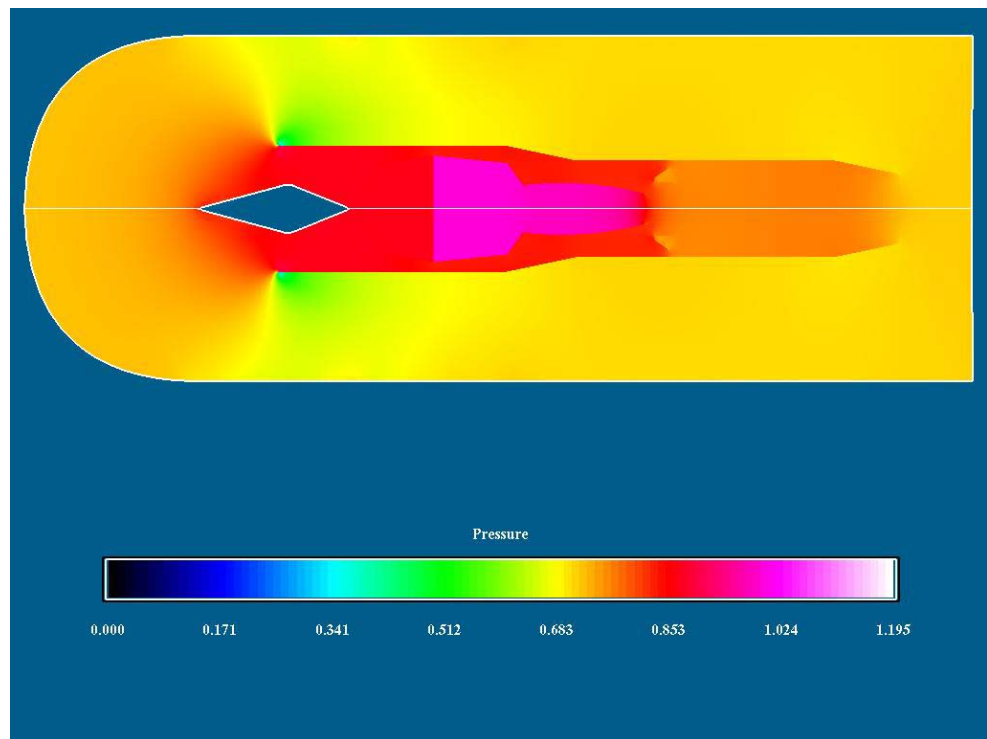


Figure C20. Pressure Distribution for the Turbo-Ramjet Engine at $M_{\infty} = 0.6$ (with Flameholder – Inflow/Outflow B.C.)

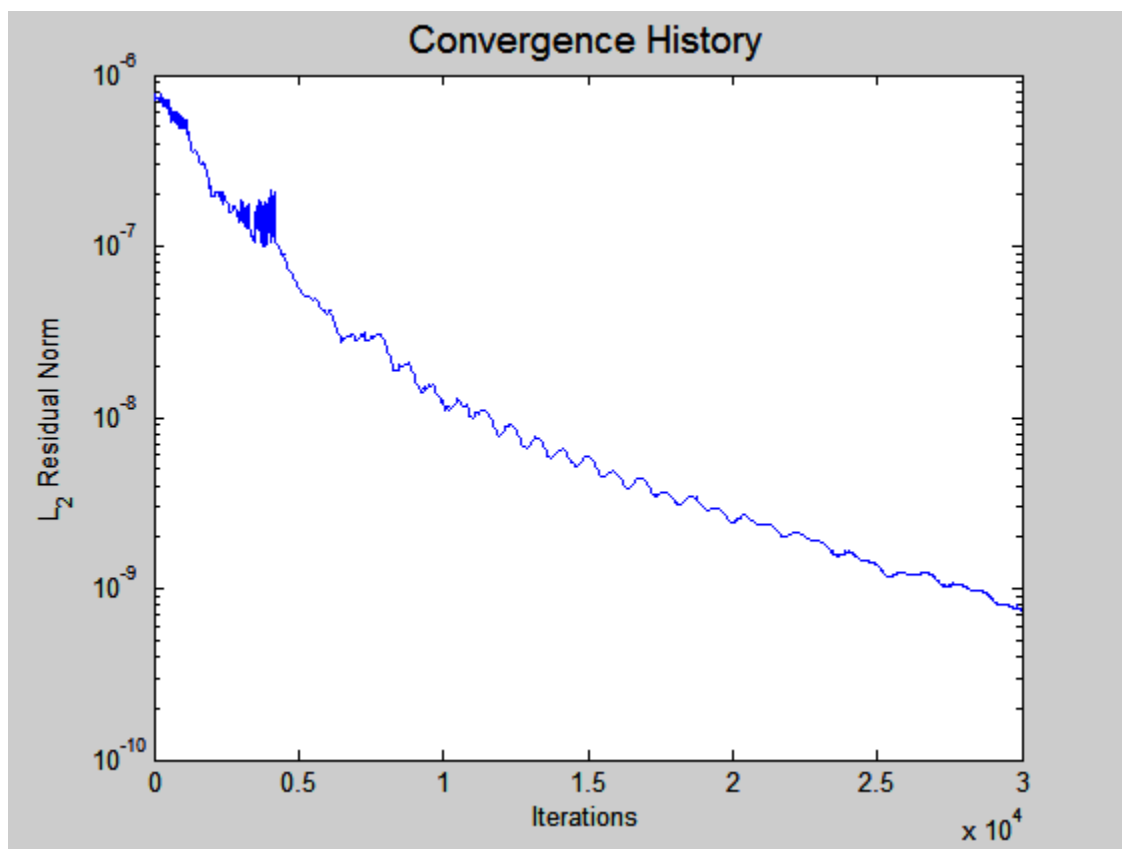


Figure C21. Convergence History for Turbo-Ramjet Engine at $M_{\infty}=0.6$ (Flameholder – Inflow/Outflow B.C.)

Overflow.in Input File for Turbo-Ramjet at $M_{\infty} = 0.6$ (Flameholder- Inflow/Outflow Boundary Condition)

```

$GLOBAL
    CHIMRA= .F.,      NSTEPS=30000,      RESTRT= .F.,      NSAVE =1000,
    NQT    = 202,
    $END
$FLOINP
    ALPHA =0,    FSMACH= 0.6000,    REY    = 1.0420E7,    TINF   = 520.000,
    XKINF=.0001, RETINF=0.1, GAMINF=1.4,
    $END
$VARGAM
    IGAM=0,
    $END
$GRDNAM
    NAME = 'Throughflow into engine heating grid TEMP change
flameholder',
    $END
$NITERS
    $END
$METPRM
    $END
$TIMACU
    ITIME=1,
    CFLMIN=1,
    CFLMAX=10,
    $END
$SMOACU
    $END
$VISINP
    VISC =.T.,
    CFLT = 1,
    ITERT = 3,
    $END
$BCINP
    NBC    = 24,
    IBTYP = 5,      5,      5,      5,      5,      5,      5,      5,      5,      5,      5,      7,
7,    7,      44,      31,      31,      22,      16,      16,      5,      5,      5,      5,      61,      44,
    IBDIR = 2,      -2,      -2,      2,      2,      -2,      2,      2,      2,      -1,      1,      2,
2,    -2,      1,      -1,      -2,      3,      1,      2,      1,      2,      1,      -2,      1,
    JBGS = 81,      81,      400,      1,      150,      386,      387,      393,      386,      387,      230,
311,  150,      228,      -1,      1,      1,      133,      393,      386,      406,      387,      539,
    JBCE = 539,      399,      539,      132,      229,      406,      393,      406,      386,      387,      310,
366,  366,      229,      -1,      -1,      -1,      1,      -1,      393,      387,      406,      392,      539,
    KBCS = 122,      121,      121,      1,      59,      59,      80,      60,      59,      82,      59,
59,    58,      1,      1,      -1,      1,      1,      62,      108,      59,      60,      1,
    KBCE = 122,      121,      121,      1,      59,      59,      80,      60,      108,      108,      59,
59,    58,      58,      -1,      -1,      -1,      -1,      1,      80,      108,      60,      79,      120,
    LBGS = 1,      1,      1,      1,      1,      1,      1,      1,      1,      1,      1,      1,
1,    1,      1,      1,      1,      1,      1,      1,      1,      1,      1,      1,      1,
    LBCE = -1,      -1,      -1,      -1,      -1,      -1,      -1,      -1,      -1,      -1,      -1,      -1,
1,    -1,      -1,      -1,      -1,      1,      -1,      -1,      -1,      -1,      -1,      -1,      -1,
    BCPAR1(11)=1000,
    BCPAR1(12)=1500,
    BCPAR1(13)=3000,
    BCPAR1(14)=.18,

```

```
BCPAR1(24)=0,  
$END  
$SCEINP  
$END
```

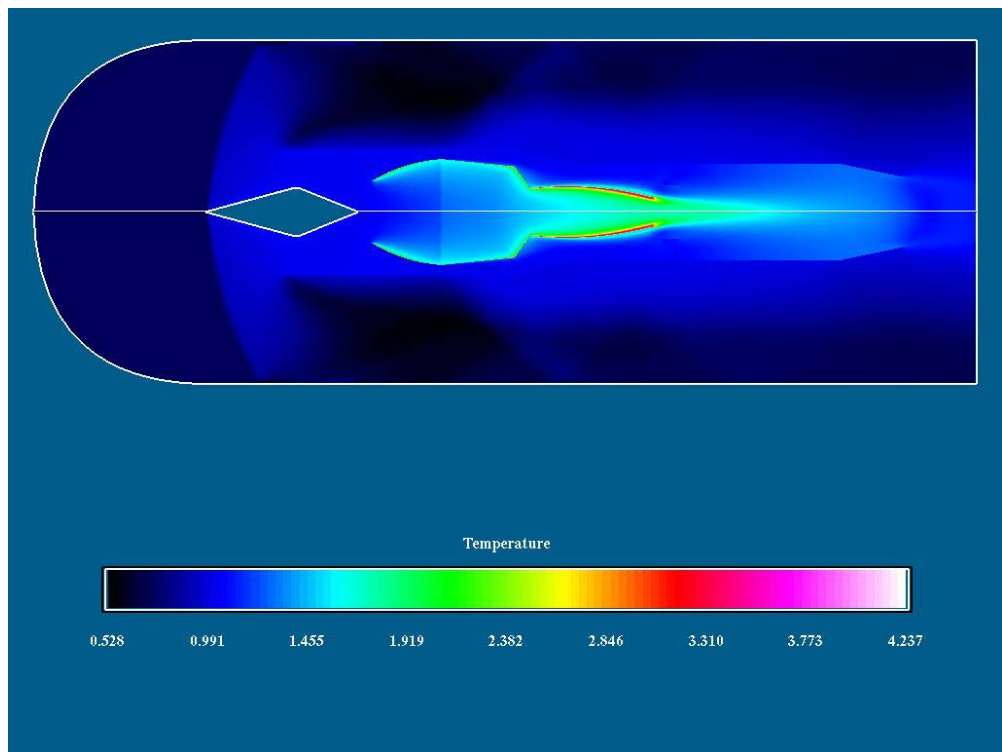


Figure C22. Temperature Distribution for the Turbo-Ramjet Engine at $M_{\infty} = 1.5$ (with Flameholder – Inflow/Outflow B.C.)

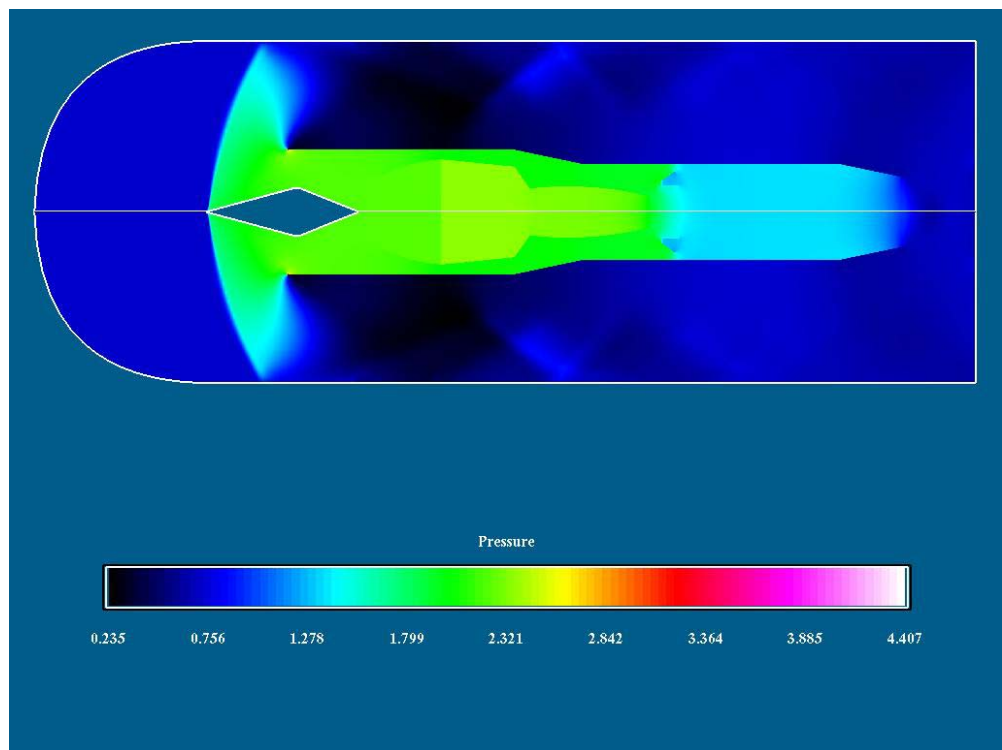


Figure C23. Pressure Distribution for the Turbo-Ramjet Engine at $M_{\infty} = 1.5$ (with Flameholder – Inflow/Outflow B.C.)

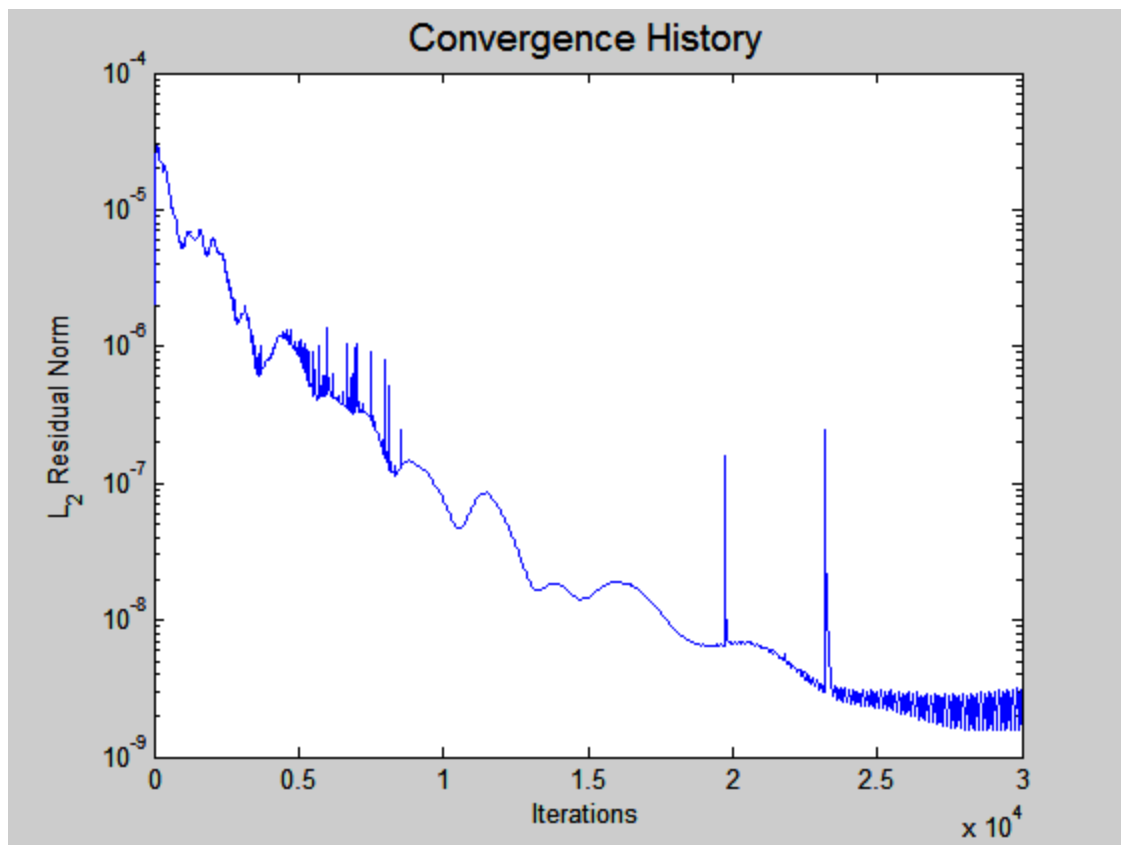


Figure C24. Convergence History for Turbo-Ramjet Engine at $M_{\infty} = 1.5$ (with Flameholder – Inflow/Outflow B.C.)

Overflow.in Input File for Turbo-Ramjet at $M_{\infty} = 1.5$ (Flameholder- Inflow/Outflow Boundary Condition)

```

$GLOBAL
    CHIMRA= .F.,      NSTEPS=30000,      RESTRT= .F.,      NSAVE =1000,
    NQT    = 202,
    $END
$FLOINP
    ALPHA =0,    FSMACH= 1.5000,    REY    = 1.0420E7,    TINF   = 520.000,
    XKINF=.0001, RETINF=0.1, GAMINF=1.4,
    $END
$VARGAM
    IGAM=0,
    $END
$GRDNAM
    NAME = 'Throughflow into engine heating grid TEMP change
flameholder',
    $END
$NITERS
    $END
$METPRM
    $END
$TIMACU
    ITIME=1,
    CFLMIN=1,
    CFLMAX=10,
    $END
$SMOACU
    $END
$VISINP
    VISC =.T.,
    CFLT = 1,
    ITERT = 3,
    $END
$BCINP
    NBC    = 24,
    IBTYP = 5,      5,      5,      5,      5,      5,      5,      5,      5,      5,      5,      7,
7,    7,      44,      32,      32,      22,      16,      16,      5,      5,      5,      5,      61,      44,
    IBDIR = 2,      -2,      -2,      2,      2,      -2,      2,      2,      2,      -1,      1,      2,
2,    -2,      1,      -1,      -2,      3,      1,      2,      1,      2,      1,      -2,      1,
    JBGS = 81,      81,      400,      1,      150,      386,      387,      393,      386,      387,      230,
311,  150,      228,      -1,      1,      1,      133,      393,      386,      406,      387,      539,
    JBCE = 539,      399,      539,      132,      229,      406,      393,      406,      386,      387,      310,
366,  366,      229,      -1,      -1,      -1,      1,      -1,      393,      387,      406,      392,      539,
    KBCS = 122,      121,      121,      1,      59,      59,      80,      60,      59,      82,      59,
59,    58,      1,      1,      -1,      1,      1,      62,      108,      59,      60,      1,
    KBCE = 122,      121,      121,      1,      59,      59,      80,      60,      108,      108,      59,
59,    58,      58,      -1,      -1,      -1,      -1,      1,      80,      108,      60,      79,      120,
    LBGS = 1,      1,      1,      1,      1,      1,      1,      1,      1,      1,      1,      1,
1,    1,      1,      1,      1,      1,      1,      1,      1,      1,      1,      1,      1,
    LBCE = -1,      -1,      -1,      -1,      -1,      -1,      -1,      -1,      -1,      -1,      -1,      -1,
1,    -1,      -1,      -1,      -1,      1,      -1,      -1,      -1,      -1,      -1,      -1,      -1,
    BCPAR1(11)=1000,
    BCPAR1(12)=1500,
    BCPAR1(13)=3000,
    BCPAR1(14)=.18,

```

```
BCPAR1(24)=0,  
$END  
$SCEINP  
$END
```

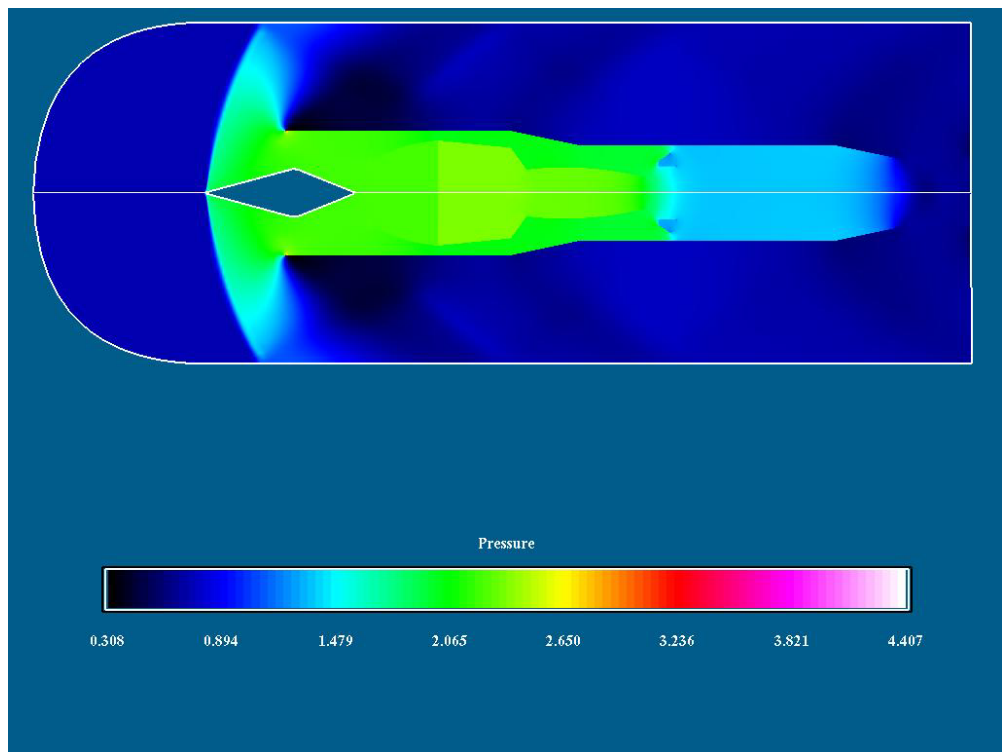


Figure C25. Pressure Distribution for the Turbo-Ramjet Engine at $M_{\infty} = 1.5$ (with Flameholder – Riemann Invariants B.C.)

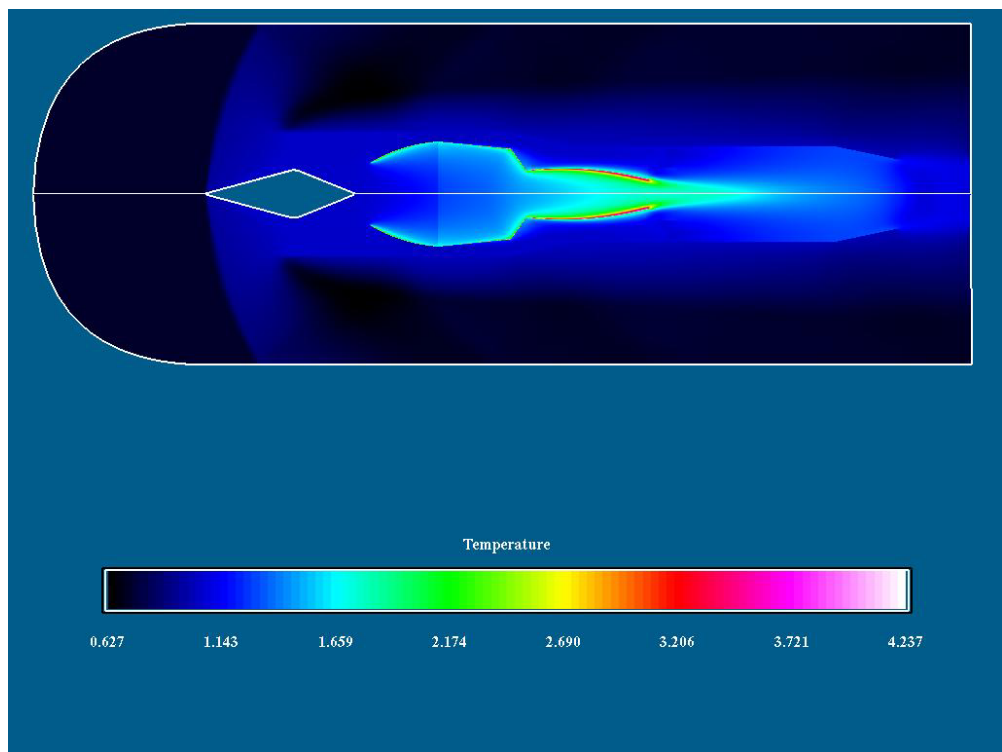


Figure C26. Temperature Distribution for the Turbo-Ramjet Engine at $M_{\infty} = 1.5$ (with Flameholder – Riemann Invariants B.C.)

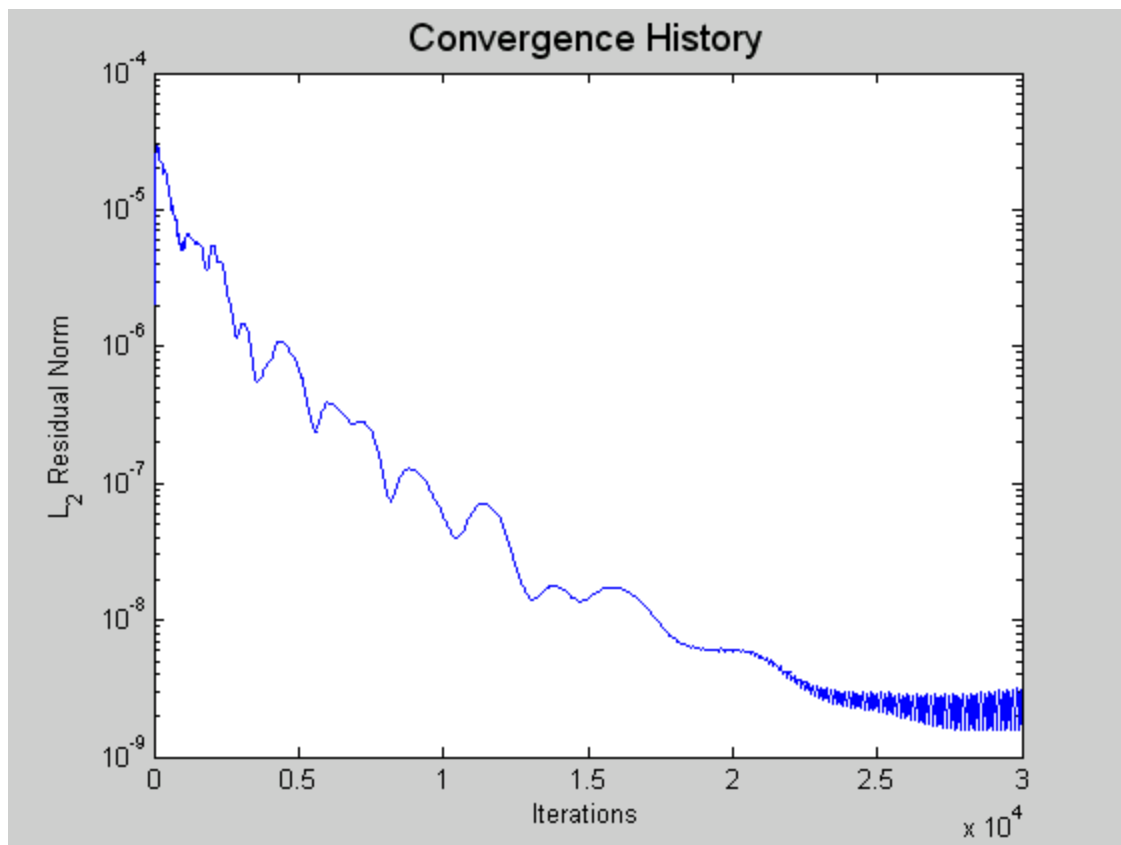


Figure C27. Convergence History for Turbo-Ramjet Engine at $M_{\infty} = 1.5$ (with Flameholder – Riemann Invariants B.C.)

Overflow.in Input File for Turbo-Ramjet at $M_\infty = 1.5$ (Flameholder- Riemann Invariants Boundary Condition)

```

$GLOBAL
    CHIMRA= .F.,      NSTEPS=30000,      RESTRT= .F.,      NSAVE =1000,
    NQT    = 202,
    $END
$FLOINP
    ALPHA =0,    FSMACH= 1.5000,    REY    = 1.0420E7,    TINF   = 520.000,
    XKINF=.0001, RETINF=0.1, GAMINF=1.4,
    $END
$VARGAM
    IGAM=0,
    $END
$GRDNAM
    NAME = 'Throughflow into engine heating grid TEMP change
flameholder',
    $END
$NITERS
    $END
$METPRM
    $END
$TIMACU
    ITIME=1,
    CFLMIN=1,
    CFLMAX=10,
    $END
$SMOACU
    $END
$VISINP
    VISC =.T.,
    CFLT = 1,
    ITERT = 3,
    $END
$BCINP
    NBC    = 24,
    IBTYP = 5,      5,      5,      5,      5,      5,      5,      5,      5,      5,      5,      7,
7,    7,      44,      31,      31,      22,      16,      16,      5,      5,      5,      5,      61,      44,
    IBDIR = 2,      -2,      -2,      2,      2,      -2,      2,      2,      2,      -1,      1,      2,
2,    -2,      1,      -1,      -2,      3,      1,      2,      1,      2,      1,      -2,      1,
    JBKS = 81,      81,      400,      1,      150,      386,      387,      393,      386,      387,      230,
311,  150,      228,      -1,      1,      1,      133,      393,      386,      406,      387,      539,
    JBCE = 539,      399,      539,      132,      229,      406,      393,      406,      386,      387,      310,
366,  366,      229,      -1,      -1,      -1,      1,      -1,      393,      387,      406,      392,      539,
    KBCS = 122,      121,      121,      1,      59,      59,      80,      60,      59,      82,      59,
59,    58,      1,      1,      -1,      1,      1,      62,      108,      59,      60,      1,
    KBCE = 122,      121,      121,      1,      59,      59,      80,      60,      108,      108,      59,
59,    58,      -1,      -1,      -1,      -1,      1,      80,      108,      60,      79,      120,
    LBKS = 1,      1,      1,      1,      1,      1,      1,      1,      1,      1,      1,      1,
1,    1,      1,      1,      1,      1,      1,      1,      1,      1,      1,      1,      1,
    LBCE = -1,      -1,      -1,      -1,      -1,      -1,      -1,      -1,      -1,      -1,      -1,      -1,
1,    -1,      -1,      -1,      1,      -1,      -1,      -1,      -1,      -1,      -1,      -1,      -1,
    BCPAR1(11)=1000,
    BCPAR1(12)=1500,
    BCPAR1(13)=3000,
    BCPAR1(14)=.18,

```

```
BCPAR1(24)=0,  
$END  
$SCEINP  
$END
```

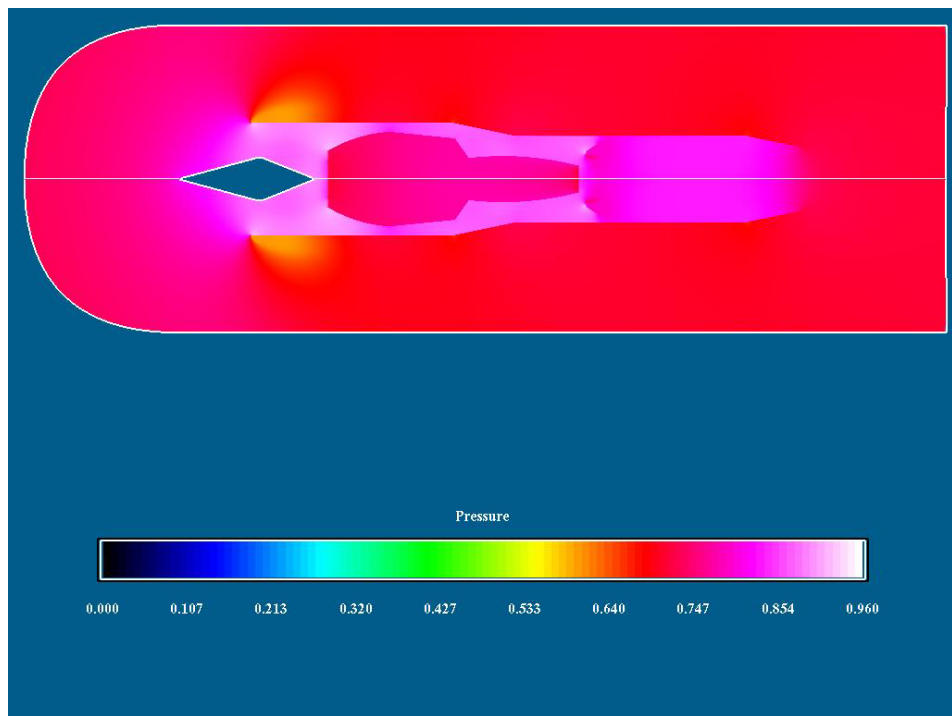


Figure C28. Pressure Distribution for the Turbo-Ramjet Engine at $M_{\infty} = 0.6$ (Engine Modeling with Q-files –Short Afterburner Duct)

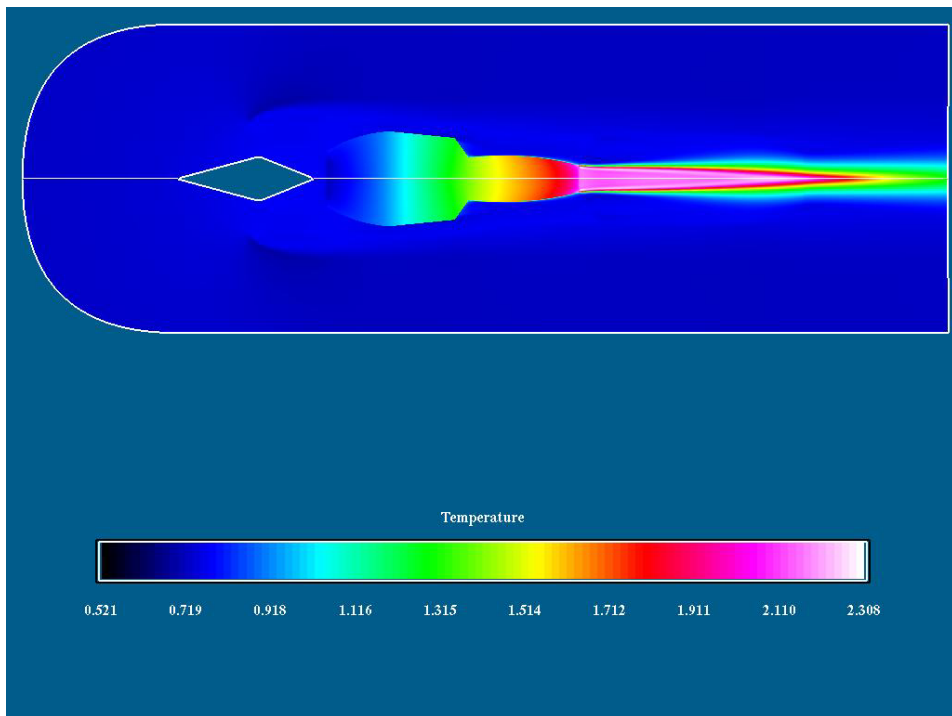


Figure C29. Temperature Distribution for the Turbo-Ramjet Engine at $M_{\infty} = 1.5$ (Engine Modeling with Q-files – Short Afterburner Duct)

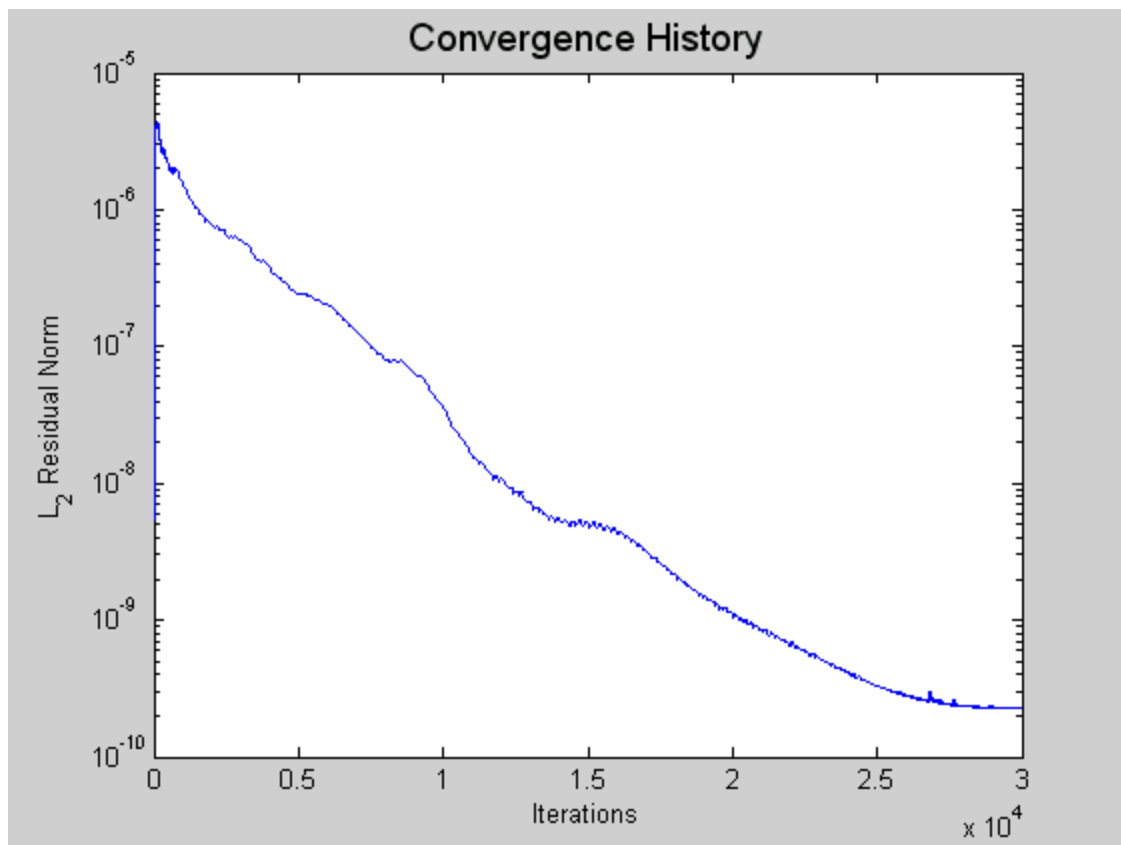


Figure C30. Convergence History for Turbo-Ramjet Engine at $M_{\infty} = 0.6$ with Engine Modeling with Q-files (Short Afterburner Duct)

Overflow.in Input File for Turbo-Ramjet at $M_{\infty} = 0.6$ for Engine Modeling with Q-files (Short Afterburner Duct)

```

$GLOBAL
    CHIMRA= .F.,      NSTEPS=30000,      RESTRT= .F.,      NSAVE =1000,
    NQT    = 102,
    $END

$FLOINP
    ALPHA =0,    FSMACH= 0.6000,    REY    = 1.0420E7,    TINF   = 520.000,
    XKINF=.01,  RETINF=1,  GAMINF=1.4,
    $END

$VARGAM
    IGAM=0,
    $END

$GRDNAM
    NAME = 'Throughflow into engine heating grid TEMP change
flameholder',
    $END

$NITERS
    $END

$METPRM
    $END

$TIMACU
    ITIME=1,
    CFLMIN=1,
    CFLMAX=10,
    $END

$SMOACU
    $END

$VISINP
    VISC =.T.,
    CFLT = 1,
    ITERT = 3,
    $END

$BCINP
    NBC    = 25,
    IBTYP = 5,      5,      5,      5,      5,      5,      5,      5,      7,      5,
5, 43, 32, 31, 22, 16, 16, 5, 5, 5, 61, 44, 61, 43,
    IBDIR = 2,      -2,      2,      2,      -2,      2,      2,      -1,      1,      2,      -2,
1, 1, -1, -2, 3, 1, 2, 1, 2, 1, -2, 1, 1, 1, 1,
    JBCS = 81, 81, 1, 150, 386, 387, 393, 386, 387, 311, 150,
150, 150, -1, 1, 1, 133, 393, 386, 406, 387, 655, 151, 366,
    JBCE = 656, 656, 132, 310, 406, 393, 406, 386, 387, 366, 366,
150, 150, -1, -1, 1, -1, 393, 387, 406, 392, 656, 365, 366,
    KBCS = 122, 121, 1, 59, 59, 80, 60, 59, 82, 59, 58,
26, 1, 1, -1, 1, 1, 62, 108, 59, 60, 1, 1, 1,
    KBCE = 122, 121, 1, 59, 59, 80, 60, 108, 108, 59, 58,
57, 25, -1, -1, -1, -1, 1, 80, 108, 60, 79, 120, 57, 57,
    LBCS = 1, 1, 1, 1, 1, 1, 1, 1, 1, 1, 1, 1,
1, 1, 1, 1, 1, 1, 1, 1, 1, 1, 1, 1, 1,
    LBCE = -1, -1, -1, -1, -1, -1, -1, -1, -1, -1, -1, -1, -1,
-1, -1, -1, 1, -1, -1, -1, -1, -1, -1, -1, -1, -1, -1,
    BCPAR1(10)=1000,
    BCPAR1(13)=10,
    BCFILE(13)='qinlet.dat',
    BCPAR1(23)=0,

```

```
BCPAR1(25)=10,  
BCFILE(25)='qexit.dat',  
$END  
$SCEINP  
$END
```

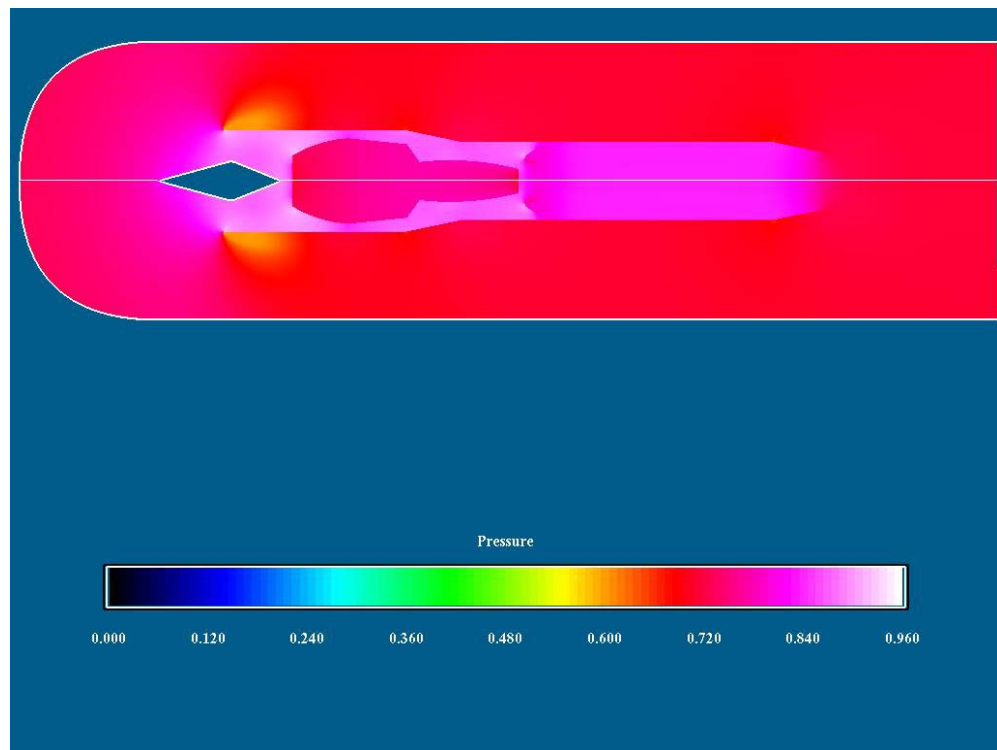


Figure C31. Pressure Distribution for the Turbo-Ramjet Engine at $M_{\infty} = 0.6$ (Long Afterburner Duct)

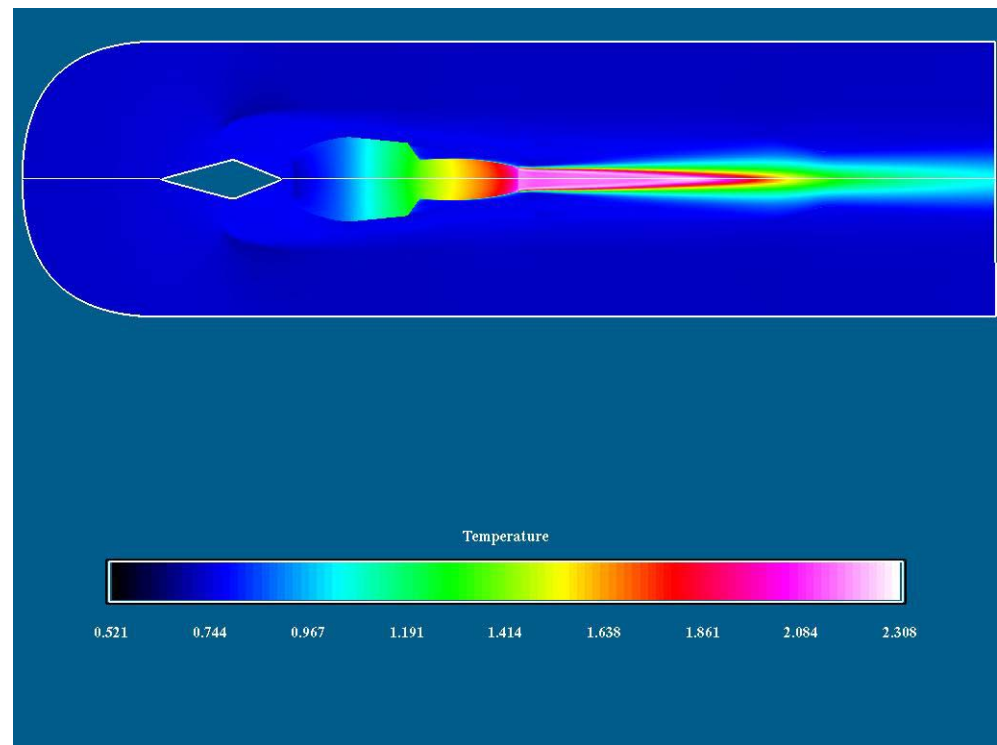


Figure C32. Temperature Distribution for the Turbo-Ramjet Engine at $M_{\infty} = 0.6$ (Long Afterburner Duct)

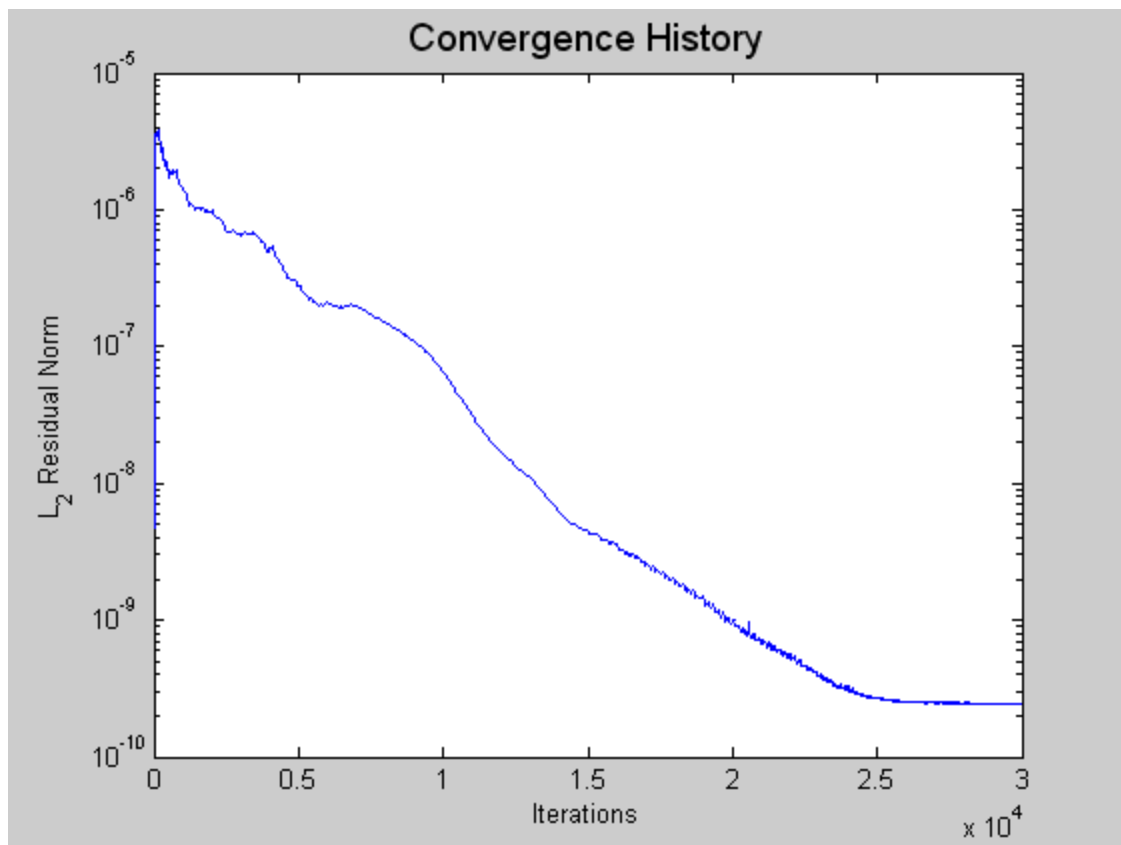


Figure C33. Convergence History for Turbo-Ramjet Engine at $M_{\infty} = 0.6$ with Engine Modeling with Q-files (Long Afterburner Duct)

Overflow.in Input File for Turbo-Ramjet at $M_{\infty} = 0.6$ for Engine Modeling with Q-files (Long Afterburner Duct)

```

$GLOBAL
    CHIMRA= .F.,      NSTEPS=30000,      RESTRT= .F.,      NSAVE =1000,
    NQT    = 102,
    $END

$FLOINP
    ALPHA =0,    FSMACH= 0.6000,    REY    = 1.0420E7,    TINF   = 520.000,
    XKINF=.01,  RETINF=1,  GAMINF=1.4,
    $END

$VARGAM
    IGAM=0,
    $END

$GRDNAM
    NAME = 'Throughflow into engine heating grid TEMP change
flameholder',
    $END

$NITERS
    $END

$METPRM
    $END

$TIMACU
    ITIME=1,
    CFLMIN=1,
    CFLMAX=10,
    $END

$SMOACU
    $END

$VISINP
    VISC =.T.,
    CFLT = 1,
    ITERT = 3,
    $END

$BCINP
    NBC    = 25,
    IBTYP = 5,      5,      5,      5,      5,      5,      5,      5,      7,      5,
5, 43, 32, 31, 22, 16, 16, 5, 5, 5, 61, 44, 61, 43,
    IBDIR = 2,      -2,      2,      2,      -2,      2,      2,      -1,      1,      2,      -2,
1, 1, -1, -2, 3, 1, 2, 1, 2, 1, -2, 1, 1, 1, 1,
    JBCS = 81, 81, 1, 150, 386, 387, 393, 386, 387, 311, 150,
150, 150, -1, 1, 1, 133, 393, 386, 406, 387, 655, 151, 366,
    JBCE = 656, 656, 132, 310, 406, 393, 406, 386, 387, 366, 366,
150, 150, -1, -1, 1, -1, 393, 387, 406, 392, 656, 365, 366,
    KBCS = 122, 121, 1, 59, 59, 80, 60, 59, 82, 59, 58,
26, 1, 1, -1, 1, 1, 62, 108, 59, 60, 1, 1, 1,
    KBCE = 122, 121, 1, 59, 59, 80, 60, 108, 108, 59, 58,
57, 25, -1, -1, -1, -1, 1, 80, 108, 60, 79, 120, 57, 57,
    LBCS = 1, 1, 1, 1, 1, 1, 1, 1, 1, 1, 1, 1,
1, 1, 1, 1, 1, 1, 1, 1, 1, 1, 1, 1, 1,
    LBCE = -1, -1, -1, -1, -1, -1, -1, -1, -1, -1, -1, -1, -1,
-1, -1, -1, 1, -1, -1, -1, -1, -1, -1, -1, -1, -1, -1,
    BCPAR1(10)=1000,
    BCPAR1(13)=10,
    BCFILE(13)='qinlet.dat',
    BCPAR1(23)=0,

```

```
BCPAR1(25)=10,  
BCFILE(25)='qexit.dat',  
$END  
$SCEINP  
$END
```

APPENDIX D. FORTRAN PROGRAMS AND INPUT FILES

PROGRAMS “*makefileinlet.f*” and “*makefileexit.f*”

```

C
C Generate Q file for powered nacelle.
C
C
PARAMETER(jdim=1,kdim=3,ldim=57,nq=8)
real dum(10)
real q(jdim,kdim,ldim,7)
CHARACTER*80 FILE
C
C Get the output filename.
C
C
READ(*,2,END=100) FILE
2 FORMAT(A)
C
ALPHA = 0
RE = 1.047E7
TIME = 0
GAMINF = 1.4
RETINF = 0.1
C
C
READ(*,*) EXP0,EXT0,EXM
READ(*,*) FSP ,FST ,FSM
READ(*,*) NI, NJ, NK

TMP = 1. + 0.5*(GAMINF-1)*EXM*EXM
TMP1 = TMP ** (GAMINF/(GAMINF-1))
C Derive Q1
C
EXP = EXP0 / TMP1 ! Exhaust pressure
EXT = EXT0 / TMP
FSP0= FSP*(1.+0.5*(GAMINF-1)*FSM*FSM) ** (GAMINF/(GAMINF-1))
EXA = SQRT(GAMINF*1716*EXT) ! Exhaust speed of sound
FSA = SQRT(GAMINF*1716*FST) ! Free stream speed of sound
EXRHO = GAMINF*EXP/EXA/EXA ! Exhaust density
FSRHO = GAMINF*FSP/FSA/FSA ! Free stream density
Q1 = EXRHO / FSRHO
WRITE(*,*) EXP, EXT , EXA , FSA
WRITE(*,*) EXRHO, FSRHO, EXP0, FSP0
C
C Derive Q2
C
Q2 = Q1*EXM*EXA/FSA
C
C Derive Q3,Q4
C
Q3 = 0.0
Q4 = 0.0
C
C Derive Q5
C
Q5 = EXP0/(FSP0*GAMINF*(GAMINF-1))
E0 = EXP/(GAMINF-1)/EXRHO+0.5*(EXM*EXM*EXA*EXA)
Q51 = Q1*E0/FSA/FSA
DO J=1,NI

```

```

DO K=1,NK
    DO L=1,NJ
        q(J,K,L,1)=Q1
        q(J,K,L,2)=Q2
        q(J,K,L,3)=Q3
        q(J,K,L,4)=Q4
        q(J,K,L,5)=Q51
        q(J,K,L,6)=GAMINF
        q(J,K,L,7)=RETINF
    ENDDO
ENDDO
ENDDO

NIJK = NI*NJ*NK
WRITE(1,*) NI,NJ,NK
WRITE(1,*) (0.0, I=1,NIJK), (((J, I=1,NI), J=1,NJ), K=1,NK),
&
           (((K, I=1,NI), J=1,NJ), K=1,NK)
C
WRITE(*,*) Q1, Q2, Q3, Q4, Q5, Q51

jmax = NI
kmax = NK
lmax = NJ
open(unit=3,file=FILE,form='unformatted')
write(3) jmax,lmax,kmax,6,0,1
write(3) FSM,ALPHA,RE,TIME
write(3) (((q(j,k,l,n),j=1,jmax),l=1,lmax),k=1,kmax),n=1,7)
close(3)
100 continue
C
stop
end

```

PROGRAM “*qinlet02.inp*”

```

qinlet.dat
2176.128,522,0.2
2116.8,520,0.6
1,47,3

```

! Name of save file (Q file)
! Exhaust Total pressure, temp. and M
! Free stream pressure, temp. and M
! NI, NJ, NK (face grid dimensions)

Input for generating a Q file

PROGRAM “*qinlet02.inp*”

```

qexit.dat
2784.96,1662,0.65
2116.8,520,0.6
1,47,3

```

! Name of save file (Q file)
! Exhaust Total pressure, temp. and M
! Free stream pressure, temp. and M
! NI, NJ, NK (face grid dimensions)

Input for generating a Q file

APPENDIX E. DATA ACQUISITION PROGRAM ANALYSIS

1. Block Diagram of the Program Operation

The program could be controlled and run by the Main page front panel shown in Figure E1.

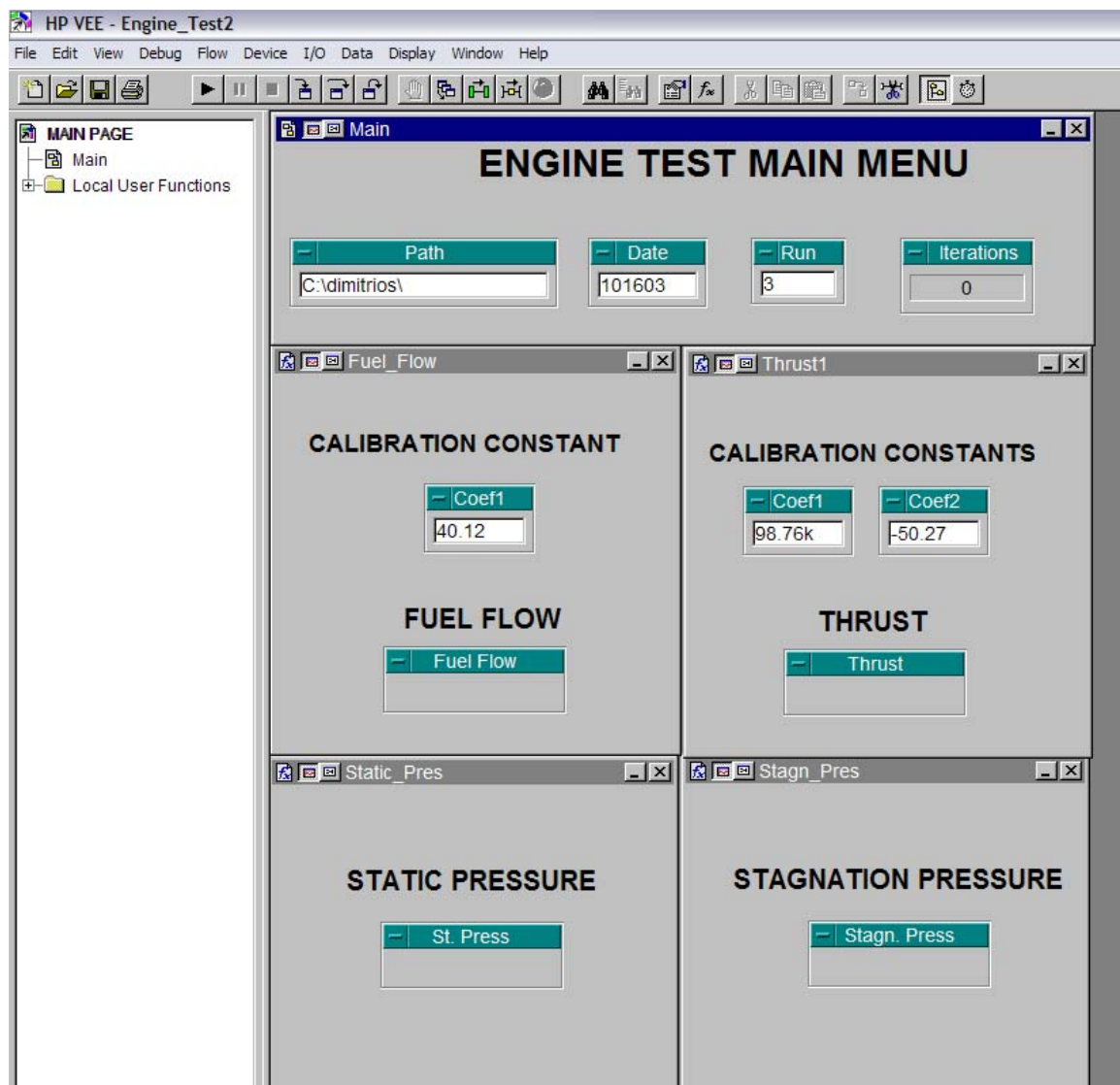


Figure E1. Control Panels

The user input the path in which the output file would be saved, the date and the run number as well as the calibration constants for the fuel flow and the thrust.

The program started by pressing the “*Run*” button. The number of iterations and the measured values of fuel flow rate, thrust, static and stagnation pressure during each iteration were presented in the corresponding windows. The program would keep running until the “*Stop*” button was pressed.

The program was also used to calibrate the thrust and fuel flow measurements, by selecting the individual functions (‘*Thrust1*’ and ‘*Fuel_Flow*’, respectively) and pressing the ‘*START*’ icon. This would run those functions only and not the rest of the application.

It was important to reset the DVM after each calibration; otherwise it would not respond to other commands.

2. Main Page Analysis

The Main page, Figure E2, consisted of the following blocks:

- An “Until Break” function, which enabled the program to operate continuously until the stop button was pressed.
- An “Iterations” counter, which counted the number of performance measurements.
- Four text constants, called “*Chan_Num*”, each of which was used to select a different channel of the DACU. It has to be noted that DACU had ten (10) channels, starting from zero (0) to nine (9), hence channel 0 read the fuel flow rate, channel 5 read the thrust, channels 6 and 7 read the static and stagnation pressures of the freejet plume, respectively.
- Four ‘calls’ for the “*Channel*” function and one for each of the “*Fuel_Flow*”, “*Stag_Pres*”, “*Static_Pres*” and “*Thrust1*” subroutines.
- An “If...then...else” function, that was used for the saving of the data file in conjunction with two “*To File*” functions.
- Six “*Constant*” and one “*Formula*” block which were used for the construction of the path and filename of the save file.

The Main page used the functions “*Chan_Num*” and “*Channel*” to command DACU to switch to Channels 0, 5, 6 and 7 to read the value of fuel flow rate, thrust, static and stagnation pressure. These values were then output to a text file (*.txt).

The output file had the following format:

DATE (alpharethmetic format)
FUEL FLOW *THRUST* *STATIC PRESS.* *STAGNATION*
PRESS.
#VALUE *#VALUE* *#VALUE* *#VALUE*
#VALUE *#VALUE* *#VALUE* *#VALUE*
#VALUE *#VALUE* *#VALUE* *#VALUE*

This format was constructed using the “If...then...Else” function and the “Iteration” counter. When “Iteration” was equal to 1, the first “To File” function was used in order to write the date, the headings and the first row of data to the text file. When “Iteration” had a value different than 1, the second “To File” function was used to write the data in rows. “Tabs” separated the data, in order to be easily read by Microsoft Excell or MATLAB for further processing.

The filename of the output file had the following format:

C:\dimitrios\RUN101603_1.txt,

where “*C:\dimitrios*” was the path of the location of the file in the hard drive,

“*RUN101603_1*” was the file name consisting of the date (16 Oct 2003, in the example) and of the run number (1).

The file name was automatically constructed using the path, date and run number provided by the user in the main panel.

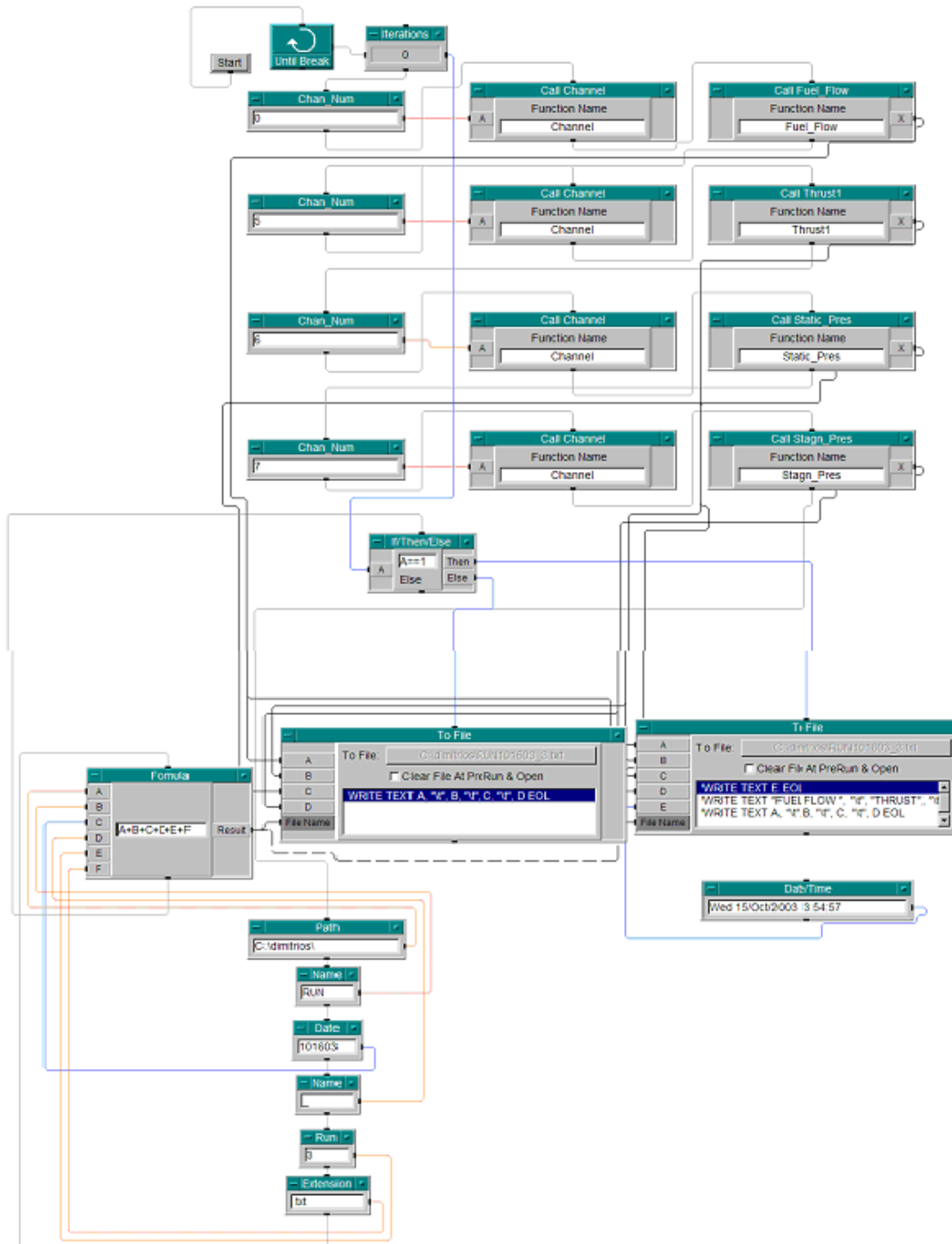


Figure E2. Main Page Block Diagram

3. “Channel” Function Analysis

The “Channel” function, Figure E3, consisted of two identical I/O functions, called “DACU”, which controlled the switching of the DACU’s channels. These two I/O

functions were used because it was found that the DACU required the repetition of the commands to switch channel.

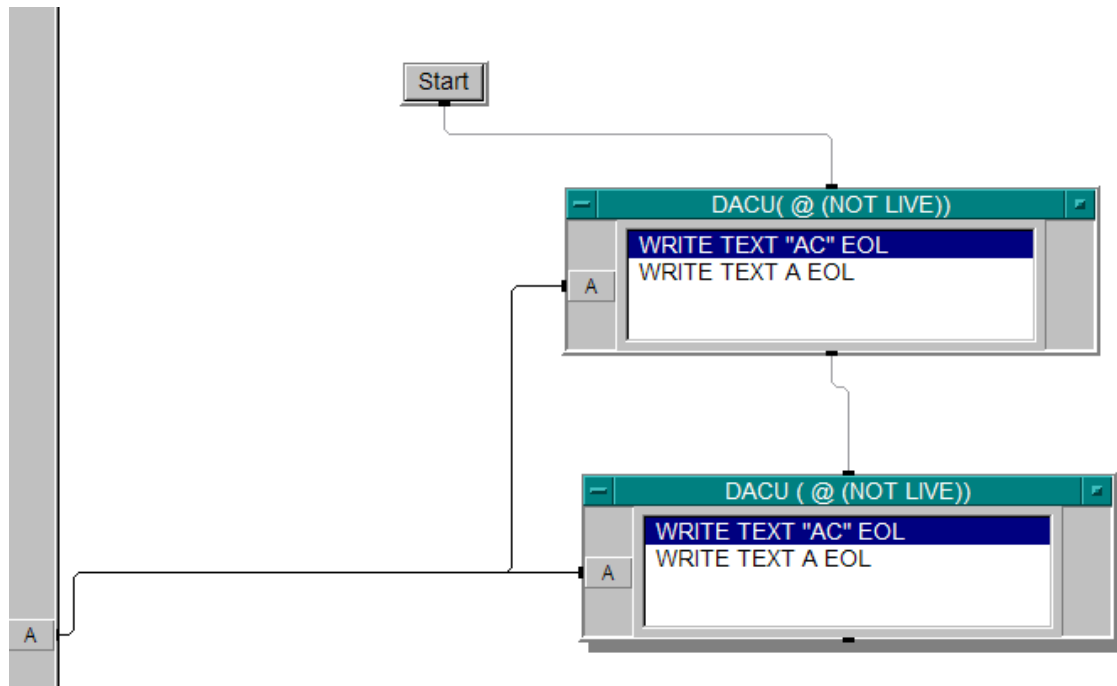


Figure E3. “Channel” Function Diagram

This function assigned the value “Chan_Num” to variable A and wrote that to DACU. The command “AC” inside the I/O function was used to open the communication port with DACU.

4. “Fuel_Flow” Function Analysis

The “Fuel_Flow” function, Figure E4, consisted of:

- a “Multimeter” block, which read the signal that corresponded to the fuel flow from the digital voltmeter (DVM). This block sampled six values, as defined in the ‘Trigger Options’ menu.
- a “Get Values” function, named “Fuel Flow Values”, which ignored the first two readings. This was necessary as it was realized that when the Channel was changed, the DVM had some hysteresis in reading the correct value of the signal.

- a “Mean” formula, which computed the average of the signal readings and assigned that to variable A .
- a “Fuel_Flow_Cal” formula, which converted the signal to a value for fuel flow rate. It used the following simple first order equation

$$\text{fuelflow} = \text{AverageSignal} * \text{Coef1} = A * B$$

where Coef1 was the calibration value, as computed using the methodology of Garcia (Ref. 6) and Piper (Ref. 1). This value was input by the user in the “Channel” panel.

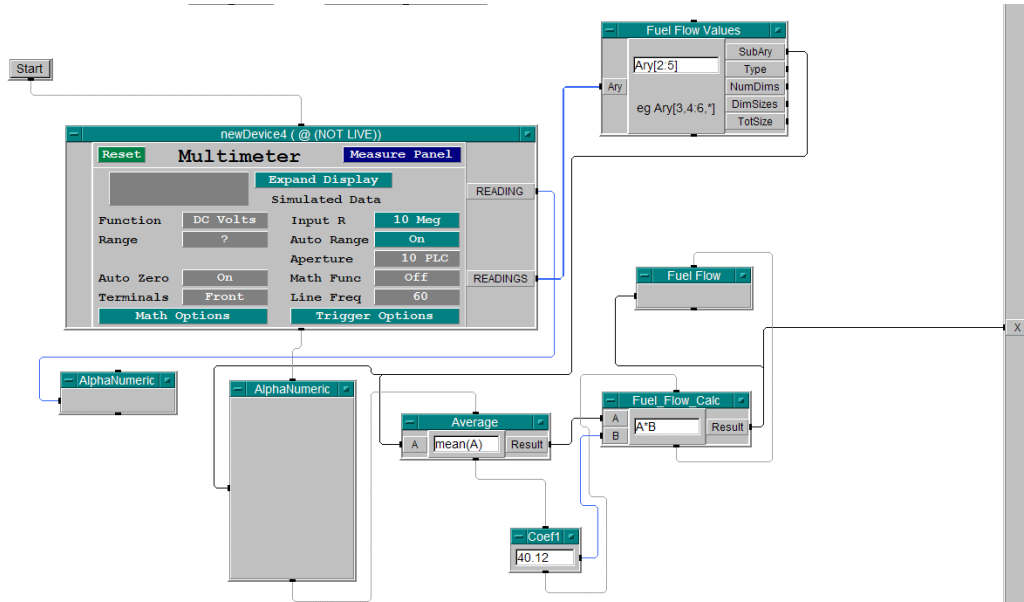


Figure E4. “Fuel_Flow” Function Diagram

5. “Thrust1” Function Analysis

The “Thrust1” function, Figure E5, had the same format as the previous one. The only difference was that it used the following equation to convert the signal to thrust:

$$\text{Thrust} = \text{AverageSignal} * \text{Coef1} + \text{Coef2} = A * B + C$$

The constants Coef1 and Coef2 were the calibration constants, as computed by the methodology of Garcia (Ref. 6) and Piper (Ref. 1) and were input by the user in the “Thrust1” panel.

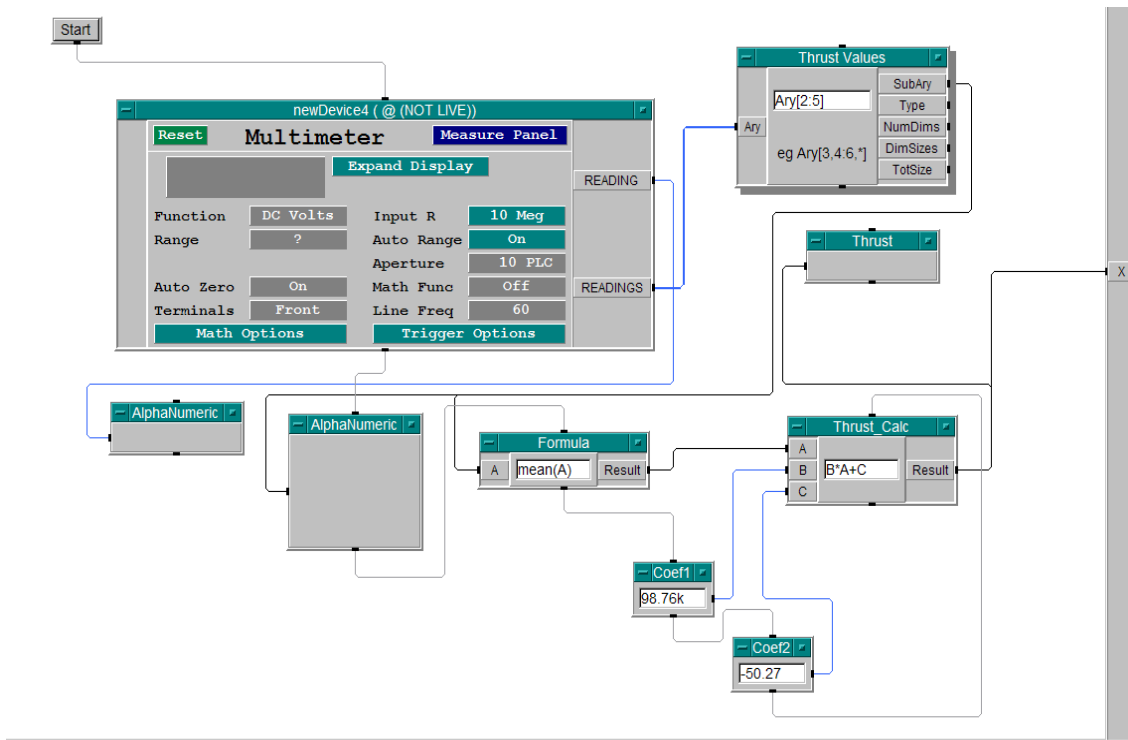


Figure E5. “Thrust1” Function Diagram

6. “Static_Pres” and “Stagn_Pres” Functions Analysis

The “Static_Pres” and “Stagn_Pres” functions are shown in Figures E6 and E7, respectively. They were also similar to the previous ones with the only difference of multiplying the average signal with a constant of 1000, in order to convert the voltage reading to a value of pressure:

$$\text{Pressure} = \text{AverageSignal} * 1000$$

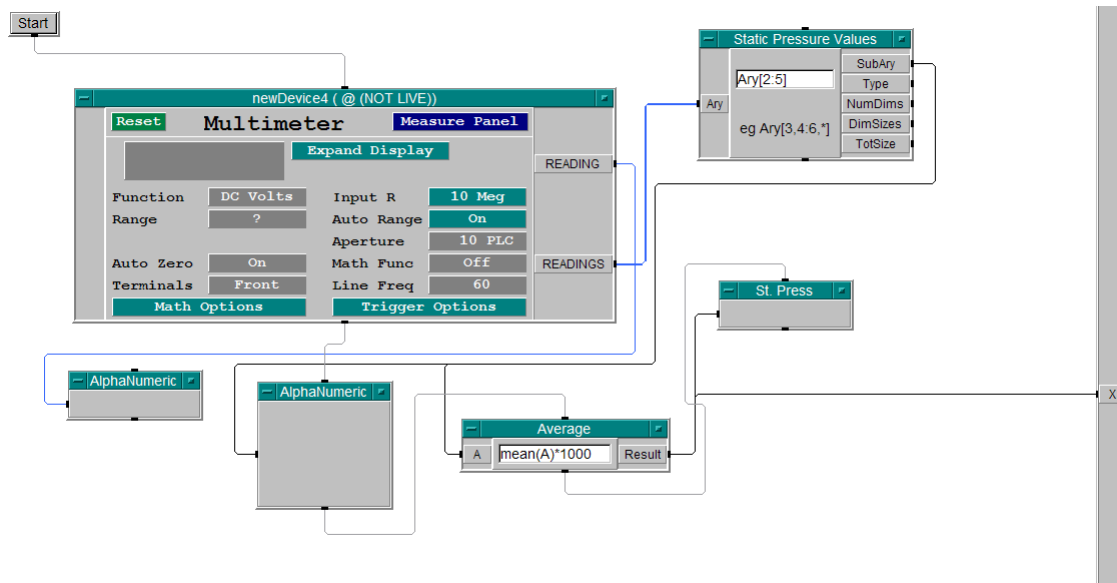


Figure E6. “Static_Pres” Function Diagram

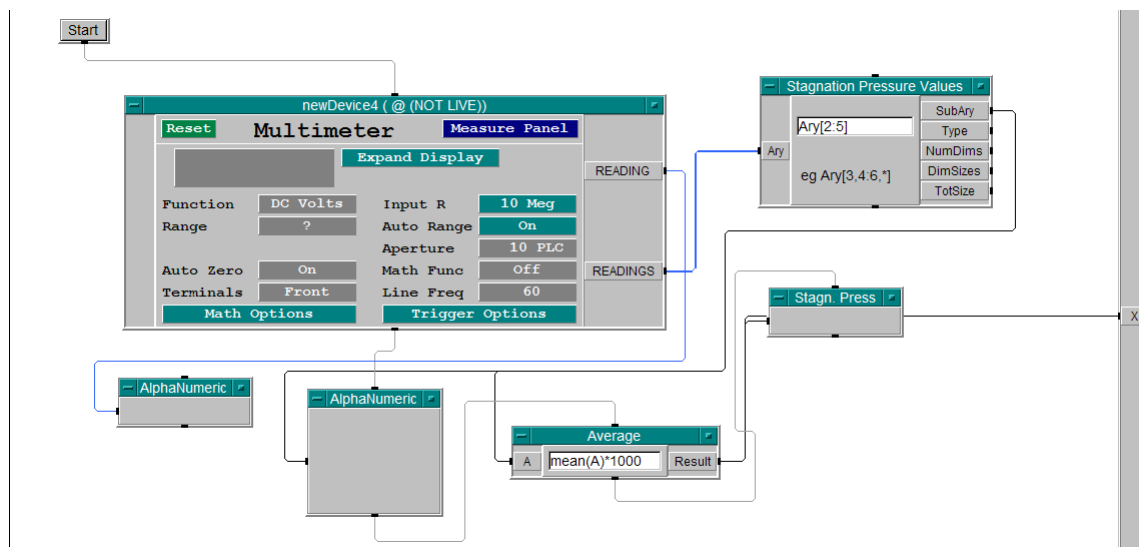


Figure E7. “Stagn_Pres” Function Diagram

LIST OF REFERENCES

1. Piper, R., *Design and Testing of a Combustor for a Turbo-ramjet for UAV and Missile Applications*, Master's Thesis, Department of Aeronautics and Astronautics, U.S. Naval Postgraduate School, Monterey, CA, March 2003.
2. Rivera, G., *Turbochargers to Small Turbojet Engines for Uninhabited Aerial Vehicles*, Engineer's Thesis, Department of Aeronautics and Astronautics, U.S. Naval Postgraduate School, Monterey, CA, June 1998
3. Hackaday, G., *Thrust Augmentation for a Small Turbojet Engine*, Master's Thesis, Department of Aeronautics and Astronautics, U.S. Naval Postgraduate School, Monterey, March 1999
4. Andreou, L., *Performance of a Ducted Micro-Turbojet Engine*, Master's Thesis, Department of Aeronautics and Astronautics, U.S. Naval Postgraduate School, Monterey, September 1999
5. Al-Namani, S.M., *Development of Shrouded Turbojet to Form a Turboramjet for Future Missile Applications*, Master's Thesis, Department of Aeronautics and Astronautics, U.S. Naval Postgraduate School, Monterey, June 2000
6. Garcia, H., *Testing and Development of a Shrouded Gas Turbine Engine in a Freejet Facility*, Master's Thesis, Department of Aeronautics and Astronautics, U.S. Naval Postgraduate School, Monterey, December 2000
7. Kurzke, J., *GASTURB 9.0 for Windows: A Program to Calculate Design and Off Design Performance of Gas Turbine Engines*, 2001
8. Mattingly, J.D., Heiser, W.H., Daley, D.H., *Aircraft Engine Design*, American Institute of Aeronautics and Astronautics Inc, 1987
9. Buning, P.G., *OVERFLOW User's Manual – Version 1.8w*, NASA Langley Research Center, Hampton VA
10. Wilcox, D.C., *Turbulence Modeling for CFD*, DCW Industries Inc., 1993

THIS PAGE INTENTIONALY LEFT BLANK

INITIAL DISTRIBUTION LIST

1. Defense Technical Information Center
Ft Belvoir, VA
2. Dudley Knox Library
Naval Postgraduate School
Monterey, CA
3. Dist. Prof. Anthony J. Healey
Naval Postgraduate School
Monterey, CA
4. Prof. Garth V. Hobson
Naval Postgraduate School
Monterey, CA
5. Prof. Kai Woehler
Naval Postgraduate School
Monterey, CA
6. Naval Air Warfare Center, Aircraft Division
Propulsion and Power Engineering
Patuxent River, MD
ATTN: C.Georgio, Code 4.4
7. Naval Air Warfare Center, Weapons Division
AirBreathing Propulsion & Controls Branch
China Lake, CA
ATTN: John B. Moore, Code 477400D
8. Dimitrios Krikellas
Athens, Greece